POLITECNICO DI TORINO

Collegio di Ingegneria Chimica e dei Materiali

Master of Science Course
in Materials Engineering

Master of Science Thesis

Bio-based polymers for Additive Manufacturing

Tutor

Prof. Roberta Bongiovanni

Candidate

Tereza Cupkova

March 2021

Table of Contents

Riassunto

I. Obiettivi

L'Additive Manufacturing (AM), conosciuto anche come stampa 3D, è una tecnologia innovativa che ha ricevuto una grande attenzione negli ultimi decenni perché offre numerosi vantaggi tra cui la possibilità di realizzare componenti con geometrie personalizzate e complesse senza l'impiego di utensili. Diversi materiali sono stati sviluppati per l'AM e tra questi, i polimeri risultano essere quelli più usati. In commercio sono disponibili polimeri sia termoplastici sia termoindurenti e nella maggior parte dei casi, il petrolio è la fonte primaria da cui vengono ricavati. Contestualmente alla diffusione delle tecniche additive e all'insorgenza dei problemi ambientali legati ai rifiuti plastici, la ricerca di materiali alternativi volti alla sostenibilità è diventata sempre più importante. L'interesse scientifico perciò si è spostato dalle fonti fossili alle numerose fonti biologiche rinnovabili come piante, alghe e microorganismi per la sintesi di nuovi polimeri. Il lavoro di tesi si colloca all'interno di questo quadro generale e si pone l'obiettivo di illustrare alcuni dei polimeri derivati da biomassa sviluppati per le principali tecniche additive.

La tesi consiste di tre parti. La prima è un capitolo introduttivo che fornisce una panoramica generale sui diversi tipi di polimeri ottenibili a partire da fonti rinnovabili, in modo da contestualizzare l'argomento centrale della tesi. In particolare, vengono presentati i polimeri bio-based che appartengono alle tre famiglie principali: polimeri naturali, polimeri di sintesi da biomassa e polimeri da fermentazione batterica. La seconda parte è dedicata alla descrizione delle varie tecniche di stampa 3D e dei relativi polimeri da biomassa riportati in letteratura. Per ogni materiale proposto vengono indicate ulteriori informazioni come il sistema di stampa usato, le caratteristiche geometriche e dimensionali del componente stampato e la fedeltà di riproduzione rispetto al modello virtuale. Dal momento che la qualità e la funzionalità di un oggetto dipendono dalla risoluzione di stampa, maggiore attenzione viene dedicata a quest'ultimo parametro. Nella terza e ultima parte vengono proposte delle considerazioni generali circa la qualità di stampa e le risoluzioni raggiunte nelle varie tecnologie di AM.

II. Risultati

Esistono diversi approcci che consentono di realizzare dei manufatti attraverso l'addizione di successivi strati di materiale, in questa tesi sono state considerate quattro modalità di deposizione: estrusione di materiale, stampa a getto, fotopolimerizzazione in vasca e tecniche a letto di polvere (Figura 3.1). Considerando le informazioni ricavate dalla letteratura scientifica, si è potuto concludere che le biomasse rappresentano una fonte idonea per la produzione di materiale destinato alla stampa 3D. Polimeri naturali, polimeri e monomeri

sintetizzati da biomassa e polimeri da fermentazione batterica sono stati impiegati per la produzione di componenti di varia complessità geometrica. Inoltre, la formulazione di blends polimerici completamente bio-based e l'aggiunta di cariche rinforzanti come le fibre lignocellulosiche, hanno permesso di regolare le proprietà viscoelastiche del feed e di migliorare le caratteristiche meccaniche dell'oggetto finale. Gran parte delle formulazioni dei feed riportate sono state preparate in laboratorio, perciò ulteriori studi dovranno essere condotti prima di ottenerne la commercializzazione. Per quanto riguarda i sistemi di stampa, nella maggior parte dei casi sono state impiegate stampanti commerciali, talvolta apportando alcune modifiche.

L'aspetto estetico e la funzionalità di un componente realizzato con le tecniche additive dipendono principalmente dall'accuratezza e dalla risoluzione di stampa, fattori che a loro volta sono determinati da alcune caratteristiche intrinseche dell'AM come l'effetto "a gradino" dovuto alla sovrapposizione degli strati e la "sfaccettatura" della superficie dovuta alla sua discretizzazione durante l'elaborazione del modello digitale. La qualità di stampa dipende anche da altri fattori come il materiale usato e il tipo di tecnica additiva adottata. Considerando questi parametri, le informazioni ricavate dalla letteratura scientifica sono state confrontate e riportate nella Tabella II.

Mentre le risoluzioni spaziali della stampa 3D dei polimeri ricavati da fonti fossili sono ampiamente riportate in letteratura, poche informazioni sono disponibili nel caso delle risoluzioni ottenibili con la stampa di polimeri da fonti rinnovabili. Poiché nella maggior parte degli articoli a cui si fa riferimento non vengono specificate le risoluzioni nel piano XY ma vengono riportate le altezze dello strato di materiale depositato, nella Tabella II. vengono indicate le risoluzioni Z. Nell'esporre le considerazioni finali ottenute dal confronto tra i dati, è necessario tenere in conto due aspetti: le considerazioni sono riferite ad un numero limitato di fonti, perciò non possono avere una valenza generale; lo spessore del layer riportato in ogni articolo dipende dal design e dall'applicazione di ciascun oggetto, quindi le risoluzioni indicate non sono da considerarsi come le più alte ottenibili.

Tabella II. Principali tecniche additive e le relative materie prime derivate da fonti rinnovabili; sono riportati inoltre il sistema di stampa usato e la risoluzione Z.

Categoria AM	Tecnica additiva	Materiale da biomassa	Stampante	Altezza layer [µm]	Rif.
Estrusione di materiale	Fused Deposition Modeling	Acido polilattico	Solidoodle Workbench Apprentice	300	[32]
			Commerciale	250	[33]
			MakerBot Replicator 2	100	[34]
		Bio-policarbonato	Personalizzata	200	[35]

		Polietilene furanoato	Ultimaker 2	50	[36]
		Zeina	ORD Bot-Hadron		[37]
		Etilcellulosa	Multirap M420, Multec GmbH	100	[38]
			MakerBot Replicator 2	300	[40]
			Prusa i3 3D desktop printer	100	[42]
		Idrossipropilcellulosa	MakerBot Replicator 2	300	[39]
			MakerBot Replicator 2	300 ÷ 400	[40]
			Prusa i3 3D desktop printer	100	[42]
		Idrossipropilmetilcellulosa	Prusa i3 3D desktop printer	100	[42]
		Idrossipropilmetilcellulosa acetato succinato	MakerBot Replicator 2X	100	[41]
		Etilcellulosa + idrossipropilmetilcellulosa	A3, JGAURORA desktop printer	100 ÷ 300	[43]
		Etilcellulosa + alginato	A3, JGAURORA desktop printer	100 ÷ 300	[43]
		Etilcellulosa + gomma di xantano	A3, JGAURORA desktop printer	100 ÷ 300	[43]
		Amido + acetato di cellulosa	Ultimaker 2+	150	[44]
		Acido polilattico + galactoglucomannano	Me3D desktop printer	200	[45]
		Acido polilattico + cellulosa microcristallina	AutoMaker, Robox		[46]
		Acido polilattico + fibre da polpa di abete	Ultimaker Original		[47]
		Bio-polietilene funzionalizzato con anidride maleica + fibre da polpa di legno	Ultimaker Original		[48]
		Poliidrossialcanoato funzionalizzato con anidride maleica + fibre lignocellulosiche	Flashforge, L2D Desktop Factory	50	[49]

	Liquid Deposition Modeling	Ink a base di nanofibre di cellulosa	Benchtop robot Fisnar F4200n	200	[57]
		Ink a base di nanofibre di cellulosa modificata	Bioplotter EnvisionTEC GmbH	~670	[58]
		Ink a base di nanocristalli di cellulosa	ABL 900010, Aerotech Inc.	~410	[59]
			Commerciale		[60]
		Acetato di cellulosa	RegenHU		[61]
			Printrbot Simple Metal (modificata)	~180	[62]
			3Dn-300, nScrypt Inc.		[63]
		Emicellulosa	Personalizzata	530 ÷ 740	[64]
		Agar	Personalizzata	300	[65]
		Alginato, alginato + metilcellulosa	BioScaffolder 2.1, GeSiM		[66]
		Acido ialuronico metacrilato	Bioscaffolder dispensing system (SYS+ENG)	200	[67]
		Chitosano	Commerciale (modificata)	~250	[68]
		Collagene	Fab@Home 3D printer, Seraph Robotics (modificata)		[69]
		Gelatina metacrilammide	Bioplotter EnvisionTEC GmbH	150 ÷ 200	[70]
		Aneroina	Personalizzata		[71]
		Fibroina della seta	ABL9000, Aerotech Inc.		[72]
		Proteine del latte + proteine del siero di latte	SHINNOVE-S2, SHIYIN Technologies Co. Ltd.	750	[73]
Stampa a getto	Drop on demand	Alginato	Personalizzata		[76]
		Collagene	Canon Bubble Jet, BJC-2100 (modificata)		[77]
		Fibroina della seta	JetLab II, MicroFab Technologies	Alcune centinaia di nanometri	[78]

Foto-polimerizzazione in vasca	Stereolitografia	Olio di semi di soia epossidato acrilato	Personalizzata	≤ 100	[86]
		Resine a base di acrilati derivati da biomassa (isobornile acrilato, 1,10-decandiolo diacrilato, pentaeritritolo tetraacrilato, oligomero acrilato)	Formlabs Form 2	50	[87]
		Saccarosio di soia epossidato (met)acrilato	Peopoly Moai SLA printer, Firmware version 1.6	100	[88]
		Vanillina metacrilata	Formlabs Form 2	100	[85]
		Albumina metacrilata	Formlabs Form 2	50	[89]
		Derivato dell'eugenolo acrilato + guaiacolo metacrilato	Formlabs Form 1+	100	[90]
		Etilcellulosa metacrilata + 2-idrossietile acrilato + monomeri derivati dalla colofonia	Creality LD 001	40	[91]
	(SLA + FDM)	Gelatina metacrilata	Sistema personalizzato		[92]
	Direct Light Projection	Olio esausto da cucina acrilato	Solus DLP	25	[96]
		Olio di semi di soia epossidato acrilato	Asiga Pico2 39 UV	97	[97]
		Olio di semi di soia epossidato metacrilato	Cubicon Lux Full HD	100	[98]
		Acido polilattico metacrilato	EnvisionTec Perfactory Mini Multilens	25	[99]
		Carbossimetilcellulosa metacrilata	Asiga UV-MAX DLP printer		[100]
		Fibroina della seta metacrilata	Personalizzata	50	[101]
		Cheratina	EnvisionTec Perfactory 4		[102]
	Direct Laser Writing	Olio di semi di soia epossidato acrilato	Personalizzata		[97]
		Vanillina dimetacrilata, vanillina diacrilata	Personalizzata		[107]
		Olio di semi di soia epossidato acrilato + vanillina dimetacrilata	Personalizzata		[108]

Tecniche a letto di polvere	Selective Laser Sintering	Poliidrossibutirrato	Sinterstation 1 2000 SLS, 3D Systems (modificata)	180	[114]
		Poliidrossibutirrato-co-valerato	Sinterstation 2000 SLS, 3D Systems (modificata)	150	[115]
		Poliidrossibutirrato-co-valerato + fosfato di calcio	Sinterstation 2000 SLS, 3D Systems (modificata)	100	[115]
			Sinterstation 2000 SLS, 3D Systems (modificata)	100	[116]
		Acido polilattico	EOS P100 Formiga		[117]
			Sinterstation 2000 SLS, 3D Systems (modificata)	100	[118]
			Personalizzata	200	[119]
		Acido polilattico + nanoparticelle di argilla	EOS P100 Formiga		[117]
		Acido polilattico + idrossiapatite	Sinterstation 2000 SLS, 3D Systems (modificata)	100	[118]
	Binder Jetting	Acido polilattico	Personalizzata		[122]
			Personalizzata	200	[123]
		Idrossipropilcellulosa, etilcellulosa	Personalizzata	200	[124]
		Amido di mais + destrano + gelatina	Z402 3D printer, Zcorp		[125]

II.I Estrusione di materiale

In riferimento alla tecnica Fused Deposition Modeling (FDM), basata sull'estrusione di materiale polimerico a partire da un filamento solido, quasi la totalità dei sistemi di stampa usati per testare i polimeri bio-based sono stampanti commerciali. Sono stati realizzati componenti con geometrie ben definite di medio-alta complessità, aventi dimensioni complessive comprese tra i millimetri e i centimetri e una risoluzione Z cha varia tra 50 µm e 400 µm.

La stampabilità dei polimeri naturali mediante il processo di Liquid Deposition Modeling (LDM), basato invece sull'estrusione di polimeri sotto forma di soluzioni, gel o paste, è stata

valutata impiegando principalmente stampanti disponibili sul mercato, ma sono stati utilizzati anche sistemi di stampa sviluppati in laboratorio e stampanti commerciali modificate. In quest'ultimo caso, alcune modifiche erano necessarie per permettere il controllo della temperatura in modo da garantire la corretta solidificazione dell'estruso. La maggiore difficoltà del processo LDM consiste nel regolare la viscosità del polimero in modo da poter costruire strutture autosupportanti durante il processo di deposizione. Con la viscosità adeguata, è stato possibile stampare componenti aventi dimensioni totali comprese tra i millimetri e pochi centimetri e con risoluzioni Z comprese soprattutto nel range 200-750 μm.

II.II Stampa a getto

Riguardo alla stampa a getto, conosciuta come Drop on Demand (DOD) e caratterizzata dall'eiezione di gocce micrometriche di polimero, un minor numero di articoli è disponibile in letteratura nel caso del processamento di polimeri da biomassa. Nei tre studi riportati, i test di stampa sono stati condotti usando stampanti commerciali o sistemi personalizzati e tutti i componenti realizzati sono oggetti di dimensioni micrometriche successivamente impiegati per le sperimentazioni di colture cellulari. Relativamente a queste prove di stampa, il diametro minimo delle gocce depositate, associabile al valore minimo della risoluzione laterale, è nell'intervallo di 10-60 μm, mentre il minimo spessore dello strato è dell'ordine delle centinaia di nanometri.

II.III Fotopolimerizzazione in vasca

Rispetto a tutte le altre tecniche additive, i processi di fotopolimerizzazione in vasca offrono una maggiore accuratezza e affidabilità, inoltre la qualità di stampa ottenuta con alcune resine ricavate da fonti rinnovabili è risultata comparabile alle tipiche risoluzioni ottenibili con alcune resine commerciali derivate da fonti fossili. Sia con la stereolitografia (SLA) sia con il processo di Direct Light Projection (DLP), è stato possibile realizzare oggetti macroporosi e in bulk aventi forme geometriche complesse. Le dimensioni totali dei componenti variano tra i millimetri e pochi centimetri, le risoluzioni Z raggiunte sono pari o inferiori a 100 μm e dettagli di centinaia di micrometri sono stati ben riprodotti. Per quanto riguarda il Direct Laser Writing (DLW), una tecnica basata sulla fotopolimerizzazione multifotone, tre studi sono stati riportati. Per mezzo di un sistema di stampa sviluppato in laboratorio, sono stati fabbricati scaffolds per applicazioni biomedicali e figure 3D con dimensioni complessive comprese tra le centinaia di nanometri e i millimetri. In un caso non è stato possibile riprodurre alcuni dettagli micrometrici, mentre negli altri due casi sono state raggiunte risoluzioni laterali di 1 μm e di alcune centinaia di nanometri.

II.IV Tecniche a letto di polvere

Per il processo di Selective Laser Sintering (SLS), basato sulla fusione selettiva di polveri polimeriche per mezzo di un laser, sono state impiegate stampanti commerciali, talvolta modificate in modo da ridurre la quantità di polvere necessaria, per costruire scaffolds macroporosi con dimensioni complessive nella scala centimetrica. Gli aspetti più critici di questa tecnica sono stati l'adesione indesiderata alle pareti del componente di particelle non

fuse, la presenza di polvere intrappolata nei canali e nei macropori, la non completa fusione delle particelle di polvere e la penetrazione del laser oltre l'area di scansione. Per questi motivi, sono stati ottenuti diversi risultati nelle prove di stampa, ma in generale le risoluzioni raggiunte sono risultate medio-basse in confronto alle altre tecniche additive. Per quanto concerne il processo di Binder Jetting, in cui le polveri vengono tenute insieme tramite la deposizione di una soluzione liquida legante, sono stati usati un sistema di stampa personalizzato e una stampante commerciale per realizzare compresse e dispositivi biomedicali impiantabili entrambi progettati per consentire un rilascio graduale e controllato di farmaci. I componenti stampati hanno mostrato forme geometriche, principalmente forme molto semplici (es. cilindri), e dimensioni, dell'ordine dei millimetri, in accordo con le caratteristiche del modello digitale.

III. Considerazioni finali

Considerando i valori delle risoluzioni che si possono raggiungere processando i polimeri più comuni (Tabella 3.1), si può concludere che alcune delle risoluzioni riportate in questa tesi sono comparabili alle prestazioni dei polimeri derivati da fonti fossili. I casi a cui si fa riferimento sono: l'acido polilattico, il polietilene furanoato, i derivati della cellulosa e i poliidrossialcanoati per il processo di FDM; tutti i polimeri naturali citati per la tecnica di LDM; i (met)acrilati ricavati dall'olio dei semi di soia, dalla vanillina, dall'eugenolo, dal guaiacolo, dai derivati della cellulosa e dalla colofonia per la stereolitografia; i (met)acrilati derivati dall'olio da cucina esausto, dall'olio dei semi di soia e dall'acido polilattico per il processo di DLP; gli acrilati derivati dall'olio dei semi di soia e dalla vanillina per la tecnica di DLW.

Lo sviluppo di nuovi materiali ecosostenibili, performanti e al contempo competitivi sul mercato è fondamentale per ottenere un impiego diffuso dei materiali ricavati da fonti rinnovabili nelle tecniche additive. I risultati ottenuti finora sono sicuramente incoraggianti ma ulteriori ricerche dovranno essere condotte per ampliare la disponibilità dei materiali da biomassa e per migliorarne la qualità di stampa.

1. Introduction

Additive manufacturing (AM), also known as three-dimensional (3D) printing, is an emerging technology which is receiving great attention due to its potential for providing objects with customized design and intricate architectures without the need for molds, dies or machining. Indeed, each component can be precisely produced by a 3D printer in a layer-by-layer fashion directly from a digital model. This approach offers a high degree of automation, reproducibility, and a rapid on-demand fabrication.
A wide range of materials that have been developed for additive manufacturing and are now available on the market, includes thermoplastic and thermosetting polymers. However, almost all of the commercial polymers for 3D printing are petroleum-sourced. As a consequence of the increasing popularization of AM techniques, the growing consumption of such plastic materials has to deal with existing environmental issues regarding the availability of resources of raw materials, the disposal of massive waste, water and soil pollution, the possible toxicity of byproducts, and the deleterious influence to human health. Due to these reasons and to the decreasing reserve of fossil fuel, it became crucial to search for alternative materials in the interest of sustainability. Therefore novel biobased polymers, defined as polymers derived from biological and renewable sources like plants, algae, and microorganisms, have been developed. Some of these environmental-friendly materials have been adapted to AM processes and this thesis intends to provide a review of 3D printing techniques in terms of the main biobased polymers utilized.

The thesis consists of three parts. The first one provides a brief overview of the different polymer types which can be derived from renewable sources. In particular, a distinction between natural polymers, synthetic polymers from biomass and bacterial polymers is given. The second part presents the main AM technologies and the relative biomass-derived materials mainly studied to print polymeric constructs. Thus, the guiding line in all the sections of this chapter is the several materials. Information such as the feedstock formulation, the printing system and the geometric properties of the printed part, is also reported. Since the quality and functionality of an object are influenced by the printing resolution, particular attention is given to this parameter. Furthermore, considerations about the results of printing from biobased polymers are provided in terms of feature size achieved and reproduction fidelity of the corresponding digital models.
The third part gathers general conclusions on the quality of the printed parts and the resolutions obtained in comparison with the typical resolution values achievable with common petroleum-based polymers.

2. Polymers from biomass: an overview

Although the aim of the thesis is to present the potential of those biobased polymers that can be used specifically in additive manufacturing, a short introductory chapter, which provide an general overview about all biomass derived polymers, is inserted in order to contextualize the topic.

Generally, polymers from short-term renewable resources could be divided into three groups[1]:

- natural polymers directly derived from biomass, including those modified chemically, such as some polysaccharides, proteins, lipids, lignin, shellac and natural rubber;
- synthetic biobased polymers synthesized from monomers obtained from natural resources;
- polymers produced by microorganisms or genetically modified plants.

2.1. Natural polymers

Polymers are very common in nature and they may derive from animal resources (as gelatin, silk, shellac, chitin, chitosan and some types of cellulose) or vegetable resources, which are classified into wood, annual plants and algae [2]. Natural polymers have numerous advantages including natural abundance, relative ease of isolation, and the possibility of chemical and physical modification to meet varying technological needs. Indeed, the approach of this first class of polymers is based on the modification of natural polymers while preserving the polymer backbone mainly intact. Some of them, such as starch, cellulose and rubber are actively used in industrial productions, while others, as lignin and chitin, have no current notable commercial applications as plastic materials but research is being done on their use as fillers for rubber and thermoplastics. For example, many investigations were done on the lignin, and two scenarios are often considered; the use of lignin as a whole or the use of defragmented lignin as monomers. In both scenarii, major issues are reported such as poor performance in the first case or too costly processes in the second case.[3]

Natural polymers can be classified according to their chemical structures, as reported in Table 2.1.

Table 2.1 List of natural polymers. [4]

Polysaccharides • Plant/algal: starch, cellulose, pectin, konjac, alginate, caragreenan, gums • Animal: hyluronic acid • Fungal: pulluan, elsinan, scleroglucan • Bacterial: chitin, chitosan, levan, xanthan, polygalactosamine, curdlan, gellan, dextran
Proteins Soy, zein, wheat gluten, casein, serum, albumin, collagen/gelatine, silks, resilin, polylysine, polyamino acids, poly(γ-glutamic acid), elastin, polyarginyl–polyaspartic acid
Lipids/surfactants Acetoglycerides, waxes, surfactants, emulsan
Speciality polymers Lignin, shellac, natural rubber

Chemical characteristics of the main categories of natural polymers are described below, while some specific polymers will be mentioned in the following chapter in the 3D printing context.

2.1.1. *Carbohydrates*

Carbohydrates includes monosaccharides, disaccharides (commonly known as sugars), oligosaccharides, and polysaccharides. Polysaccharides are high molecular weight polymers composed of monosaccharides linked together through glycosidic bonds to form linear or with branched side chains structures. Polysaccharides have a general formula of $C_x(H_2O)_y$ where x is usually a large number between 200 and 2500, but considering that the repeating units are often six-carbon monosaccharides, it can also be represented as $(C_6H_{10}O_5)_n$ where n is a number between 40 and 3000. Polysaccharides exist in a variety of chemical compositions, molecular weights and structures, hence they possess various physicochemical properties which allow them to perform diverse functions such as stores of energy (e.g. starch), cell wall structural components (e.g. cellulose in plants and chitin in arthropods), protective barriers, participants in signal recognition and intracellular communication[5]. However, their structure offers available hydroxyl, carboxylic, and amine groups as source of chemical modification in order to tune the polymer physicochemical properties for specific applications.

2.1.2. *Proteins*

Proteins are linear heteropolymers made of amino acids which condense with the formation of a peptide (or amide) bond linking them. The structure, shape, and function of a polypeptide is determined by the sequence of 20 different amino acids having an amino-functional group (-NH_2) and a carboxyl group (-COOH). The chain of amino acids, due to forces such as hydrogen bonds, disulfide bridges, and ionic interactions between charged monomers, folds into a particular three-dimensional conformation that constitutes the primary level of protein structure. Moreover, hydrophobic and hydrophilic interactions cause bending, coiling, or folding into a secondary structure such as the alpha helix and beta-pleated sheet. The last two forces are also responsible for even more compact configurations, as globular proteins, giving rise to a tertiary protein structure. Lastly, a quaternary structure is formed when a protein contains more than one polypeptide chain.[6,7] The structure of a protein determines its function that can be regulatory, transport, protective, storage, contractile or structural (e.g. collagen, elastin).[8]

2.1.3. *Lipids*

Lipids are water-insoluble molecules that can be classified as fats, phospholipids, waxes, and steroids. Fatty acids (carboxylic aliphatic acids) and glycerol are lipid monomers, the carboxyl group of a fatty acid and the hydroxyl group of the alcohol monomer react via dehydration synthesis forming an ester linkage. A polymeric structure, namely triglyceride, is formed when the hydroxyl groups of glycerol join the carboxyl groups of three, usually different, fatty acids to form three ester bonds.[9] Natural waxes are formed through biochemical processes and they can have an animal or a vegetable origin. Biological wax synthesis occurs in many plants, particularly carnaúba palm, and animals such as bees. Natural waxes are seldom used industrially in their original form, they are generally modified by refining or by chemical processes. Waxes have been employed as a raw material for modeling, in the production of casting molds, as a pigment carrier, and for surface protection, while nowadays they are used mostly as additives and active substances.[10]

2.2. *Synthetic biobased polymers*

The second group of biobased polymers presented here includes polymers obtained from biobased precursors, derived from a variety of molecular biomass. Usually the approach consists of a two-step biomass conversion. The route starts from the production of bio-based precursors by means of biochemical and/or chemical transformation and ends with the polymerization of the biobased monomers. If the biobased monomers structures are already available from fossil resources, they are called "drop-in" and the final materials cannot be distinguished, neither chemically nor by performance, from their petrochemical counterparts. Polymers synthesized from biobased monomers that have new structures are called "novel" and often show an improved functionality. [11] Polyesters (such as polylactide, polybutylene succinate, polyethylene terephthalate, polyethylene furanoate, polycarbonate), polyamides, polyolefins (polyethylene, polypropylene, polybutylene, polybutadiene, polyisoprene), acrylic resins, polyurethanes, and phenolic, epoxy and alkyd resins can be obtained from renewable resources. [1,3]

2.2.1. *Polyesters*

Polyesters, polymers that contain the ester functional group, are prepared via condensation polymerization of diols with dicarboxylic acids or diesters, ring-opening polymerization of lactones, and acyclic diene metathesis (ADMET) polymerization (Fig. 2.1). [3] Due to the promise of compostability and biodegradability through hydrolysis of the ester linkage, research in the production of various fully and partly bio-based polyesters has received great attention. Long-chain aliphatic polyesters can be derived from fatty acid, naturally present in some vegetable oils, by olefin metathesis and by isomerizing alkoxycarbonylation, a reaction that enables to prepare dicarboxylic acids from the hydrocarbon chain, carbon monoxide and an alcohol. [3]

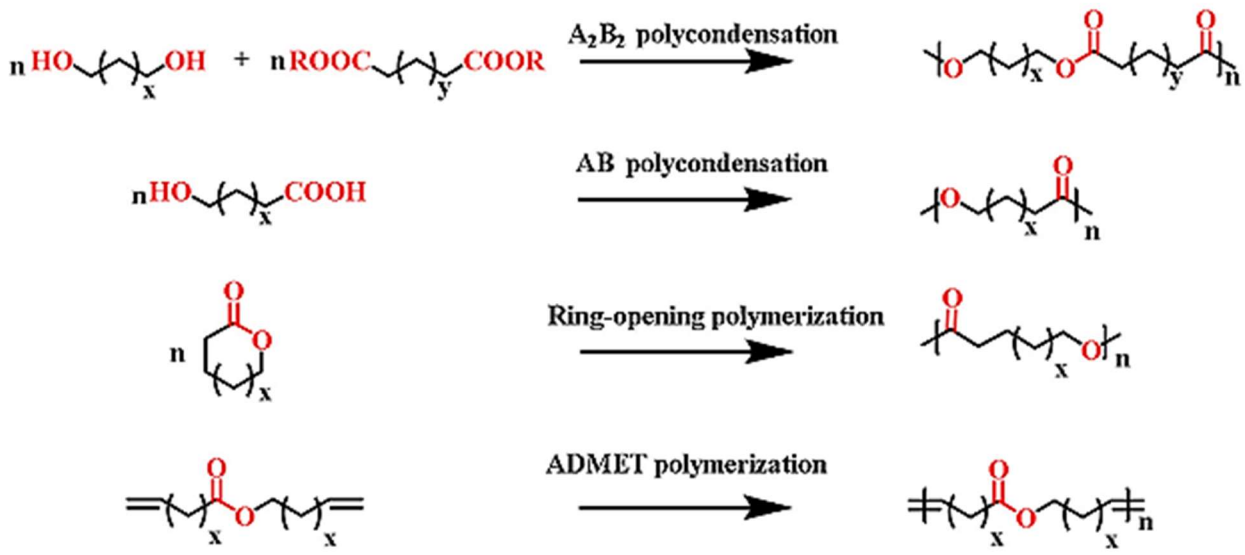

Figure 2.1 Synthesis methods of polyesters.[3]

Among "novel" biobased polyesters, the most studied are polylactic acid (PLA), synthesized through polycondensation of lactic acid obtained by fermentation of hexoses, and polybutylene succinate (PBS), produced by bacterial fermentation of organic feedstock like starch and glucose. Instead, "drop-in" monomers are ethylene glycol (EG) and terephthalic acid (TPA) whose product polycondensation is polyethylene terephthalate (PET), predominantly employed

in textiles and packaging applications. Bio-EG is obtained by oxidation of biobased ethylene or through hydrogenation of sugar pyrolysis products, and its use allows to synthesize 30% biobased PET. Fully biobased PET also requires bio-TPA whose production is not as simple. In one of the most advanced processes, bio-TPA is a result of multiple catalytical conversion steps starting from isobutanol which is produced by dehydration of sugars. Alternatively, bio-TPA can be obtained from muconic acid, limonene-derived building blocks and furan derivatives. Another "drop in" monomer is 2,5-furandicarboxylic acid (FDCA), a dicarboxylic acid produced from carbohydrates that is combined with EG for the preparation of polyethylene furanoate (PEF), a valid biobased replacement for PET.[1,11,12]

2.2.2. *Polyamides*

Polyamides, polymers with repeating units linked by amide bonds, have excellent mechanical and thermal properties but also some limitations as high-water absorption and poor low-temperature properties. However, some features like melting points and mechanical properties, can be tuned regulating the density of amide groups. Biobased polyamides are developed starting from fatty acids, carbohydrates, terpenes, and rosin acids. Terpenes are hydrocarbons with one or more carbon–carbon double bond, contained in the volatile fraction of vegetable resin; rosin acids are carboxylic acids present in the nonvolatile solid form of resin. [13] For instance, PA 11 is synthesized through pyrolysis of ricinoleic acid (castor oil derivative), PA 6 10, PA 10 10 and PA 10 12 through the polycondensation of sebacic acid (a ricinoleic acid derivative) with a diamine, PA 12 from lauric acid (obtained from palm kernel oil), and others polyamides through ring opening polymerization of lactams.[14]

2.2.3. *Polyolefins*

Polyolefins are used in a wide variety of fields due to their excellent mechanical properties, high chemical stability, and good electrical insulation. The pathways to produce bio-polyethylene are steam cracking of biomass, catalytic conversion into ethylene of bio-ethanol which is obtained by anaerobic fermentation of biomass (such as starch, sucrose, cellulose), conversion of bio-methanol and dimethyl ether into ethylene, and through plants and microorganisms metabolisms. Likewise, bio-polypropylene can be effectively produced from biomass through bio-olefin metathesis, steam and fluid-catalytic cracking of hydrocarbons, dehydration of bio-alcohols and conversion of glycerol into olefins. Other polyolefins such as polybutylene, polybutadiene, and polyisoprene can be also derived from biomass following pathways similar to the previous ones. [3,15]

2.2.4. *Polyurethanes*

Thermosetting polymers are high-performance materials due to their high cross-linking density achieved by curing at elevated temperature and/or by irradiation. Polyurethanes, polymers containing a significant number of urethane linkages (–NH-COO–), are obtained through reactions of various polyols and polyisocyanates in presence of a catalyst or by activation with ultraviolet light. Their mechanical properties can be tailored by selecting appropriate reacting components at suitable ratios, indeed polyols with long and flexible aliphatic chains confers elasticity and flexibility, while cyclic isocyanates provide mechanical strength to the resulting polyurethane. [16] Biopitches (fusible solid oligomers obtained from Eucalyptus tar fractionation after vacuum distillation), soy flours, vegetable oils (e.g. soy, lin, sunflower, canola, cor, castor, passion fruit, macauba oils), natural cork and cardanol derivatives can be some natural sources of polyols. As regards isocyanates production, the most promising feedstocks are triglycerides (e.g. soy bean oil trygliceride) and fatty acid (e.g. oleic acid). [17,18]

2.2.5. *Phenolic resins*

Phenolic resins, polymers synthesized from phenol and formaldehyde, are widely applied because of their superior performances enabled by the presence of aromatic rings in the polymer backbone which imparts rigidity, high glass-transition temperatues and good thermal stability. Bio-based phenolic resins can be produced by substitution of phenol with counterparts of bio-renewable origin. Cashew nut shell liquid, an agricultural by-product obtained from the cashew tree (Anacardium oxidentale), is one of the major resources of natural phenols. A range of phenolic resins, more flexible than the conventional ones, are produced by reactions of cardanol with formaldehyde. Owing to its abundance and similar structure with phenol, lignin is considered as a potential substitute for phenolic-based resins. However, because of steric hindrances, lignin reactivity with formaldehyde is limited therefore it has to be previously chemically modified.[18] Other bio-sources are phenolic compounds (e.g. chavicol, tyrosol, eugenol) extracted from certain plant oils, and tannin compounds, extracted from wood, bark, leaves, and galls of plants.[17]

2.2.6. *Epoxy resins*

Epoxy resins are made from resin precursors containing epoxy groups. These functional groups are treated with curing agents (e.g. amines, anhydrides, amides), sometimes in presence of catalysts. Almost 90% of all commercial epoxy resins is based on the reaction between bisphenol A (BPA) and epichlorohydrin, yielding diglycidyl ether of bisphenol A (DGEBA). To obtain bio-epoxy resins, epoxidized plant oils (e.g. epoxidized castor oil, epoxidized soybean oil, epoxidized linseed oil, epoxidized canola oil, epoxidized grapeseed oil) and fatty acids are some promising options. However, most natural vegetable oils do not contain naturally occurring epoxy groups, thus they have to be introduced on unsaturation sites via either chemical or enzymatic routes. One exception is the case of oils containing vernolic acid, for example a natural epoxidized oil that contains 60-65% of vernolic acid is available in Vernonia galamensis and other Vernonia species.[16,18] Furthermore, natural phenolic acids, such as salicylic and 4-hydroxybenzoic acids, can be used as a replacement for DGEBA in the biobased epoxy resin formulations. Other bio-renewable sources that allow the development of several aromatic epoxy resin systems are tannins, lignin, cardanol, cellulose and hemicelluloses. For instance, the reaction between tannins extracted from green tea leaves and epichlorohydrin allows the production of polyfunctional epoxy monomers, subsequently used for epoxy resins preparation.[17]

2.2.7. *Alkyd resins*

Alkyd resins are organic polyesters which can be obtained from plant oils through the monoglyceride method. The process consists firstly of oil alcoholysis to produce monoglyceride or diglyceride in the presence of an acid or base catalyst, and secondly of a polycondensation reaction between monodiglycerides and anhydrides (e.g. maleic, succinic, phthalic and glutaric anhydrides). Types and content of anhydride and the oil length determine the properties of the resultant alkyd, for instance aromatic anhydrides confer high heat and moisture resistance because of the presence of a stable benzene ring, while a higher anhydride content results in a lower drying time. The most widely used polyalcohol in alkyd resin is glycerol and the fatty acid moiety derives from fatty oils like palm, coconut, peanut, tung, sunflower, linseed, soybean, rapeseed, jatropha, and rubber seed oils. In addition to the monoglyceride method, there is the fatty acid method. This second route is performed in a single step in which the polyacid, polyol, and fatty acid are added and heated at the same time.[19,20]

2.3. Bacterial polymers

Two different macromolecular structures are synthesized by bacteria: cellulose and polyhydroxyalkanoate (PHA).

2.3.1. *Bacterial cellulose*

Bacterial cellulose is a renewable natural nanomaterial and although its chemical structure is identical to that of any other vegetable cellulose, it has unique threedimensional porous network structures. The properties associated with this original material are unique over plant cellulose, such as the absence of lignin and hemicellulose, a high degree of polymerization combined with the 60–70% of crystallinity, a very high waterholding capacity, an excellent biodegradability and biological affinity.[21]

2.3.2. *Polyhydroxyalkanoates*

PHAs are thermoplastic, amorphous or semicrystalline, polyesters produced via bacterial fermentation of renewable feedstocks or in genetically engineered plants. The polymer is in the form of granular submicron inclusions inside the microorganism, hence the fermentation process has to be followed by solvent based precipitation, mechanical disruption, and chemical and enzymatic digestion. The extraction and purification steps allow to destroy the bacterial cell and remove the protein layer on the granules. After drying, the final purified PHA is obtained. More than 150 different PHA monomers have been identified and the first discovered PHA was poly(3-hydroxybutyrate) (P3HB), that is the simplest one. Different PHAs are produced by different bacteria, thus the properties of the final polymer can be tailored by using mixed cultures and by varying the organic feedstock. Copolymers biosynthesis of 3-hydroxybutyrate with other hydroxyalkanoate comonomers is another possible strategy to adjust the performance of the final PHA. Currently, copolymers of P3HB and 3-hydroxyvalerate, copolymers of P3HB and 4-hydroxybutyrate, copolymers of P3HB and 3-hydroxyhexanoate, as well as 3-hydroxyhexanoate and 4-hydroxybutyrate, are produced.[1,11,21]

3. 3D printing of bio-based polymers

3D printing, or additive manufacturing, is a techniques for constructing three-dimensional physical structures with complex geometries through successive layer-by-layer deposition of material.

By referring to ASTM Standard F2792, the American Society for Testing and Materials (ASTM) has classified 3D printing technologies into seven specific categories, the same subdivision will be adopted in this thesis. The techniques that will be addressed are shown in the diagram below (Figure 3.1). An overview of the seven categories is presented in the Appendix A.

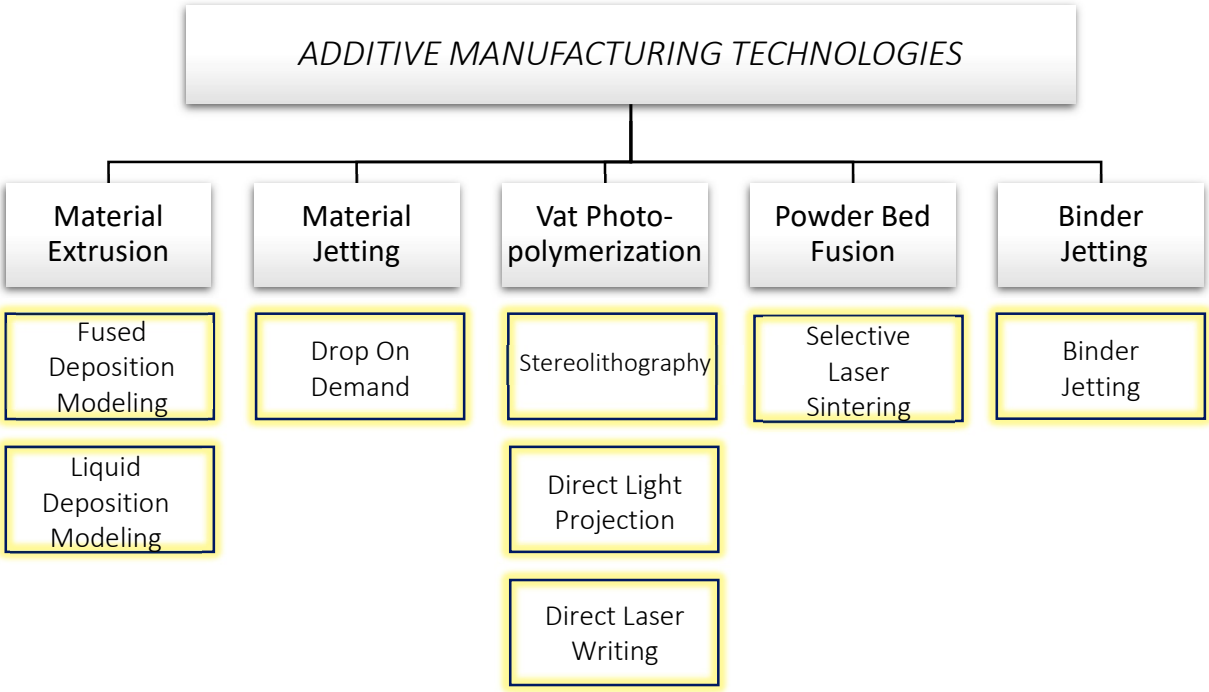

Figure 3.1 Additive manufacturing technologies classification. (Adapted from [23])

In any AM process, virtual models are first designed using a computer aided design (CAD) software. The models created are then converted into Standard Triangle Language (STL) for the contour data. The object is sliced horizontally according to the required layer thickness into many two-dimensional layers, then the slicing software uses the information of each layer to create the G-code which provides the necessary tool-path along the X, Y and Z directions for direct manufacturing. In some techniques the movement along Z axis is carried out by the platform. The layer thickness can vary according to the geometry and the capability of the machine. In general, the thinner the layer, the higher the surface finishing and better the detail reproduction. [22]

It is important to notice that 3D printing, is a relatively young technology (around 40 years old) and since the last decade, thanks to the expiration of patents, a tremendous growing had been observed. In these particular technologies, bio-based polymers are seen as interesting materials in order to replace petrochemical polymers or to develop new solutions. The attention of the

researchers and studies are mainly focused and reported for biomedical or pharmaceutical applications because of the relative biocompatibility of the bio-based polymers. That is why most of the reviewed articles in this thesis are linked to a biomedical application.

The various 3D printing processes differ in terms of cost, maximum spatial resolution, composition of the feed materials and how layers are generated.
Dimensional characteristics such as resolution (intended as the minimum obtainable feature size), dimensional accuracy (intended as the fidelity of part geometry to the virtual design) and surface roughness are functions of process and product design parameters.

In many studies, the feasibility of the printing, i.e printability, is qualitative and that is why in the following, a great attention will be given on the spatial resolution in order to have a quantitative property even if it is not relevant by itself.
Resolutions related to 3D printing of the most common polymers are reported below in order to have reference values for a comparison with those obtained with the printing of polymers derived from renewable sources (Table 3.1).

Table 3.1 Printing resolution of main AM technologies (Adapted from [24])

Technology	**Typical feature resolution (spatial resolution) [µm]**
Fused deposition modeling	100-150
Liquid deposition modeling	100-1000
Material jetting	10-30
Single-photon lithography	25-100
Multi-photon lithography	0.1-5
Selective laser sintering	50-100
Binder jetting	100

In the following chapters, materials, applications, and geometric properties (resolution included) will be detailed.

3.1. Material extrusion

The first category concerns additive deposition techniques based on material extrusion. The feedstock can be a continuous solid filament of thermoplastic polymer or a viscous liquid depending on whether the process is Fused Deposition Modeling (FDM) or, Liquid Deposition Modeling (LDM).

3.1.1. *Fused Deposition Modeling (FDM)*

3.1.1.1. FDM generalities

FDM is an extrusion method in which a filament is supplied via an electric motor-controlled pinch roller mechanism to the liquefier, an heating system where the polymer reaches the melting temperature. Other FDM techniques exist, which employ pelleets instead of filaments, but up to now are marginal. The process using a filament can be described as follow [25,26]:

- the melt is "pushed" through the liquefier towards the nozzle generating an extruded filament recognized as a "road";
- the printhead is moving along XY plane thanks to stepper motors (Fig. 3.2) in order to deposit the filament either on the platform or upon previously printed layers;
- after the completion of the layer deposition, either the platform moves down or printhead moves up along the Z axis according to one layer thickness.

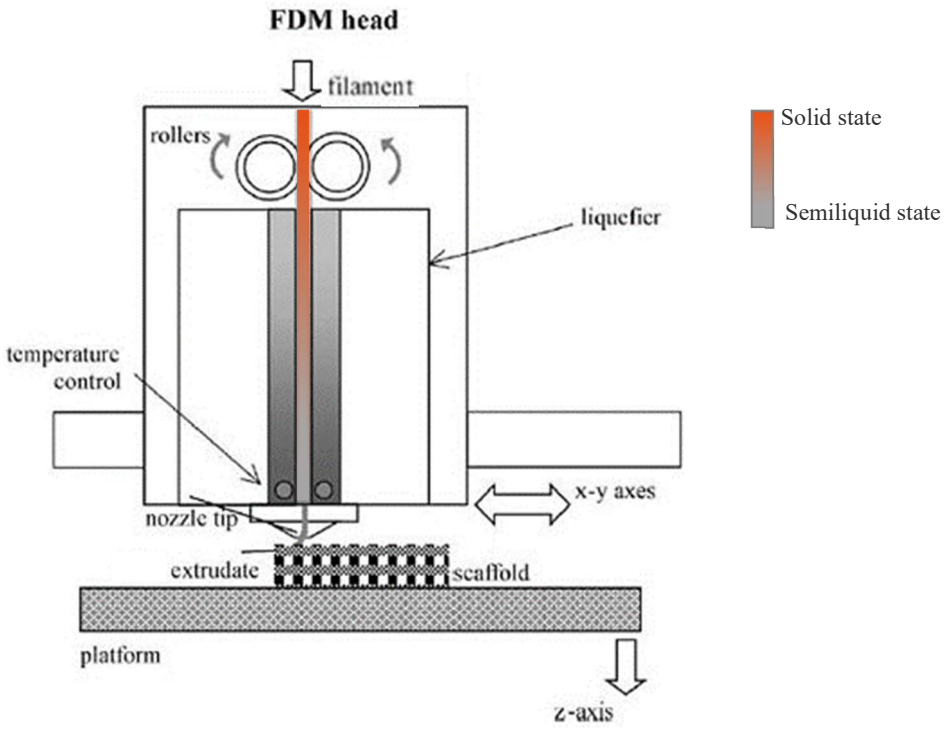

Figure. 3.2 Schematic picture of FDM process. (Adapted from [28])

The main benefits of FDM are low cost, high speed and greater simplicity. While its limits are a restricted accuracy, due to the approximation involved in surface discretization and in virtual model slicing, and poor surface quality related to filament solidification problems.[27]

Dimensional characteristics such as resolution (intended as the minimum obtainable feature size), dimensional accuracy (intended as the fidelity of part geometry to the virtual design) and surface roughness are functions of process and product design parameters.

In particular, the resolution that can be achieved is limited by width and thickness of the roads which are laid down in the XY plane and the road dimensions in turn depends on the deposition rate, the accuracy of the motors controlling print head motion, the quality of the control algorithm and the print nozzle diameter. The road width cannot be smaller than 1.2-1.5 times the size of the nozzle diameter because of die swelling phenomenon as the melt leaves the print nozzle. Smaller nozzle diameters would lead to better resolutions but the pressure required to push the melt increases as the nozzle diameter decreases and consequently, the required motor power increases as well. In addition, the compression of the feed filament between the feed rollers and the liquifier entrance, can cause the feed filament buckling above some critical applied pressure.[25] Typically, the minimum feature size obtainable with a desktop FDM printer is in the order of 100 μm in case of common polymers.[25,29]

3.1.1.2. Biobased polymers for FDM and applications

In FDM, the thermoplasticity of the polymer is an essential property because it allows the filament to fuse together during printing and to solidify at room temperature after printing.
The most common filament materials are acrylonitrile butadiene styrene, polyethylene terephthalate, other engineered thermoplastics have been introduced (polyamides, polycarbonates, high-density polyethylene, polyetheretherketone) to offer some benefits over the traditional ones.[30] However, because of environmental issues related to the massive consumption of such petrochemical polymers, focus has begun to shift to the development of sustainable thermoplastics from renewable sources.

PLA is one of the most representative polymer originating from the biomass of fermented plant materials. PLA has been widely studied for use in medical applications due to its biocompatibility and biodegradability and nowadays it is commercially available with an attractive price. Many companies provides PLA filaments suitable for their FDM machines, for example Sharebot has developed some printer models with different resolutions. In particular, Sharebot Viper and Sharebot 43 are printer models with the best resolutions, both achieve an XY resolution of 11 μm and a Z resolution of 25 μm.[31]
Miao *et al.*[32] have printed a sacrificial mold to create a biomimetic scaffold with graded porosity and a PLA filament was used. A cylindrical scaffold (Fig. 3.3a), 5 mm of diameter and 3 mm in height, with a gradient distribution of pores from the top to the bottom as the distance between pores increases from 240 to 560 μm, was printed via a Solidoodle Workbench Apprentice 3D printer. With a nozzle diameter of 250 μm, a layer thickness of 300 μm was obtained. A "square pore shaped" cylindrical scaffolds (Fig. 3.3b) composed of stacked units with a 200 μm line distance and a wall thickness of about 200 μm, were printed by Cui *et al.*[33] with a FDM printer. Moreover, a series of interconnected horizontal and vertical channels of 500 μm were present in order to mimic the microvascular network in native bone. In this case the layer thickness was 250 μm. A higher Z resolution was achieved in the printing of a surgical instrument (Fig. 3.3c) with a MakerBot Replicator 2 printer.[34] The prototype replica of a common Army/Navy retractor measured 17 cm x 1.5 cm x 4 mm and the layer was 100 μm high.

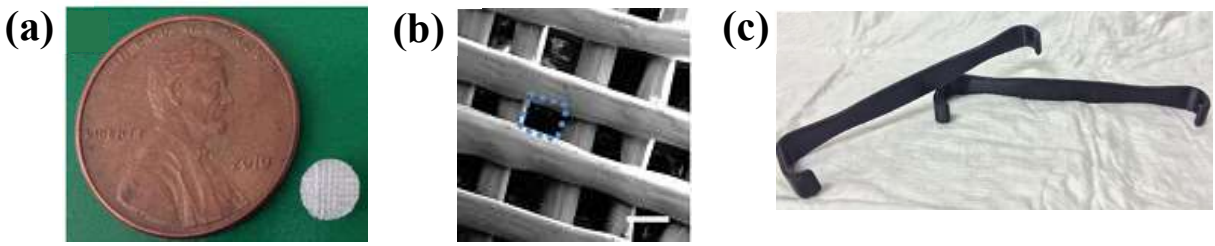

Figure 3.3 (a) PLA cylindrical scaffold compared to a cent.[32] **(b)** SEM image of porous PLA scaffold. The blue square shows 200 µm pores. [33] **(c)** Two FDM printed surgical instrument prototypes made of PLA.[34] (The scale bar indicates 200 µm.)

Another bio-based thermoplastic tested in additive manufacturing is bio-polycarbonate (bio-PC). In the study performed by Park *et al.*[35], filaments were developed starting from bio-based PC pellets (DURABIO, Mitsubishi Chemical, Japan). The as-processed filaments were the feedstock material of a customized FDM system and they were printed into specimens for tensile testing (ASTM D638 type I). The layer height was set to 200 µm. The same developed machine and the bio-PC filament feedstocks were used to realize daily life objects such as cookie cutter, spoon holder, sauce bowl, dog bowl, toy block and cell phone holder (Fig. 3.4a).

Objects with higher chemical resistance than PLA were created with cellulose-derived polyethylene-2,5-furandicarboxylate (PEF) by Kucherov *et al.* (Fig. 3.4b).[36] To evaluate its printing quality, sample objects were produced using an Ultimaker^2 machine. Performance reliability of the developed PEF polymer was confirmed by changing nozzle sizes and layer heights. The maximum resolution corresponded to a nozzle diameter of 250 µm and a layer thickness of 50 µm (Fig. 3.4c).

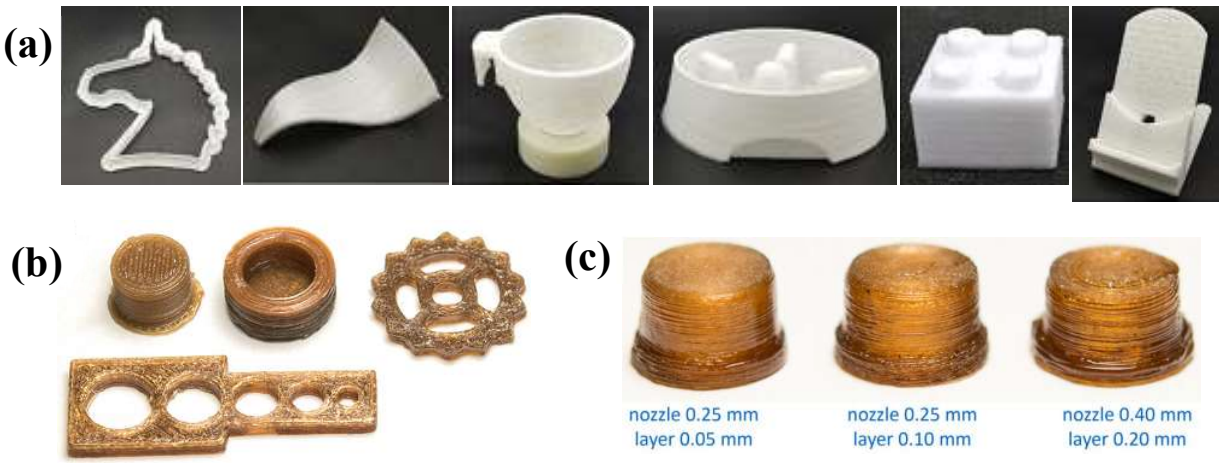

Figure 3.4 (a) Daily life objects printed with bio-PC.[35] **(b)** Objects produced from PEF.[36] **(c)** PEF-objects (7.8 mm in diameter) printed by various nozzle sizes and with different layer heights.[36]

An interesting candidate for FDM is zein, a storage protein from maize seed endosperm, used as a water barrier in food or pharmaceutic applications and for obtaining degradable plastics. In the work of Chaunier *et al.*[37] zein was purchased from Sigma-Aldrich and blended with glycerol. The plasticized zein allowed to print a “ring” geometry model of 1 cm diameter with an ORDBot-Hadron 3D printer.

FDM is a promising method for preparation of medical implants and tablets since shape adaption as well as the control of drug delivery are feasible. Such applications require biodegradable, bioabsorbable, biocompatible, and mechanically robust materials and cellulose-based polymers are potential candidates. Due to its strong hydrogen bonds, pure cellulose does not go through a fluid phase before degradation, thus a chemical modification is required. Examples of cellulose derivatives used as biofeedstock in FDM, are cellulose ethers and cellulose esters. The latters can be obained by substituting hydroxyl groups of cellulose by acetate groups, while the formers can be divided into carboxymethyl cellulose, methylcellulose, ethylcellulose, hydroxyethyl cellulose, hydroxypropyl cellulose, hydroxypropyl methylcellulose and hydroxypropyl methylcellulose acetate succinate according to the functional groups that substitute the hydroxyl groups of cellulose.[38]
In the study of Kempin *et al*.[39], drug loaded implants as hollow cylinders were produced from ethylcellulose filament loaded with quinine and triacetin in order to investigate the drug release (Fig. 3.5a). The filaments production consisted in two steps, firstly drug loaded polymer films were prepared by a solvent casting technique and secondly, after cutting the film into small pieces, tha filaments extrusion with a self-constructed extruder was carried out. Then a standard FDM printer Multirap M420 (Multec GmbH) was used and a layer thickness of 100 µm was set, resulting in a final implant of 3 mm for 30 layers.
Melocchi *et al*.[40] manufactured capsular devices for oral pulsatile release starting from hydroxypropyl cellulose filament (Fig. 3.5b). The polymer filament needed to be of pharmaceutical grade, hence it was in-house produced because commercially not available. While a commercial MakerBot Replicator 2 printer was used to built cap and body parts through deposition of layers at first with a nominal thickness of 400 µm. The assembled capsule shell had a nominal thickness of 600 µm, while the overlapping portions of the body and cap were only 300 µm thick. The wall thickness and the locking mechanism were the most challenging details of the hollow structure and some changes to the 3D printer software were requested to improve the resolution and obtain the desired thickness values. The same MakerBot Replicator 2 printer was used in two other works. In the first one[41], a disk (30 mm in diameter, 600 µm in height) of pure hydroxypropyl cellulose was built through a deposition of layers 300 µm high. The study demonstrated that such material is suitable for fabrication of capsule shells and coatings for either immediate or modified release. In the second one [42], cylindrical printlets (i.e. tablets made by 3D printing) loaded with paracetamol were printed from three different grades of hydroxypropyl methylcellulose acetate succinate (Fig. 3.5c). In this study, the layer height was set to 100 µm which is the minimum value of the last three examples having in common the same FDM printer.

Figure 3.5 (a) Hollow cylindrical implant of ethylcellulose in side view (outer diameter of 5 mm, inner diameter of 3 mm).[39] **(b)** Capsular device made of hydroxypropyl cellulose (diameter of 7 mm, height of 13 mm).[40] **(c)** Printlets (10 mm in diameter, 3.6 mm in height) incorporating 5% paracetamol: increasing hydroxypropyl methylcellulose acetate succinate grade from left.[42]

The use of ethylcellulose, hydroxypropyl cellulose and hydroxypropyl methylcellulose to prepare drug loaded filaments suitable for FDM printing, was investigated by Zhang *et al*.[43] Controlled-release tablets were fabricated with in-house extruded filaments using a commercial

Prusa i3 3D desktop printer. The tablet dimensions were 10 mm in diameter and 4.5 mm in thickness, while the Z resolution was set to 100 µm. Ten batches of each filament type were tested and those that could be printed without break or squeeze aside more than six times, were defined adequate for 3D printing. Ethylcellulose and hydroxypropyl methylcellulose passed the printing test, while hydroxypropyl cellulose filaments were too soft and flexible to be fed into the printer. In order to improve the mechanical properties of these filaments based on single-polymer formulations, binary combinations of polymer blending ratio were tested.
In another work,[44] ethylcellulose were also blended with sodium alginate, xanthan gum, as well as hydroxypropyl methylcellulose, for 3D printing of tablets with different fill patterns (Fig. 3.6a). A desktop JGAURORA A3 printer was used with different settings. The layer height was increased from 100 to 300 µm reducing the number of deposited layers from 68 to 23. Tablets with thinner layer had better print precision and appearance, but longer print time.
Also cellulose acetate blended with corn starch has a good innovative potential to manufacture medical devices. Paggi *et al*.[45] used the blend in the form of granules to fabricate filaments by a laboratory-scale extruder. The filaments fed an Ultimaker 2+ printer and through a deposition of layers 150 µm high, test specimens were obtained under different process conditions.
Another bio-based polymeric blend developed for FDM process by Xu *et al*.[46] is based on PLA and galactoglucomannane, a common derivative of hemicellulose, which was isolated from Norway spruce wood. Scaffold prototypes were built with Me3D desktop printer and each layer was 200 µm high (Fig. 3.6b).

Figure 3.6 (a) Printed tablets of ethylcellulose and hydroxypropyl methylcellulose blend (12.0 mm diameter, 7.0 mm height, 200 µm layer height).[44] **(b)** Printed scaffold (20 mm x 20 mm x 2 mm) and top view SEM image, referred to blend ratio of 20:80 in weight of galactoglucomannane and PLA.[46]

Another study[47] reported the production of microcrystalline cellulose reinforced PLA with different concentrations. The filaments containing 1 and 3 wt% cellulose, were used by an AutoMaker Robox 3D printer to realize biomedical scaffold prototype with a diameter of 15 mm and height of 1 mm.
Filgueira *et al.* produced two fully biobased polymer filaments reinforced with thermomechanical pulp (TMP) fibers. TMP fibers are a relatively cheap raw material and have a high aspect ratio allowing to manufacture biocomposites with good mechanical properties. However, hydrophylic fibers and hydrophobic matrices are chemically incompatible, thus physical or chemical modifications of lignocellulosic fibers are necessary to improve interfacial adhesion.[48] The first developed biocomposite filament had PLA as matrix and modified spruce TMP fibers as reinforcing material.[48] The reinforced filament was used to print model figures (Fig. 3.7a) and dog bone specimens with length of 80 mm, width and height of 3 mm, on a Ultimaker Original 3D printer. The second biocomposite filament was made from bio-PE and modified spruce TMP fibers.[49] Square objects and circular figures were printed by the same FDM machine used in the first study (Fig. 3.7b).

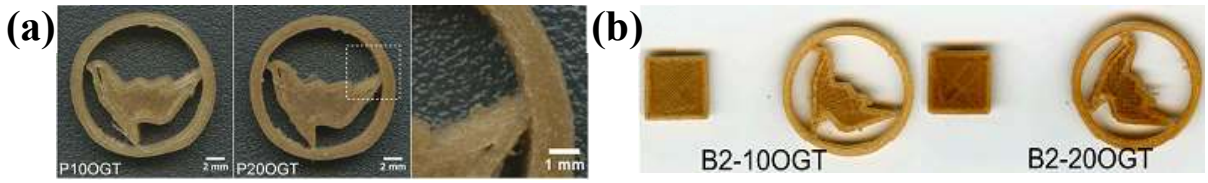

Fig. 3.7 (a) Model figure (15 mm in diameter) of PLA reinforced with 10% and 20% modified TMP fibers. The right image shows the local area marked with dashed rectangles.[48] **(b)** Model figure of bio-PE reinforced with 10% and 20% modified TMP fibers. The squares are 10 mm × 10 mm and the circles are 20 mm in diameter.[49]

Polyhydroxyalkanoate (PHA) filaments can be used to print medical devices by FDM process. Wu *et al*.[50] evaluated the mechanical properties of a composite material made from maleic anhydride-grafted PHA and coupling agent-treated palm fibers. The treatments ensured a better adhesion at polymer-filler interface resulting in higher Young's modulus and tensile strength at break compared with the untreated composite PHA/palm fibers. In the study, the filament printability has not been investigated in detail. However, it was possible to realize some specimens with a Flashforge (L2D Desktop Factory) printer through a deposition of 50 µm thick layers.

3.1.2. *Liquid Deposition Modeling (LDM)*

3.1.2.1. LDM generalities

LDM is also known as Direct Ink Writing or robocasting[23,51]. In this technique, solutions, gels or pastes are used as inks for the system, hence there is no need to increase the temperature during the extrusion process. A computer-controlled three-axis translation stage precisely moves a syringe-like reservoir where the viscous ink is stored. The reservoir is connected to a dispensing nozzle which deposites continuos beads of material, onto a platform or on the previous layer, with a print resolution of 5 µm to millimeters wide. The most common methods to extrude the material are pneumatic or mechanical systems. Pneumatical dispensing printers have simpler drive-mechanism components and their force is limited only by the air-pressure capabilities of the system, but they are less efficient in the direct control over the material flow because of the compressed gas volume delay. Mechanical dispensing printers have smaller and more complex components, a greater spatial control but often reduced force capabilities. Mechanically driven printers can be based on a screw system or on a piston mechanism (Fig. 3.8). [52]

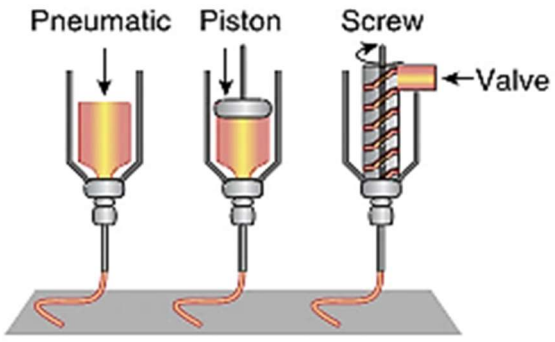

Figure 3.8 Types of LDM dispensing system.[52]

The correct ink preparation is an essential aspect to achieve a good printability. The ink formulation must meet certain requirements [51]:

- low resistance flow through tiny nozzles to facilitate printing and avoid clogging;
- shear thinning properties in order to decrease in viscosity as the shear rate increases in the nozzle and sharply increase in viscosity as the shear rate decreases at the nozzle exit;
- high viscosity at zero shear and enough stiffness to steadily retain the filamentary shape after extrusion;
- high yield stress and rapid elastic recovery to prevent the collapse of the wet printed part;
- easy polymerization by rapid cross-linking methods such as ionic, thermal and UV-induced curing if viscoelastic properties cannot support the 3D printed structures;
- sufficient solid content after drying to avoid large deformations.

3.1.2.2. Biobased polymers for LDM and applications

Direct-writing inks are either gels or polymer solutions in a low boiling organic solvent (such as dichloromethane, tetrahydrofuran or dimethyl sulfoxide) that rapidly evaporates upon extrusion.[53] Another strategy to maintain the printed structures stable, is the extrinsic increase of elastic moduli through cross-linking or providing a physical support. The latter concerns the gel-in-gel 3D printing, also known as 3D plotting [53], that is based on extruding a viscous liquid from a pressurized syringe into a supporting liquid or gel. The supporting liquid can be a thermo-responsive matrix, a medium containing crosslinking agents, or a cooler medium that induces a rapid solidification of the extrudate.[54,55]

Mainly natural polymers are employed in LDM techinque, especially polysaccharides and proteins. Among polysaccharides, cellulose solution or suspension is a suitable candidate because of its shear thinning behavior and a sufficient zero shear viscosity.[56]
An interesting category of cellulose derivatives is nanocellulose, which includes cellulose nanofibrils (CNF) and cellulose nanocrystals (CNC).[38] In a static state, the hydrogen bondings between individual fibers form a hydrogel network, while under the application of a shear force, the entangled fibers break up and align to the printing direction, resulting in a decrease of viscosity. Once the shear is removed, the hydrogen bondings between nanocellulose fibers are recovered.[56]
Cao *et al.*[57] fabricated electrodes for lithium metal batteries using a CNF ink with a concentration of 8.3 wt%. In particular, a two-step approach was adopted to prepare the Li anode. Firstly, a porous scaffold of CNF was printed and secondly, molten Li was infused into the freeze-dryed and subsequently carbonized scaffold. A benchtop robot (Fisnar F4200n) with three-axis micro-positioning stage, was used to print anode scaffolds through a deposition of 6 to 24 layers, each 200 μm thick (Fig. 3.9a). The ink viscosity ranged from 10^2 to 10^3 Pa·s at the shear rate of 1 s^{-1} and the minimum viscosity required to hold structure stable during printing was 400 Pa·s.
In the study conducted by Rees *et al.*[58], cellulose nanofibrils were pretreated with a combination of carboxymethylation and periodate oxidation. The printability of an ink containing 3.9% of the modified nanocellulose was assessed by manufacturing a grid construct and a scaffold (25 mm in diameter and 6 mm in height) composed of nine layers. Good results were achieved with a commercially available 3D Bioplotter EnvisionTEC GmbH. The grid showed a solid structure with well defined tracks and the scaffold was self-standing during deposition and after freeze-drying.

With CNC inks, higher solid loadings may be achieved at a given viscosity and storage modulus.[59] Viscoelastic aqueous inks with 20 wt% of CNC were prepared by Siqueira *et al.*[59] to print 3D cellular architectures. Also this ink formulation had a viscosity of about 10^3 Pa·s at the shear rate of 1 s^{-1}. Each layer of the printed structures was composed of filamentary features with a diameter of 410 µm, arrayed with a center-to-center spacing varying from 1 mm to 320 µm resulting in a grid (Fig. 3.9b) or in a block (Fig 3.9c), respectively. Such feature dimensions were obtained with a pneumatically driven ABL 900010 Aerotech printer.
In another study[60], 3D printing of CNC inks with different concentrations up to 30 wt%, was reported. It has been shown that the print quality was improved as the CNC weight percent and, consequently the viscosity, increased. To further improve the printing quality, nozzle tips of various sizes were tested in the printing of bowl structures and the best printing resolution was achieved with the smaller tip size (200 µm) (Fig. 3.9d). Moreover, to demonstrate the possibility of obtaining well controlled shapes, 20 wt% CNC ink was printed into various structures, such as octet cube, pyramid, hexagonally twisting vase, nose model, ear model and honeycomb (Fig. 3.9e).

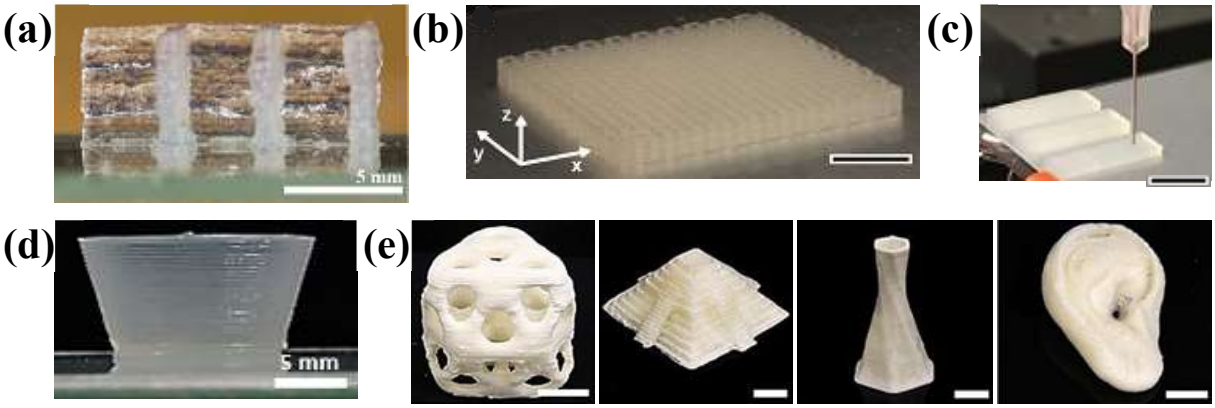

Figure 3.9 (a) Electrode scaffold printed with CNF ink.[57] **(b)** Grids and **(c)** blocks composed of eight layers made from CNC ink (scale bars: 10 mm). [59] **(d)** Bowl structure from 20 wt% CNC ink and 200 µm nozzle tip size.[60] **(e)** Freeze-dried structures printed from 20 wt% CNC ink and 500 µm nozzle tip (scale bars: 1cm).[60]

Another category used in LDM are cellulose esters. For instance, Khaled *et al.*[61] printed cellulose acetate into the so called "polypill", a personalised tablet containing separate compartments each loaded with a specific drug. This strategy ensured that the active ingredients were separated avoiding incompatibility issues, and dissolved at different release rates. The cellulose acetate, mixed with D-mannitol and a plasticizer, was first extruded to form the tablet shell, then a hydroxypropyl methylcellulose matrix loaded with the active drugs was extruded into the segmented compartments, and finally sodium starch glycolate, mixed with other excipients, was deposited directly on the top to cover the sustained release compartments. All the pastes were loaded into separate ink cartridges and extruded through a 500 µm print tip mounted on a RegenHU 3D printer. The dimensions of the polypill were 5.85 mm in height and 12 mm in diameter, and a series of raised dots were printed onto the top of the tablet to facilitate the formulation identification both visually and by touch.
Slightly larger objects from cellulose acetate were realized by Pattinson *et al.*[62] Three separate pieces that can be assembled in a miniature eyeglass frame, and a small rose were printed with a modified desktop Printrbot Simple Metal printer. The standard filament extruder of the machine was replaced by a capillary nozzle connected to a fluid dispenser where the cellulose acetate solution was stored. The cm sized products had a minimum feature size of 200 µm and a nominal layer thickness of 180 µm. To demonstrate the promising possibility of printing

customized medical instruments with tailored biochemical functionality, antimicrobial forceps with custom circular grippers were also realized using the cellulose acetate ink.
The relatively linear structure of cellulose acetate leads to the production of rigid structures. Instead, flexible and amorphous solid structures can be obtained with acetoxypropyl cellulose which has a more branched molecular structure.[63] This cellulose derivative is synthetized from hydroxypropyl cellulose by acetylation as reported by Tenhunen *et al*.[63] In their work, the printing of both cellulose derivatives on cotton and viscose fabrics was studied. To evaluate the adhesion of the structures, test strips were printed with a commercial 3Dn-300 nScrypt printer on cellulosic textiles. Moreover, an in-house built printer was used for prototyping purposes. Refractive, thermoresponsive, rigid structuring and flexible structuring prototypes were developed to demonstrate that different functionalities can be embedded into cellulosic textiles without external glues or labour intensive processing (Fig. 3.10a,b). Ionic liquid dissolved cellulose was also prepared for decorative prototypes and to experiment visual effects such as the smocking of the fabric (Fig. 3.10c).

Figure 3.10 (a) Refractive structures from an ink based on cellulose acetate. **(b)** Thermoresponsive structures from an ink based on acetoxypropyl celullose. **(c)** Structures printed using cellulose dissolved in ionic liquid for smocking effect. **[63]**

Although hemicellulose is the second most abundant polysaccharide in nature following cellulose, limited attention has been given to this biopolymer.[64] For the first time, Bahçegül *et al*.[64] 3D printed hemicellulose without any chemical modifications or blending with other polymers. Pastes with five different water contents, with and without NaOH addition, were tested. All the formulations demonstrated a shear thinning behaviour and the viscosity was extremely responsive to even very small variation of water content. The presence of NaOH in the pastes reduced the viscosity and made viscosity less responsive to changes in water content. The temperature and the amount of flowing material were other parameters to take into account for a continuos deposition process. A successful printing process was achieved in a very narrow window considering all these parameters. Three-layered grids, a flower-shaped model, a hollow cube and a scaffold prototype were manufactured with a custom-made printer capable of printing high viscosity pastes (Fig. 3.11). The minimum average line thickness achieved in the grid printing was 740 µm, while for the cube, the flower and the scaffold, the layer thicknesses were about 700 µm, 680 µm and 530 µm, respectively. However, higher resolutions could be achieved using smaller tips.

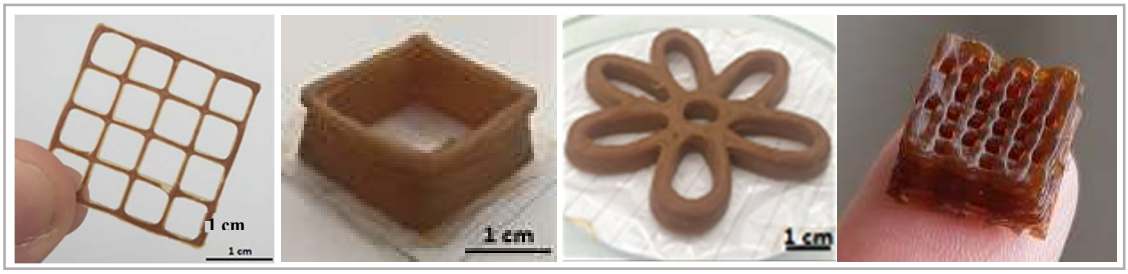

Fig. 3.11 From left: a three-layered grid, a hollow cube (2 cm x 2 cm x 1 cm), a flower model and a scaffold prototype (10.5 mm x 10.5 mm x 5.3 mm) made of hemicellulose.**[64]**

In addition to lignocellulosic derivatives, other polysaccharides from vegetable sources, such as agar and alginate, have been studied for 3D printing. For instance, Landers et al.[65] fabricated macroporous scaffolds for application in tissue engineering through plotting of thermoreversible alginate hydrogel in a liquid medium. The plotting material was an aqueous alginate solution with low viscosity, while the medium was a gelatin hydrogel which avoided the 3D architecture collapse due to the compensation of gravity forces by means of buoyancy forces. The polymer solution was plotted in the liquid medium at a temperature higher than the liquid medium whose temperature was below the gelation temperature of alginate. Thus the plotting material solidified immediately when extruded into the cold medium. The plotter was based on a CNC-milling machine (Diadrive 2000 from Mutronic Feingeratebau GmbH); the milling head was replaced by a metal cartridge adapted for the dispensing nozzle and a thermostat was used to heat the cartridge. The system plotted a cubic scaffold with an edge length of 1 cm through a deposition of layers 300 µm high. Each layer was composed of parallel strands of 500 µm in diameter and the distance between them was again 500 µm.
Alginate, one of the most commonly used biopolymers for biofabrication, was evaluated by Schutz *et al.*[66] for 3D plotting. A low concentrated alginate sol was loaded into the BioScaffolder 2.1 GeSiM machine and a four layered scaffold was printed using air as plotting medium. However, pure alginate sol exhibited a poor printability because of the inaccurate geometry of the construct. In order to enhance the sol viscosity, different amounts of methylcellulose was added to the 3 wt% alginate sol. The resulting sol had a viscosity of 750 Pa·s at a shear rate of 1 s^{-1}, while the viscosity of the pure 3 wt% alginate sol was 0.77 Pa·s at the same shear rate. The strong enhancement of viscosity improved printability and allowed a precise strand deposition. Scaffolds with various numbers of layers (4, 20, 28, 50), edge lenghts (6, 15, 20 mm) and strand distances (2.5, 2, 1.87, 1.5, 1, 0.75 mm) were successfully built (Fig. 3.12a). At a distance of 750 µm or below, the strands fused togheter and a construct without macropores was obtained.
As regards polysaccharides from non-vegetable sources, hyaluronic acid and chitosan have been considered as potential biopolymer feedstocks for 3D printing. Modification of hydroxyl groups with methacrylate groups, allows hyaluronic acid to be polymerized upon UV exposure in presence of a photoinitiator.[67] Methacrylated hyaluronic acid hydrogel was used by Poldervaart *et al.*[67] to print photo-crosslinkable scaffolds for bone tissue engineering. A porous scaffold measuring 20 x 20 x 3 mm^3 and a non-porous human vertebrae scaffold measuring 20 x 25 x 1 mm^3 were produced through a deposition of strands 200 µm thick using the Bioscaffolder SYSENG dispensing system (Fig. 3.12b). A strand distance of 200 µm led to the non-porous structure, while the porous scaffold was obtained with a strand distance of 1 mm. After printing, the scaffolds were UV irradiated to increase elastic modulus and fixate their shape.

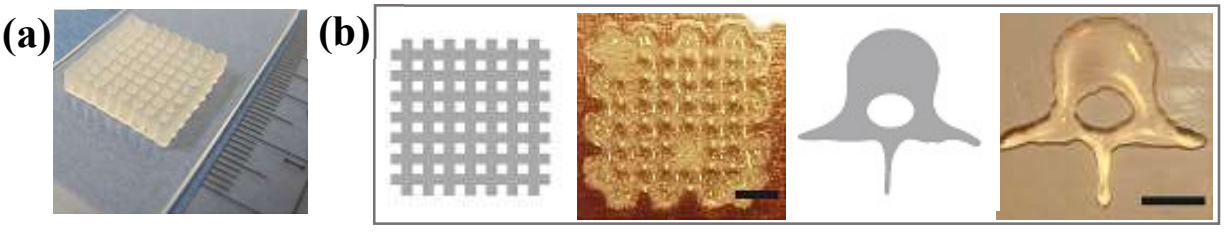

Figure 3.12 (a) Scaffold of alginate mixed with methylcellulose (20 layers).[66] **(b)** Structure design and relative printed part of a cubic scaffold and a vertebrae shaped scaffold. The polymer used is methacrylated hyaluronic acid. (Scale bars: 500 µm) [67]

A different printing approach was adopted by Elviri *et al.*[68] for the preparation of chitosan scaffolds. A low temperature manufacturing (LTM) system was developed at a laboratory scale: a commercial FDM printer was modified by implementing a new deposition system based on a syringe pump and replacing the platform with a cooling plate. In this way, the extruded chitosan solution immediately froze once in contact with the substrate allowing the proper mechanical characteristics of the structure. After printing, the frozen scaffold was immersed in an aqueous KOH solution in order to gel it. Through a deposition of strands of 250 μm in diameter, scaffolds of different thickness and with a mesh structure having a 400 μm nominal opening, were accurately reproduced.

Proteins have been studied especially as tissue engineering scaffold material, but other applications have also been proposed. An example of common ink for biomedical applications evaluated by Rhee *et al.*[69] for tissue printing, is collagen hydrogel. Collagen constructs, such as a sheep meniscus and half-cylinders, were printed using a modified commercial Fab@Home (Seraph Robotics) 3D printer and collagen hydrogels with different concentrations. Modifications were made adding a heatable ceramic baseplate, an infrared heat lamp and a cooling system aroung the deposition tool, in order to enable a heated printing setup. The results data showed that the collagen parts fabricated at higher temperature had a greate geometric fidelity, while without the addition of heat to polymerize the construct, the parts collapsed under the weight of upper layers. As concerns the hydrogel densities, with too low collagen concentrations the material spread over the substrate prior to gelation, while at the highest concentration the gel polymerized in the deposition tool.
Another biopolymer widely used in biomedical field is gelatin due to the low production costs and its excellent biocompatibility.[70] In the work of Billiet *et al.*[70] bovine gelatin was reacted with methacrylic anhydride in order to obtain a photosensitive polymer. A liquid solution of gelatin methacrylamide mixed with a photo-initiator was loaded in an adapted Envisiontec GmbH Bioplotter dispensing system. The Bioplotter device adaptations enabled a homogeneous heating of the dispensing syringe and a cooling of the platform to temperatures below the gelling point. Solutions with a low gelatin concentration led to a collapse of subsequent strands caused by insufficiently fast physical gelation. On the contrary, higher concentrations allowed well-defined porous scaffolds to be printed. Constructs of 13 x 13 mm and 1-3 mm high, were created through a regular deposition of strands 350 and 500 μm spaced, and 150-200 μm thick. The final step was the photo-initiated crosslinking under UV irradiation.
Park *et al.*[71] evaluated printability of a new ink based on aneroin, a sea anemone-derived silk-like protein. In order to enhance viscosity and shear-thinning property, 2 wt% of hyaluronic acid was added to the aneroin solution. Thus, the final ink had approximately 26 Pa·s of viscosity at a shear rate of 1 s^{-1} and a higher print resolution was achieved. By controlling the printing parameters, such as pneumatic pressure, printing speed, and nozzle size, a minimum strand width of 100-270 μm was obtainable. Using a custom-made printing system, rectangular parallelepiped lattices (20 x 5 x 0.5 mm^3) with strands of 400 μm, human ear model (35 x 50 x 18 mm^3), vascular graft, and nose model were successfully fabricated and subsequently photo-crosslinked (Fig. 3.13a,b).
Regarding non-tissue engineering applications, silk fibroin and milk protein have been investigated for LDM. An aqueous silk fibroin solution was printed by Parker *et al.*[72] into straight and wavy optical waveguides. The ink was extruded into filamentary shapes from ABL9000 Aerotech printer and directly deposited in a methanol-rich reservoir where coagulation occurred. The dimensions of the waveguide cross-section were approximately 5 x 5 μm and neither defects nor porosity were present, enabling a proper light propagation.

The printing performance of milk protein blended with whey protein, a byproduct of cheese production, was evaluated by Liu *et al.*[73]. The study aimed establish a high protein food simulant for 3D printing. Printing tests were made with a SHINNOVE-S2 (SHIYIN Technologies Co. Ltd.) machine through a deposition of layers 750 µm high, and the printed models were a Chinese character (春, 38 mm × 38 mm × 4.75 mm), a cylinder (16 mm × 16 mm × 20 mm) and other objects (Fig. 3.13c). The successful results demonstrated that 3D printing can also lead to the production of food products with customized designs and personalized nutrition values.

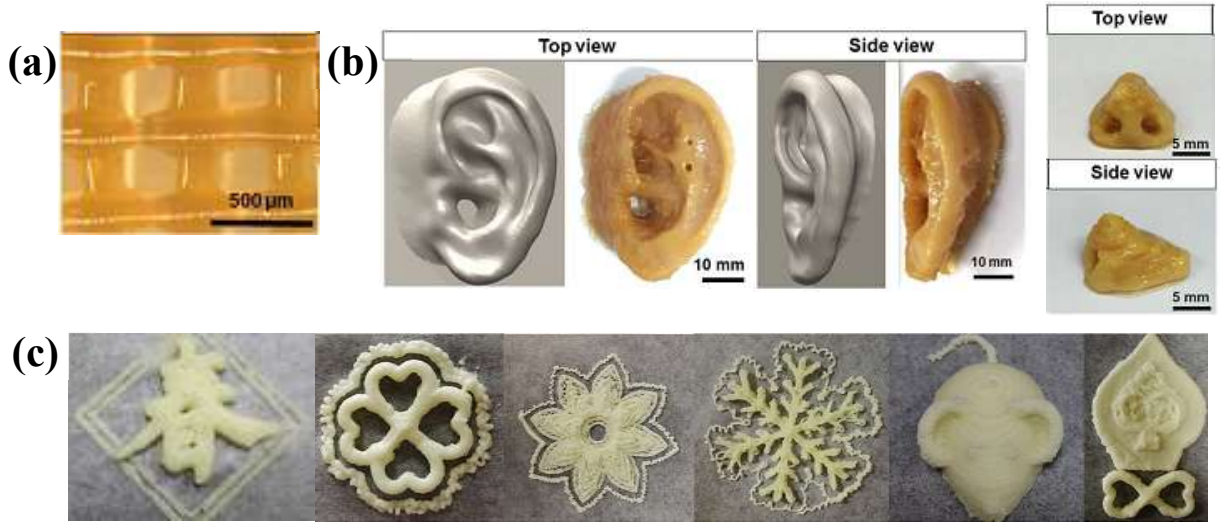

Fig. 3.13 (a) Top view of two-layer rectangular scaffold made from aneroin ink.[71] **(b)** CAD image of a human ear and printed part (left), nose model (right); both made from aneroin ink .[71] **(c)** Printed objects made from milk protein-whey protein blend.[73]

3.2. Material jetting

Material jetting techniques are divided in three groups based on the droplet generation mechanism. In the first one, namely continuous inkjet (CIJ) printing, a continuous stream of droplets is involved, in the second one, known as drop-on-demand (DOD) printing, droplets are expelled only when necessary, and in the last one, electrohydrodynamic (EHD) printing, droplets are ejected through high-ranges of electric voltage.[74] Papers present in literature report mainly DOD printing as material jetting technique for biopolymer processing, indeed DOD printers are more used for research purposes[75] because more economical, handy to control and easy to pattern biologics without contamination[74]. For this reason, the following examples of biopolymer jetting are focused on DOD printing.

3.2.1. *Drop On Demand (DOD)*

3.2.1.1. DOD generalities

DOD printing enables deposition of individual droplets of ink from a nozzle to a printing surface placed on an electronically controlled elevator stage. DOD printers consist of a single or multiple printheads each of which contains a fluid chamber and a single or multiple nozzles.[74] The deposition rate is high (up to 10 000 drops per second) and can be controlled electronically, as for droplet size.[52] The liquid volume of each drop ranges from 1 to 100 picoliters and the drop diameter is in the range of 25 to 50 µm. The small and controllable

droplet volume, together with a placement with positional accuracy of about 10 μm in XY plane, allow a deposition with high resolution and precision.[53]

The liquid is ejected by means of a thermal or a piezoelectric or an electrostatic actuator (Fig. 3.14).[74] The latter method relies on deflection of a pressure plate to generate droplets. When a voltage pulse is applied between the plate and an electrode, the plate deflects and when the voltage pulse is removed, the plate regains its original shape resulting in a brief increase in volume of the fluid chamber that subsequently ejects droplets.[74] Piezoelectric printers use piezoelectric materials which, under an applied voltage, change rapidly in shape deforming the fluid chamber and generating the pressure needed to dispense droplets at regular intervals. This type of inkject printers are capable to control a uniform droplet size and ejection directionality. Such advantages are not obtainable with thermal inkjet printers.[52] In thermal inkjet heads, as a result of short and localized heating, the ink vaporizes inducing bubble expansion that pus hes the liquid through the printhead.[75] The dispensed drop is solidified by solvent evaporation and then, the material can be polymerized by cross-linking methods such as UV light, chemical, and ionic cross-linking.[51,75]

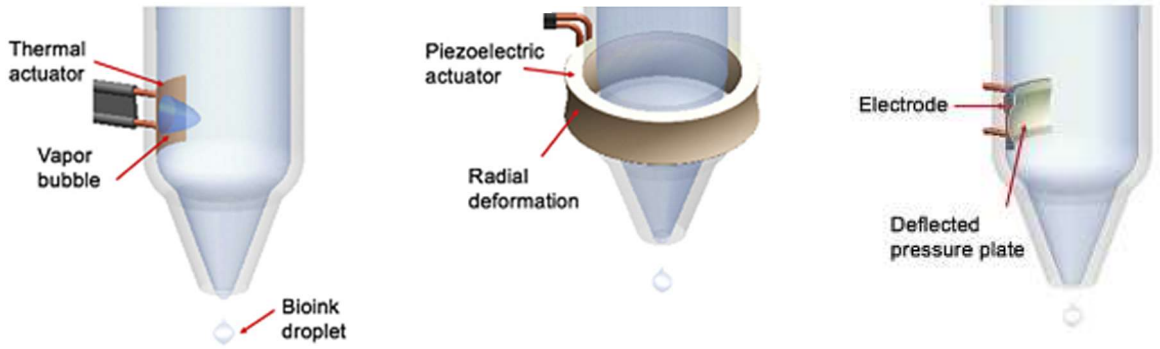

Figure 3.14 Types of DOD dispensing system.[74]

The success of the printing process depends on two important ink properties: viscosity and surface tension. The surface tension determines the shape of the drop both at the nozzle exit and on the substrate, while the proper value of ink viscosity, usually below 10 mPa·s at shear rates between 10^5 and 10^6 s^{-1}, allows to avoid excessive pressure required to eject the liquid. Furthermore, resolution and accuracy of the printed part depend on the interaction between adjacent drops and the wettability of the substrate.[53]

3.2.1.2. Biobased polymers for DOD and applications

DOD printing has been mainly used for tissue engineering (e.g. bioadhesives, scaffolds) and pharmaceutical applications (e.g. drug delivery systems).[53] Both polysaccharides and proteins have been employed for these purposes.

Cell supporting structures were fabricated by Nishiyama *et al.*[76] using alginate gel and a custom-made printer. The printing system had an EPSON SEA-Jet™ (Seiko Epson Corp.) inkjet nozzle head equipped with twelve channels, but only a single kind of ink was possible to print because the inlets of all channels were connected to the same tank of material. The tank was loaded with sodium alginate solution as the precursor of the gel, and calcium chloride was used as the substrate for gelation. To improve substrate viscosity, polyvinyl alcohol (PVA) was added to calcium chloride, alternatively hyaluronic acid could be used as viscosity enhancer. When the solution was ejected from the nozzle, sodium alginate droplets gelated by the contact

with the substrate surface and an alginate gel was obtained. At the end of the printing process, the object was extracted from the calcium chloride solution. Gel beads were the minimum unit of printed structure and they had the same dimension as the droplets supplied, which were sized at 8-160 pl in volume. The beads were approximately 10-60 µm in diameter and the positioning resolution was 0.2 µm, thus a high print resolution was achieved. 3D gel tubes were fabricated by repeatedly drawing circular patterns at the same position on the substrate surface (Fig. 3.15a).

A protein based ink and a slightly modified commercial DOD printer, were used by Roth *et al.*[77] to create patterns for cell culture studies. In detail, two solutions of both rat-tail and calf-skin collagen were prepared and maintained at 4°C, above which the gelling occurs, until printing. Each solution was ejected from a modified Canon Bubble Jet (BJC-2100) onto a substrate to form patterns such as lines, rings, circles and dot arrays (Fig. 3.15b). In this case, the droplet size was approximately 10-20 pl in volume and, according to the printer specifications, the lateral resolution was 100 µm. However, the reported resolution value is probably valid only if paper is used as substrate and a standard ink is used as printing material. Since the substrate was a microscope cover slip, the maximum resolution was compromised by the different surface properties of the glass cover slip. For this reason, a resolution in the range of only 300-400 µm was achieved.
Another protein was used to fabricate microscopic arrays capable of hosting live cells. Suntivich *et al.*[78] printed silk fibroin "nests" through an alternating deposition of silk polyelectrolytes chemically modified with side chains in order to stabilize the pattern by ionic interactions. Precisely, a solution of silk-polyglutamic acid was deposited with a JetLab II inkjet printer (MicroFab Technologies) on top of silk-polylysine dots at the same positions to generate the first silk bilayer, and the printing process was repeated until the desired number of bilayers (from 1 to 10) was reached. Each bilayer had an average thickness of 115 nm, and droplets were 60-90 pl in volume. After the printing process, a drying step allowed to obtain an insoluble crystalline silk. The nest-shaped microstructure of 70-100 µm in diameter and several hundred nanometers in thickness (Fig. 3.15), provided a biotemplated platform for immobilization, encapsulation and growth of biological cells.

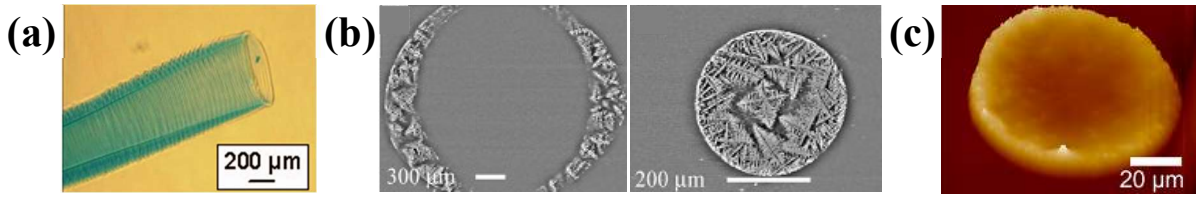

Figure 3.15 (a) Opening at the tip of alginate tube.[76] **(b)** Light microscopy images of ring-shaped and circular patterns made from collagen.[77] **(c)** 3D surface morphology of silk nest (one bilayer).[78]

3.3. Vat photo-polymerization

Vat photo-polymerization techniques are light-assisted printing methods. In general, a vat is filled with a resin or a monomer solution, and then the photo-reactive liquid surface is irradiated to initiate the polymerization of the first layer. In the layer, the resin is cured and solidified according to the pattern of the specific section, while the uncured monomer remains in the bath. After polymerization, the build stage move in the vertical direction and the next layer is cured on top of the previous. There are two types of polymerization mechanisms: free-radical

polymerization and cationic polymerization (Fig. 3.16). The first one occurs when photopolymers form long chains, get close to each other and crosslink. The most common resin is based on acrylates which offer high reaction rates but cause high shrinkage and warping. The second one happens when polymer ring structures, such as epoxies, open leading to formation of chemical bonds which are in number and structure, very similar to the original ones. Hence, this polymerization mechanism results in little warping, curling and shrinkage. The solution fomulation also contains photoinitiators to decrease polymerization activation energy and sometimes non-reactive components, such as UV absorbers, to achieve good part quality.[79] After printing, post-processing steps are required to remove any extra unreacted resin, achieve a fully polymerized part with better mechanical properties by heating or photo-curing further, and enhance surface quality by finishing operations.[79,80]

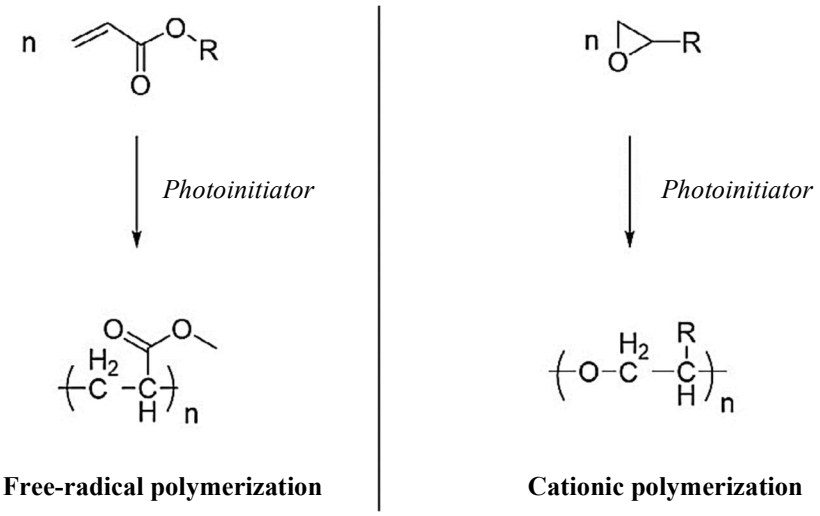

Figure 3.16 Polymerization mechanisms for vat polymerization process.[79]

There are three configurations depending on which light sources are employed: stereolithography (SLA), direct light projection (DLP), and direct laser writing (DLW). SLA and DLP can be performed in two ways, with a bottom-up or a top-down approach. In bottom-up fabrication, the radiation source is placed above the tank and the structure is built on a support platform that moves downwards after every layer. In top-down fabrication, the light source is localized beneath a tank with a transparent bottom plate and the structure, attached to a platform that moves upwards, is built facing upside down.[81] In the latter setup, althought the printed part is subjected to larger mechanical forces, several advantages compared with bottom-up approach are present: recoating of the structure with resin is not required, the exposed surface is always smooth, lower amounts of resin are required, and the illuminated layer is not exposed to the atmosphere.[82]

In all vat polymerization methods, kinetics of the reaction and the curing process are complex. The energy of light source, the exposure of the resin to radiation, the chemistry and amount of the monomer and photoinitators control the kinetics and determine the thickness of each layer.[54,80]

3.3.1. *Stereolithography (SLA)*

3.3.1.1. SLA generalities

SLA was developed in 1986 by 3D Systems and it is one of the earliest methods of additive manufacturing. The light source is a computer-controlled laser beam and each layer is built by scanning the surface bath and drawig the pattern.[82] The laser rasters the layer through the focus and projection using optics and a scanning galvanometer (Fig. 3.17).[79] As described above, the platform movement and the photoinduced polymerization of an individual pattern in each layer of resin, are repeated until a three-dimensional object is obtained.[82]

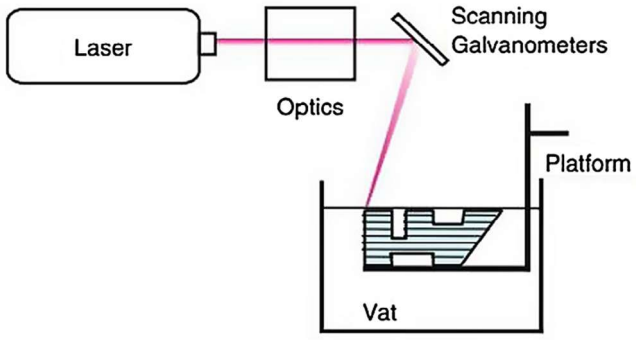

Figure 3.17 Schematic of SLA process.[79]

Of all the printing methods, SLA has one of the highest manufacturing accuracy due to the high resolution of light source. Thus, smaller layer thickness, higher detail information, and better surface quality can be achieved.[56] Regarding the thickness of a solidified layer, namely cure depth C_d (μm), a semi-empirical equation relates it to the light irradiation dose E (mJ/cm^2):

$$C_d = D_p \ln\left(\frac{E}{E_c}\right)$$

where D_p is the light penetration depth, and E_c is the critical energy (mJ/cm^2) required to reach the gel point and solidify the resin. The depth at which the resin is cured (C_d) increases logarithmically with the applied irradiation dose and depends linearly on the penetration depth.[82] The penetration depth can be decreased by increasing the photo-initiator concentration or by including a dye in the resin, while the dosage can be controlled by the laser scan velocity V_s and the laser power P_L in accordance with the relation:

$$E = \left(\frac{P_L}{V_s h_s}\right)$$

where h_s is the scan line spacing.[82,83]

3.3.1.2. Biobased polymers for SLA and applications

Feedstock materials for stereolithography must be photocurable. Since high-resolution photocurable resins have a significant cost , several monomers and oligomers derived from biomass have been used to prepare the photoreactive liquid. However, a prior modification of their chemical structure is often necessary to allow for photo-crosslinking capability. For instance, naturally derived resins were formulated using linseed oil and epoxidized linseed oil, mixed with a photoinitiator.[84] In both compositions, it was possible to induce

photopolymerization reaction after an exposure of at least 150 s to UV radiation. Compared with commercial resin, linseed oil-based resins required longer exposition times to solidify. The lower photosensitivity can be explained by the presence of longer and bigger monomer molecules which need more time to bond with each other.[84]

In most of the works found in literature, functional groups of biomass-derived monomers are modified with acrylic or methacrylic groups due to their higher reactivity and faster curing times and availability of easy modification processes.[85] Miao *et al*.[86] solidified a renewable soybean oil epoxidized acrylate, using a SLA technique, into biomedical scaffolds capable of supporting cell growth. The printing system was custom-made, a solid-state UV laser was mounted on the existing Solidoodle 3D printer platform. The system had a positioning resolution of 100 μm in X, Y and Z axis, and the spot size was 190 ± 50 μm. The effect of various printing speeds and laser frequencies on struts' thickness and width of cured resin, were investigated. Both the minimum thickness and the minimum width, less than 100 μm and 250 μm respectively, were obtained with the highest of the tested print speeds and, on the contrary, thickness and width decreased with decreasing laser frequency.

A successful fabrication of complex shaped prototypes from biobased acrylate photopolymer resins, was reported by Voet *et al*.[87] Four distinct resins were prepared mixing a photoinitiator, an optical absorber, and the bioderived acrylates (isobornyl acrylate, 1,10-decanediol diacrylate, pentaerythritol tetraacrylate, and multifunctional acrylate oligomer) with different concentrations. All formulations had a Newtonian behaviour and an adequate viscosity. The resin based on pentaerythritol tetraacrylate had the highest viscosity (7.3 Pa·s), however the value was on the same order of those of other commercial photocurable resins. In general, low viscosities allowed appropriate recoating of the liquid resin on the top of the last layer, but more viscous resins led to printed parts with lower shrinkage stress, higher feature resolution and excellent surface finishing. Besides test specimens, prototypes with a rook tower design having complex microarchitectures of about 700 μm, were printed using a Formlabs Form 2 desktop SLA printer. A layer thickness of 50 μm was selected and final structures of almost 2.5 cm in height were realized (Fig. 3.18a).

Bioderived methacrylate and acrylate resins have been synthesized by Silbert *et al*. [88] from epoxidized sucrose soyate and compared with commercial urethane acrylate resins in terms of mechanical and thermomechanical properties. Epoxidized sucrose soyate contains flexible aliphatic chains, a rigid sucrose core and many epoxy sites that can be modified with other functional groups. Silbert and co-workers prepared three different resins from the reaction of epoxidized sucrose soyate with: acrylic acid, methacrylic anhydride and methacrylic acid, or methacrylic anhydride and butyric anhydride. All the liquid resins were Newtonian and had a viscosity within the range of 1.5-3 Pa·s. A Peopoly Moai SLA printer (Firmware version 1.6) was used to print test specimens and a detailed structure in order to ascertain wheter more complex shapes could be fabricated within the printer setting capabilities. Therefore, a ring having pinhole details was printed with a layer height set to 100 μm and no imperfections were noted (Fig. 3.18b).

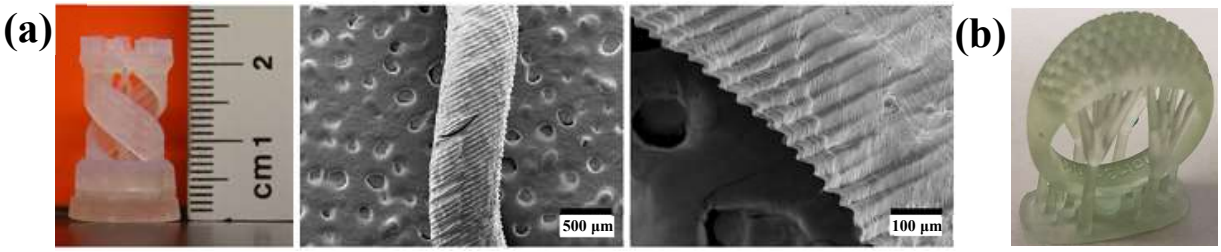

Figure 3.18 (a) Photograph of the rook tower prototype printed with the most viscous biobased acrylate resin and corresponding SEM images of the internal helix.[87] **(b)** Ring prototype printed with a biobased functionalized sucrose ester resin.[88]

Methacrylate resins based on monomers derived from other renewable sources such as vanillin, albumin, guaiacol, rosin and cellulose have been explored as alternatives to petrochemically derived resins.
Vanillin, which can be derived from lignin as well as other biomass sources, was methacrylated and used by Bassett *et al*.[85] as building block for vinyl ester resins and SLA feedstock material. The functionalized vanillin, in addition to a crosslinker and a photoinitiator, was poured in the tank of a Formlabs Form 2 SLA printer and a layer thickness of 100 µm was selected for printing process. The low viscosity (≈ 0.1 Pa·s) of the Newtonian resin, due to low interactions between resin monomers and low molecular weights of the monomers, allowed an easy recoating of the cured layer with the resin as the build platform moved down. Final printed parts were rectangular samples (35 × 12 × 2.5 mm^3 and 35 × 12 × 1.5 mm^3) for tensile testing.
Smith *et al*.[89] synthesized and formulated aqueous resins containing methacrylated bovine serum albumin. Commercially available bovine serum albumin was functionalized by reaction with methacrylic anhydride in an aqueous buffer. Final resin formulations containing 10 to 40 wt% methacrylated bovine serum albumin, were evaluated via rheometry. Formulations up to 35 wt% maintained a relatively low viscosity (under 1.56 Pa·s) while for a concentration of 40 wt% a viscosity of 29.4 Pa·s was reached. Since resins that have a viscosity higher than 10 Pa·s are more difficult to process, only resins with a concentration lower than 35 wt% were considered. Before pinting, an additive had to be added to the formulation because the cure rate was not sufficiently high. Robust protein-based constructs were fabricated in two steps: a first 3D printing via stereolithography, and a thermal curing in order to improve mechanical properties. Thus, the final part was comprised of both chemical and physical crosslinks. A slightly modified Formlabs Form 2 SLA printer was used to fabricate cylindrical disks (10 mm in diamenter x 5 mm in height) for swelling experiments, structures with various sized features for resolution tests, and objects with complex lattice geometries. The structures for evaluation of resolution capabilities of the albumin-based resin was designed to have square holes that increase in size from 400 µm to 2000 µm and fins that range from 100 µm to 1000 µm (Fig. 3.19a). The smallest fin printed was 243 µm and the smallest square hole resolved was 700 µm, while for a commercial acrylate resin the values were 173 and 400 µm, respectively. Regarding the lattices, more complex geometries with good resolution (250 µm struts) were successfully printed (Fig. 3.19b). It should be noted that all the resolutions above reported refer to "as printed" dimensions and printed constructs with features resolved down to 170 µm were obtained after thermal curing.

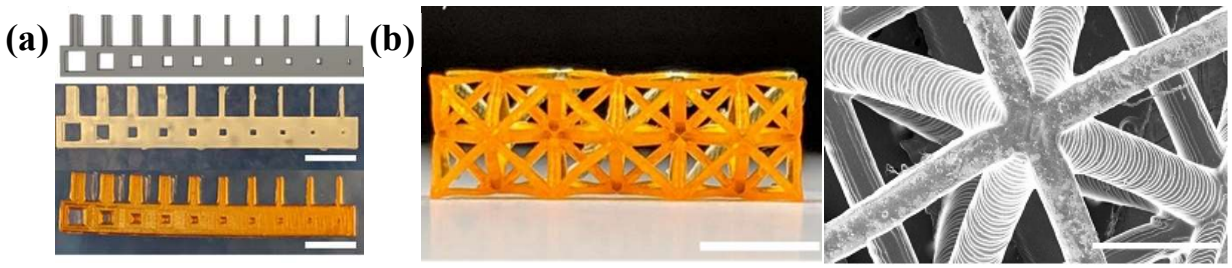

Figure 3.19 (a) From top to bottom, comparison of the original CAD, printed commercial resin, and resin based on methacrylated bovine serum albumin. Scale bars: 5 mm. **(b)** Optical image (left) and SEM image (right) of lattice structure made of resin containing methacrylated bovine serum albumin; in the SEM image 50 µm layer heights are visible. Scale bars: 5 mm (left), 1 mm (right).[89]

In the work reported by Ding *et al*.[90] natural phenolic-based (meth)acrylates were developed for sustainable and 3D printable formulations. In detail, binary formulations contained a structural diacrylate and a mono-methacrylate diluent, while for ternary formulations a

methacrylate crosslinker was added. The diacrylate was synthesized by dimerization of eugenol with a dithiol through the radical thiol-ene reaction, while guaiacol methacrylate was selected as a low viscous reactive diluent. Both molecules are 2-methoxyphenol derivatives which can be found in softwood lignin. Printing test was performed with a Formlabs Form 1+ desktop printer and a 3D model of a logo ("M", 20 x 11.8 x 2.9 mm) and a standard dogbone specimen (31.8 x 4.8 x 1.6 mm) were created using the ternary formulation (Fig. 3.20). The Z resolution was set to 100 μm, but the actual layer height varied from 60 to 90 μm. At high magnifications of SEM images, the stair-case effect were visible on sloping surfaces due to the layer-by-layer manufacturing (Fig. 3.20a,b). However, the high curing rate and the low viscosity of the monomers allowed a successful printing of designed models.

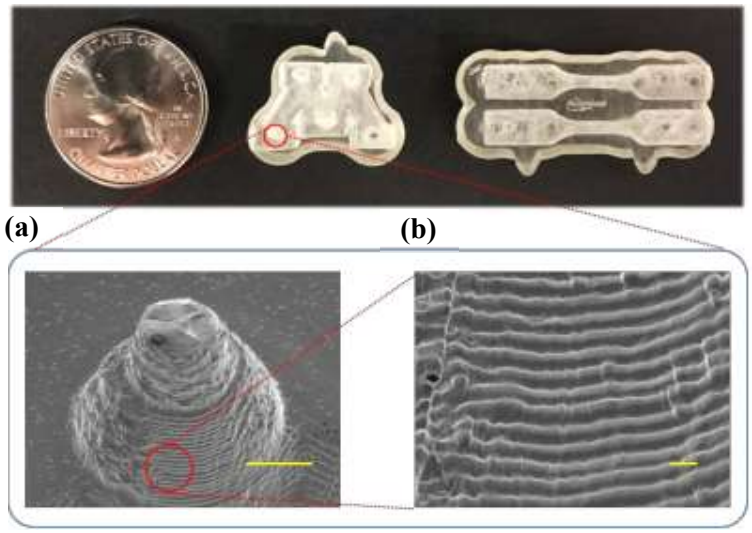

Figure 3.20 "M" logo and dogbone tensile bars printed from natural phenolic-based (meth)acrylates. **(a)** SEM image of a support cone which shows stair-casing feature (scale bar: 1 mm) and **(b)** magnified image with scale bar of 100 μm.[90]

A two-step polymerization strategy was employed by Lu *et al*.[91] in the preparation of 3D printed thermoset synthesized from cellulose and rosin. The stereolithography process was first performed to form a crosslinked network by UV-induced chain-growth polymerization, subsequently a thermally induced step-growth polymerization formed a second crosslinked network. The thermosetting polymer solution consisted of rosin derived monomers, 2-hydroxyethyl acrylate as monomer, mathecrylated ethylcellulose macromonomer as crosslinker in chain-growth polymerization, hexamethylene diisocyanate as crosslinker in step-growth polymerization, and a photoinitiator. Thus, in the first step, acrylate functional groups reacted under UV radiation and in the second one, reaction between the hydroxy and isocyanate occurred upon heating. The final thermoset had a dual-cure networks that resulted in enhanced mechanical properties. Printing process was performed with a commercial Creality LD 001 printer and, setting the layer thickness to 40 μm, a chess piece was realized. Furthermore, the ability to repair damaged parts using the biobased resin was investigated. The missing part of a seriously damaged chess piece was printed and, after polishing of the damaged site, the two parts were spliced by coating the photosensitive resin solution at the interface. The resin solution was then UV irradiated in order to generate new hydrogen bonds between the hydroxy group of monomer and cellulose at the interface. Finally, the partially repaired object was heated in order to induce the second polymerization mechanism. As a result, a complete

chemical crosslinking network was restored and a homogeneous repaired solid was obtained (Fig. 3.21).

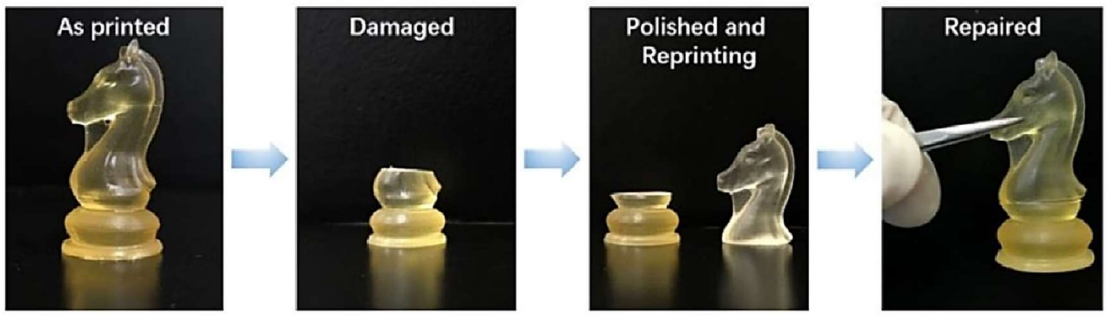

Figure 3.21 Demonstration of capability of thermosets derived from cellulose and rosin to repair a damaged chess piece.[91]

Generally, each object is fabricated through a single 3D printing technique. However, especially in the field of tissue engineering there is a need to produce intricate hierarchical structures with different intrinsic characteristics.[92] To address this issue, an integrated approach was proposed by Cui *et al*.[92] combining multiple 3D printing platforms for the fabrication of a complex vascularized bone construct. The dual custom-made platform was comprised of a SLA printer and a FDM printer that used gelatin methacrylate and polylactide as feedstock materials, respectively. The biphasic component, a cylindrical scaffold with 9 mm in diameter and 4 mm in thickness, had a PLA matrix of high mechanical strength and a vascular network of high flexibility. Hard bone regions were deposited first using the FDM machine, subsequently the remaining spaces in the construct were filled with gelatin methacrylate hydrogel wich was then cured via stereolithography to form the elastic vascular network. The porous scaffold was composed of stacked units with a 200 μm line distance, 250 μm line width, and a 200 μm layer height; a channel of 1.5 mm internal diameter was located in the centre of the construct and eight channels of 200 μm internal diameter were arranged around the central channel. The actual structural dimensions matched the nominal values demonstrating a good printing precision and reliability.

3.3.2. *Direct Light Projection (DLP)*

3.3.2.1. DLP generalities

Since the surface scanning with a laser beam can be slow, DLP technique was developed to cure an entire layer of photoreactive liquid at a time resulting in a high building speed. The radiation source is a light projector that generates a large two-dimensional pattern using an array of up to 1-4 millions of aluminum micromirrors that can be rotated independently to an on and off state. The mirrors system, called digital micromirror device, reflects incoming light from UV source to project a cross-section image of a CAD model. The projected image which is composed of small square pixels called “voxels”, passes through an optical lens and cures the photopolymerizable resin (Fig. 3.22).

Consecutive patterns are fabricated by moving the stage or the light focal plane along the Z axis.[79,82,93,94] The resolution of the printed structures depends on the size of the projected voxels, but parameters such as the curing time of each layer, layer thickness, and intensity of the UV light are also important to achieve high resolutions.[94,95]

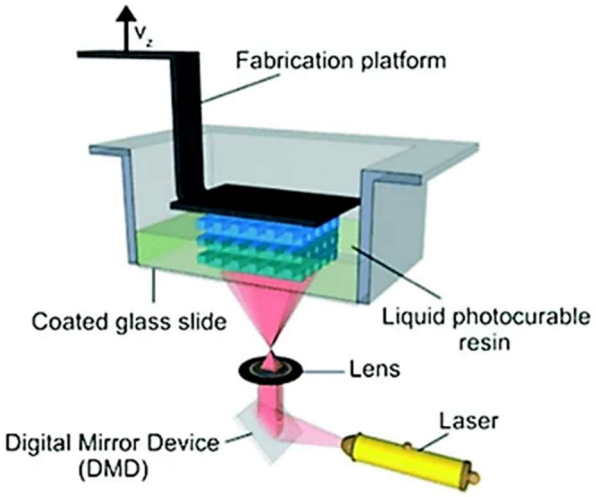

Figure 3.22 Schematic of DLP process.[95]

3.3.2.2. Biobased polymers for DLP and applications

As for stereolithography, the feedstock material is a photopolymerizable resin based mainly on (meth)acrylates or epoxies. Since the main requirements for resins are, in addition to sustainability, low cost and ready availability, vegetable oils have been considered a potential renewable source for the preparation of photocurable formulations. Some vegetable oils contain unsaturated molecules whose double bonds permit acrylation with acrylic acid, allowing crosslinking to take place during UV exposure.[96] Due to the growing consumption of healthier unsaturated oils, Wu *et al*.[96] thought of exploiting waste cooking oil for the formulation of acrylate resins suitable for the printing process. The unsaturated oil was obtained directly from the cooking vats of a McDonald's restaurant and its acrylation was then performed. A mixture of the acrylated oil and a photoinitiator was poured in the vat of a commercial Solus DLP printer. Setting the XY resolution at 41.7 µm and the layer height at 25 µm, a butterfly model consisting of larger and smaller structural features was printed. The resulting prints showed an outstanding resolution with features down to 100 µm which is comparable with the performance of some of the most expensive commercial resin (Fig. 3.23a). For comparison, an acrylated epoxidized soybean oil was also tested. This latter resin had the tendency to overcure and as a result, some of the open spaces were filled in and the design definition was reduced in comparison to the resin derived from waste cooking oil (Fig. 3.23b).

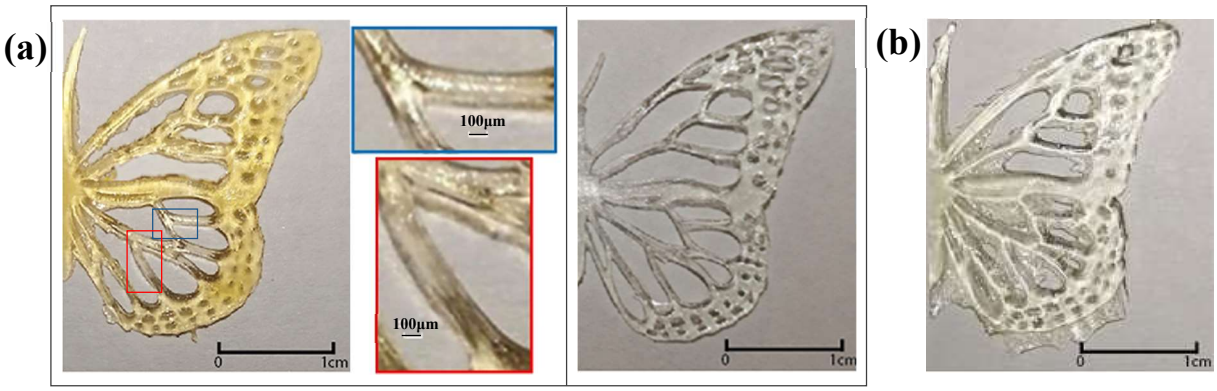

Figure 3.23 (a) Butterfly model printed from waste cooking oil (left) and from commercial resin (right). **(b)** Butterfly model printed from epoxidized soybean oil.[96]

An unsaturated, mass-produced and most inexpensive vegetable oil is that extracted from soybean seeds.[96] Soybean oil has been used both in the form of acrylate and methacrylate for DLP printing. In the work reported by Skliutas *et al*.[97] , acrylated epoxidized soybean oil mixed with a diluent and a photoinitiator, was chosen to produce centimeter sized chess-like figures and monolayer membranes on supportive pillars for evaluation of the polymerization depth under different exposure doses. A commercial Asiga Pico2 39 UV printer with a XY resolution of 39 μm was employed. Among the tested exposure durations, the lowest one led to an average monolayer thickness of 52 μm.
Other biobased resins derived from soybean were developed by Guit *et al*.[98] using methacrylated epoxidized soybean oil with various functionalities in addition to a biobased monofunctional diluent and a photoinitiator. Formulations with different types and ratios of oligomer and diluent were prepared and those having a viscosity lower than 1 Pa·s at a shear rate of 50 s^{-1} were selected for print testing. A Cubicorn Lux Full HD printer was employed to build various specimens for stress-strain analysis, a 3D logo, and complex shape prototypes with rook tower design (Fig. 3.24a). A first visual inspection of the rook tower prototypes revealed accurate print quality with smooth surface finishing and the SEM image of an internal detail within the prototype showed a complete fusion between the layers 100 μm high (Fig. 3.24b). Moreover, tensile tests demonstrated that the fully methacrylated resin allowed to have enhanced stiffness and tensile strength with respect to the pure acrylated soybean oil resins.

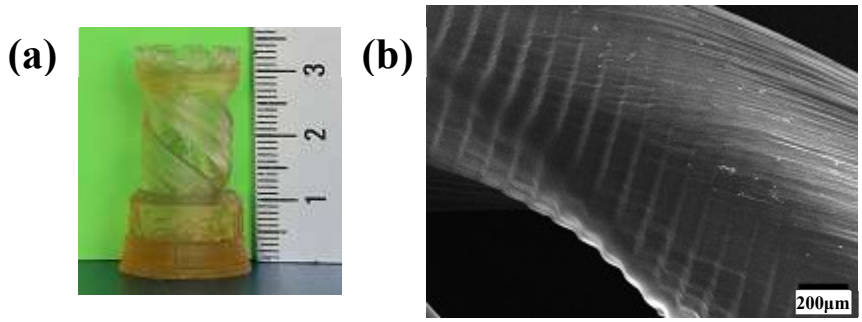

Figure 3.24 (a) Rook tower prototype printed with methacrylated epoxidized soybean oil. **(b)** SEM image of the internal double helix within the prototype.[98]

In tissue engineering and regenerative medicine, some of the desired requirements for a material are biocompatibility, biodegradability, and sometimes bioabsorption. The number of resins available having the required properties is limited, however in recent years naturally-derived photopolymers have been developed for biomedical applications. The following examples will concern resins based on polylactide, cellulose and two types of protein.
For tissue engineering of hard tissue like bone, in addition to the characteristics listed above, proper mechanical properties are necessary to simulate the original tissue. For this purpose, Melchels *et al*.[99] used the amorphous form of PLA, poly(D,L-lactide), for the construction of porous structures for bone cells culturing. In general, the polymer network can be formed by radical polymerization of polylactide oligomers end-functionalized with methacrylate, acrylate, or fumarate group.[99] In Melchels's work, the resin was formulated with methacrylated polylactide of varying molecular architectures, ethyl lactate as non-reactive diluent, a photoinitiator, an inhibitor, and a dye. The diluent was necessary to reach the appropriate viscosity, which was decreased to approximately 1 Pa·s. The liquid resin was used to built non-porus specimens for tensile tests (ISO 37-2), films (70 x 24 x 0.5 mm^3) and a porous scaffold with a gyroid architecture. By means of an EnvisionTec Perfactory Mini Multilens apparatus, it was possible to print relatively large scaffolds (up to 42 x 33 x 200 mm^3) and at high

resolutions, as well (Fig. 3.25a). The size of the smallest printable feature was determined by the size of the light pixels (32 x 32 μm^2), the layer thickness (25 μm), and the overcure.

Although lignocellulosic biopolymers and their derivatives have a huge potential for light-assisted printing, few studies have reported their use for preparation of photocurable resins for DLP. In particular, carboxymethyl cellulose, an attractive natural polymer for biomedial applications due to its biocompatibility, has advantageous properties, such as water-solubility and susceptibility to further functionalization, that enables it to be an ideal candidate for the production of photosensitive inks.[100] In the work reported by Melilli *et al.*[100] two formulations based on methacrylated carboxymethyl cellulose and a photoinitator, were prepared. Each solution was tested using an Asiga UV-MAX DLP printer with an XY resolution of 62 μm. From the first formulation, which contained water as solvent, simple massive structures like cylinders and parallelepipeds with low resolution were obtained (Fig. 3.25b). While the second formulation, based on a culture medium solution, had an improved printability and resolution due to phenol molecules contained in the medium that acted as a dye. Hence the latter resin allowed to print more complex geometries with suspended structures or with thin walls having sub-millimetric details (Fig. 3.25b).

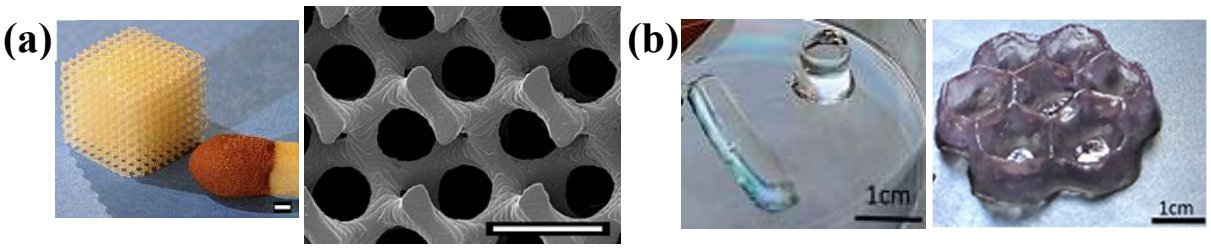

Figure 3.25 (a) Photograph (left) and SEM image (right) of PLA scaffold with a gyroid architecture. Scale bars represent 500 μm.[99] **(b)** Parts printed from methacrylated carboxymethyl cellulose: on the left, simple cylinder and parallelepiped (solvent: water) and, on the right, a more complex object (solvent: culture medium solution). [100]

Regarding protein-based resins, the first example refers to the study of Kim *et al.*[101] A hydrogel for DLP printing was prepared from silk fibroin through a methacrylation process. Methacrylated silk fibroin was synthesized by adding methacrylate groups to the amine-containing side groups of the protein using glycidyl methacrylate. The modified silk protein was mixed with a photoinitiator and used in a high-quality custom-made DLP projector. The printing system had a resolution of 30 μm in XY plane and the layer thickness was adjustable from 5 to 200 μm. A printing thickness of 50 μm was selected for the construction of various structures. However, tests were conducted to get the actual resolution of the developed photocurable formulation, and observable features were formed when nominal X and Z dimensions were at least 100 and 300 μm, respectively. For the printability test, complex shapes were chosen to demonstrate the versatility of the resin. Scaffolds with small and highly interconnected pores, a replica of the Eiffel Tower in miniature, and complex organ structures in miniature, such as ear auricle with helical fold, brain with cerebral sulcus and grooves, trachea, lung, heart, and vascular network with small caliber, were accurately realized in accordance to the designed digital models (Fig. 3.26). Hence, solid as well as tubular constructs with multiple branches and capillary networks, were successfully fabricated. Moreover, unlike the majority of other hydrogels, stable parts layered up to 45-50 mm (e.g. brain and Eiffel Tower) were printable. The second example of photo-crosslinkable ink is based on keratin, a polymer that can be derived from a renewable and low cost resource typically considered waste: the cortex of human hair. Placone *et al.*[102] demonstrated that photosensitive initiator-catalyst-

inhibitor solution can be coupled with the oxidized form of keratin in order to crosslink constructs via DLP printing. The formulated resin was processed by an EnvisionTec Perfactory 4 printer to assess print resolution. Cubes, cylinders and pyramids with dimensions of a few millimeters and features as small as one millimeter, were designed (Fig. 3.26b-d). The average printed dimensions of the cross-sections did not differ significantly from the nominal ones, but the height values had a significant variation. Moreover, squared and pyramidal geometries did not show well-defined right angles (Fig. 3.26c,d). The results suggests that further studies should be carried out to refine the crosslinking between layers on the height dimension and to achieve greater resolution also with a view to printing more complex geometries.

3.3.3. *Direct Laser Writing (DLW)*

3.3.3.1. DLW generalities

The vat photo-polymerization techniques considered so far, refer to the linear lithography category. The second main category is the nonlinear lithography which is know also as direct laser writing, two-photon polymerization, or multi-photon lithography.[97] Differently from SLA and DLP that involve an one-photon absorption, in DLW process the laser is focused to a tightly confined region within a photosensitive resin and two or more photons are simultaneously absorbed by the polymer that locally solidifies.[103] The radiation source is a near-infrared femtosecond laser and, through the two-photon absorption, it induces the same energy transition as ultraviolet photons which are involved in the one-photon absorption.[104] Since photosensitive resins are highly absorptive in the UV region, single-photon absorption occurs within the first few micrometers and the printing results in a planar process restricted to the exposed surface (Fig. 3.27a). While, because the resins are transparent in the infrared range,

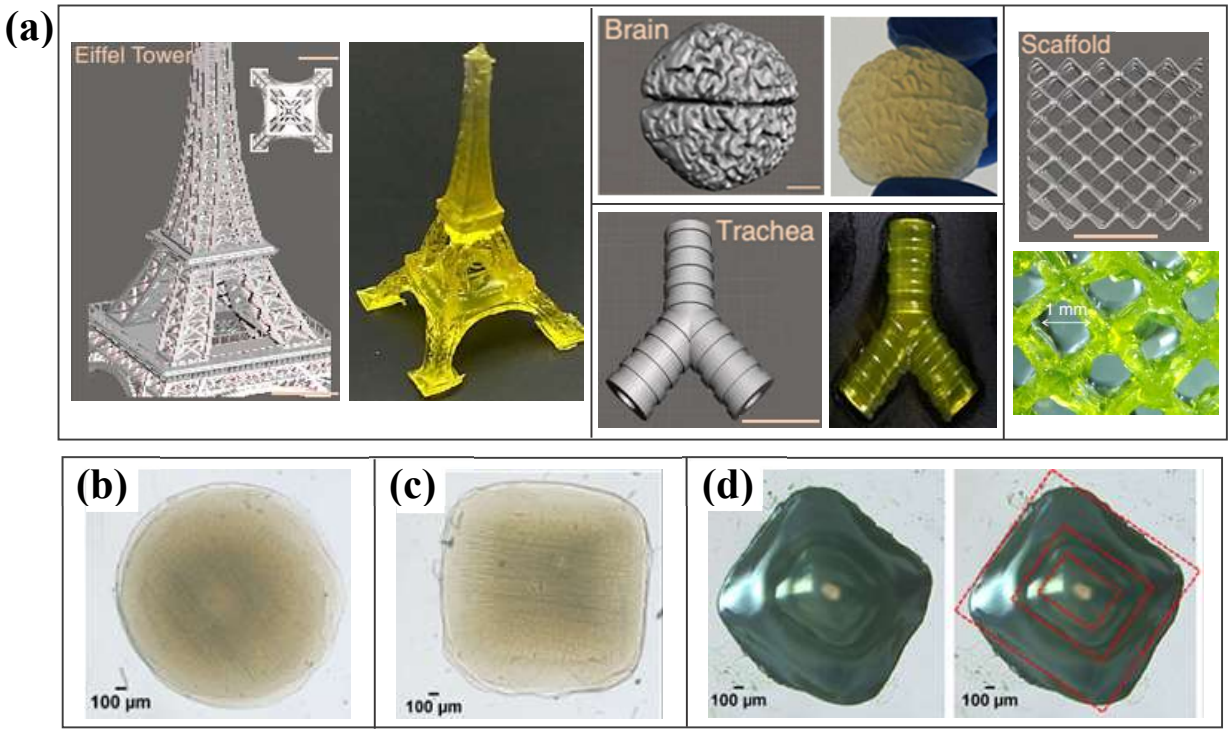

Figure 3.26 Printability of two different protein-based resins. **(a)** CAD images and relative printed structures from methacrylated silk fibroin: Eiffel Tower imitation (5 cm height), brain and trachea (2×2.5×1 cm^3) mimicked shape, and a scaffold.[101] (Scale bars: 1 cm) **(b-d)** Geometrical constructs printed from keratin: cylinder (2 mm diameter, 2 mm height), cube (2×2×2 mm^3), and pyramid with cube steps (the red boxes highlight the steps obtained).[102]

the local area where the femtosecond laser pulses are focused, is essentially a "floating" point within the volume of the resin (Fig. 3.27b).[105,106]

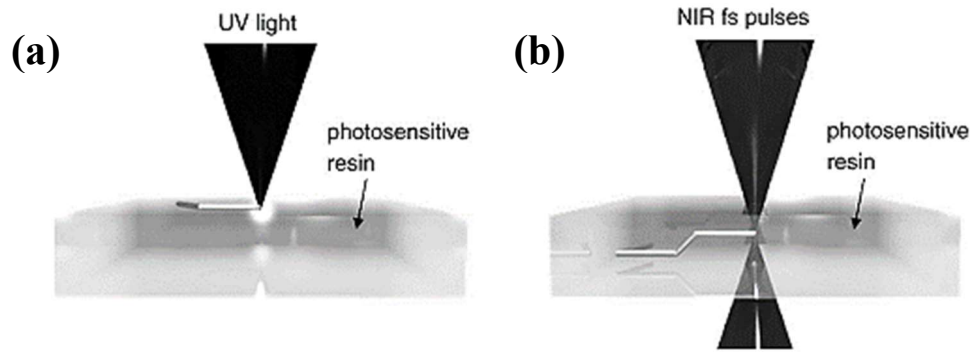

Figure 3.27 (a) UV light is absorbed at the surface of a photosensitive polymer. **(b)** Femtosecond pulses of NIR light can be focused within the volume of the resin enabling full 3D (nonlayered) fabrication.**[106]**

A typical DLW apparatus includes either galvanometric scanners that raster the laser focus in the XY plane and a positioning system to move the sample in the Z axis, or a piezoelectric stage that performs sample maneuvering in each direction.[106] This technology offers the highest resolution out of available 3D printing process, thanks to the smaller two-photon excited spot in comparison with the single-photon excited spot. This allows the fabrication of smaller structures with resolution down to the submicron-size, in particular a lateral resolution of 100 nm and an axial resolution of 30 nm have been reported.[103,106] As for previous techniques, the spatial resolution is dominantly determined by laser power and exposure time.[104]
Due to its fabrication capability for precise microstructures with high spatial resolution on both the microscopic and the nanometric scale, DLW has been applied in the fields of micro/nanophotonics, micro-electromechanical systems, microfluidics, biomedical implants and microdevices.[104]

3.3.3.2. Biobased polymers for DLW and applications

Also DLW uses photocurable resins mainly based on (meth)acrylates or epoxies, usually in addition to a photoinitiator. Although the functional groups can be the same, generally the resin is proper only for either linear or nonlinear lithography because of its properties, such as optical characteristics, viscosity, impurities, photopolymerization, mechanism sensitivity to development and post-processing.[97] However, a recent study[97] reported the preparation of a biobased material suitable for both technological fulfillments, ensuring high throughput and spatial resolution. The custom-made resin contained acrylated epoxidized soybean oil and its formulation was the same of the resin mentioned in the previous section dedicated to DLP. To perform DLW printing, a custom setup consisting of a femtosecond laser, galvano-scanner, positioning stages, and objectives, was used. Before fabrication of more complex structures, 75 × 75 μm^2 sized bi-layer scaffolds having 15 μm wide and 75 μm high logs, and hanging beams on supportive columns were printed in order to assess fabrication parameters and to evaluate the size of a single voxel, respectively. Due to the bending, twisting and stretching of the beams, precise measuring was not possible, however it was estimated that the lateral dimension of a voxel could reach several hundreds nm. For printing experiments, a well-defined grating (75 × 75 μm^2) having 0.8 μm wide and 2 μm high logs, a 7 layers scaffold (1.065 × 1.065 mm^2) having 25 μm wide logs, and chess-like bulky objects with fine features were manufactured (Fig. 3.28).

Due to the fact that the material was relatively soft, some parts of the models were deformed (Fig. 3.28a). However, a multi-scale manufacturing, from hundreds nanometers to millimeters, using a single material from renewable sources was successfully achieved.

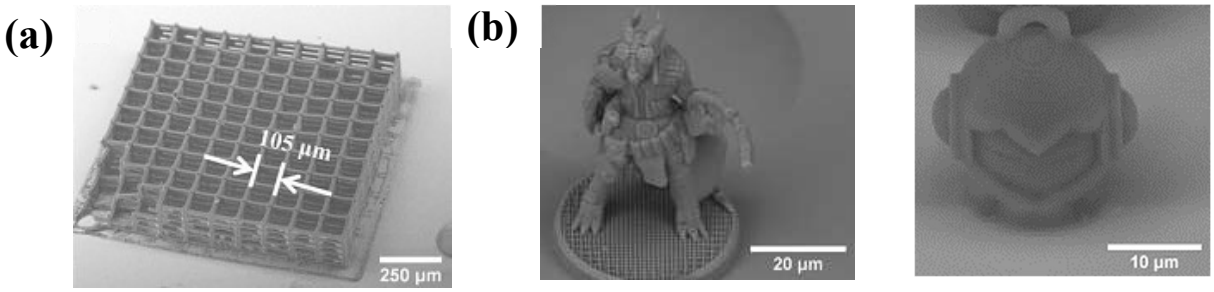

Figure 3.28 SEM images of objects printed from acrylated epoxidized soybean oil: **(a)** 7 layers scaffold, **(b)** chess-like figures ("Tower" and "Marvin").[97]

The same printing setup was employed in other two works[107,108] with vanillin acrylate-based resins. Vanillin has an aromatic structure which confers high mechanical properties, thus it could replace petro-based aromatic monomers. This natural compound can be derived by extraction from beans of vanilla orchids or by chemical modification of lignin. [107] In both studies two commercially available vanillin derivatives, vanillin dimethacrylate (VDM) and vanillin diacrylate (VDA), were tested in the custom DLW system described above. In one case, [107] VDM or VDA were mixed with a photoinitator. The mixtures were then placed in the vat and woodpile structures, were polymerized through ultrafast laser pulses. The 3D model consisted of two layers of two-dimensional gratings (75 × 75 μm^2) comprised of logs 15 µm wide and 75 µm long, spaced with a 15 µm gap. The gratings were connected by vertical columns 20 µm high. Printed constructs corresponded to the designed model, but tilted columns and not fully formed logs were visible in SEM images (Fig. 3.29a). Moreover, a chess-like figure ("Marvin") was manufactured but only the basic shape was polymerized and some details such as the face, ears and the loop were missing (Fig. 3.29b).
In the other case, [108] the vanillin acrylate-based resins were mixtures of VDM or VDA and acrylated epoxidized soybean oil without any photoinitiator. The high printability of the soybean oil derivative was combined with the high mechanical properties of the vanillin derivative. In order to assess the optimal process parameters, a printing test was performed through the fabrication of five straight lines supported by the long edges of rectangle-shaped

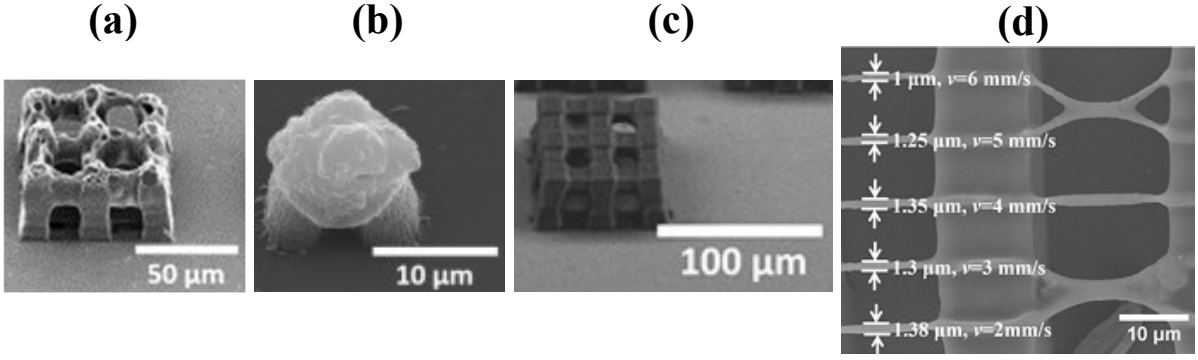

Figure 3.29 (a,b) SEM images of objects printed from VDA resins: **(a)** woodpile structure, **(b)** chess-like figure ("Marvin").[107] **(c,d)** SEM images of objects printed from mixtures of VDA and acrylated epoxidized soybean oil: **(c)** woodpile structure, **(d)** top view of lines supported by rectangle-shaped columns. [108]

columns having 15 μm width and 15 μm height. Each line was scanned with a different velocity to evaluate the smallest feature. The minimum line width was 1 μm (Fig. 3.29d). Further woodpile structures with various dimensions (from μm to mm scale) were tested, but only those printed using a sufficiently high laser power were able to sustain themselves. In particular, the woodpile structures having the same design of those built in the previous case (two layers, 75 × 75 μm^2) were successfully created with the proper light intensity (Fig. 3.29c).

3.4. Powder bed-based printing

Referring to the status of raw materials, the additive manufacturing categories described above use liquid-based and/or solid-based materials. The last category which is here reported, refers to powder-based printing technologies and, as its name suggests, polymers in the form of powders are employed. Selective laser sintering (SLS) and binder jetting belong to this class. In both techniques, the construction of a 3D component consists of consecutive steps repeated until the final part is built: [51]

1) a roller spreads horizontally and, at the same time, compacts a thin layer of very fine powders on the build platform while removing excess powder into an overflow box;
2) the cross-sectional pattern is traced by means of either a heat source (Fig. 3.30) or a binder (Fig. 3.33) depending on the technique;
3) the powder reservoir is lifted and the platform is lowered one layer in order to proceed with the next deposition.

After the part is completed, the loose powder is removed from the part by blowing compressed air in order to reuse it in successive runs.

Resolution is affected by the powder particle size, the particle size distribution, material binding properties, and laser or binder width.[53] For both technologies, the particle size is in the range of 10-100 μm, lower dimensions would cause poor spreading, too fast sintering and safety issues, while larger particles lead to lower spatial resolution and higher surface roughness.[24,53,54] The maximum particle size determines the effective minimum layer thickness, a parameter that has the greatest impact on the density of the final component. In particular, layer thickness for denser products must be set to the minimum value and vice versa.[109]
The layer thickness is also determined by the flowability of the powder. The flowability in its turn, as well as the packaging efficiency, is affected by the particle size distribution and the particle morphology.[110] Typical commercial powders include a major share of particles having dimensions in the range of 60 μm and a minority fraction with average particle sizes below 10 μm.[24] While, as concerns particle shape, well-defined spherical particles offer higher flowability than rough-edged and irregular particles.[24] Flowability of powders is an essential parameter to obtain high resolution. Too little flowability causes a low fabrication resolution due to insufficient recoating, and on the other hand, very high flowability does not provide sufficient bed stability.[109]
Unlike in previous additive manufacturing categories, temporary support structures are not needed since unfused or unbound particles support any cantilever structures. Because of this embedment, this fabrication method is used especially for scaffolds, implants and fixation devices for biomedical applications where the absence of rigid support structures is strongly recommended.[109]

3.4.1. *Selective Laser Sintering (SLS)*

3.4.1.1. SLS generalities

In SLS, powders are selectively melted and fused togheter by thermal energy. The heat source is a laser and its beam is scanned by laser optics according to the digital slices (Fig. 3.30). The chamber is kept at an elevated temperature, in order to decrease processing time and reduce the amount of curl distortions and thermally induced internal stresses.[24]

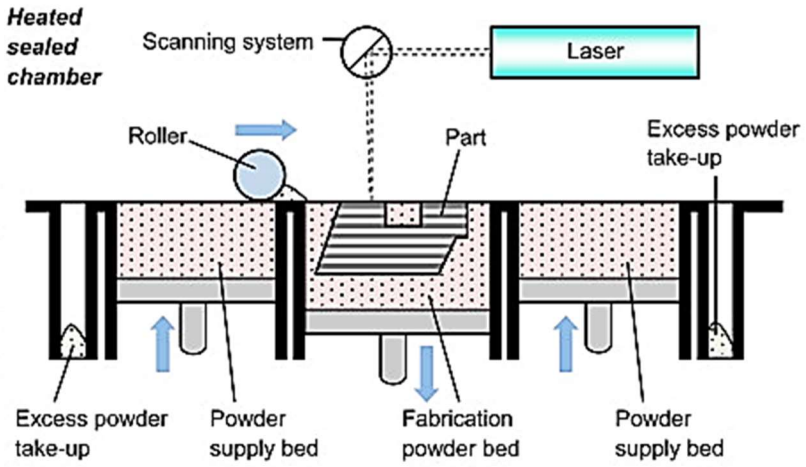

Figure 3.30 Schematic of SLS process.[111]

Due to the absorption of the laser radiation, the local heating of the powder cause the temperature to raise above the glass transition point. During sintering, capillary forces and molecular diffusion along the outermost surface of the softened particle lead to neck formation between adjacent particles.[24,54]
Besides the characteristics of powder particles, the laser beam diameter, the scan spacing, and the laser absorption have a crucial role in the quality of printed parts.[54,24] In particular, the Z resolution is dependent on laser absorption bacause this limits the sintering depth of the laser beam.[24]

3.4.1.2. Biobased polymers for SLS and applications

In general, polymers for SLS are mainly semi-crystalline thermoplastics, but may also be amorphous thermoplastics, dual-segment thermoplastics or elastomers.[110]
Among thermoplastics from renewable sources, aliphatic polyesters are the most explored because of their attractive properties, such as non-toxicty, biodegradability, and biocompatibility, suitable for the biomedical field.[112] The following examples will focus on two most important classes of thermoplastic aliphatic polyesters: polyhydroxyalkanoates and polylactic acid.
Printing tests with a polyhydroxyalkanoate were done by Oliveira et al.[113] They worked with a polyhydroxybutyrate powder in pure form and structures of about 2.5 in height (up to 10 layers) with 1 mm holes were printed by SLS.
P3HB porous structures were built by Pereira *et al*.[114] via SLS process. The polymer was provided directly in powder form by PHB Industrial S/A and loaded in a commercial Sinterstation 2000 (3D Systems) printer. A layer thickness of 180 µm was selected for the fabrication of porous cubes. Their nominal dimensions were 10.407 x 10.350 x 10.140 mm^3 and the internal architecture was composed of 16 circular pins with a 1.668 mm diameter

arranged orthogonally with 32 pins with a 1.641 diameter (Fig. 3.31a). The printed cubes showed similar geometry compared to its correspondent digital model (Fig. 3.31b). However, the resolution of pores and pins was low due to the size of the laser spot and the undesirable thermal adhesion of loose particles that made their removal difficult. The incomplete removal resulted in channels clogged with powder particles (Fig. 3.31c).

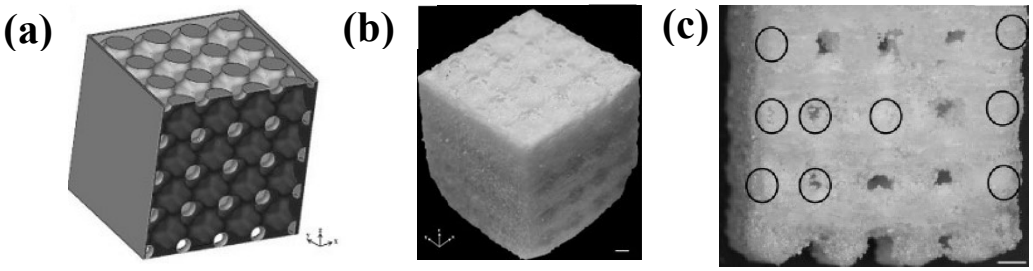

Figure 3.32 (a) Cube digital model and **(b)** the relative printed part from P3HB. **[114]** (Scale bar: 1 mm) **(c)** Internal view of the porous cube.**[114]** (Scale bar: 1 mm)

Duan *et al.*[115] prepared scaffolds for bone tissue engineering starting from the preparation of PHBV microspheres and calcium phosphate/PHBV (Ca-P/PHBV) nanocomposite microspheres. Such materials were used as feedstock powders on a Sinterstation 2000 (3D Systems) printer slightly modified in order to reduce the consumption of raw materials. The tetragonal porous scaffolds had nominal dimensions of 8 x 8 x 15.5 mm^3 and an orthogonal periodic architecture composed of struts 0.5 mm wide (Fig. 3.32a). To facilitate handling, a solid base (9 x 9 x 3 mm^3) was incorporated in the scaffold design. For producing PHBV and Ca-P/PHBV structures, the layer thicknesses were set to 150 µm and 100 µm, respectively. As printing results, the height, width and thickness of the scaffolds, were in accordance with the macrostructure of the digital model (Fig. 3.32b). Furthermore, for both materials the morphology and architecture of each layer were well preserved and the pores were clearly identified (Fig. 3.32c). Using the Ca-P/PHBV nanocomposite particles and the same printing system, Duang and Wang reported in another study[116] a successful fabrication of rod-shaped scaffolds, bar-shaped scaffolds, and more complex constructs such as geometrical models and a model of human proximal femoral condyle. The femoral condyle model was printed in the form of a cm-sized porous scaffold composed of cubic cells, and a strut size of 1.0 mm was achieved.

The feasibility of processing neat PLA and PLA nanocomposites by SLS was also investigated. In the work carried out by Bai *et al.*[117], PLA and nanoclay reinforced PLA were used to print flexural test samples in order to characterize and compare the mechanical properties of sintered parts. The powder particles of boh materials were prepared in laboratory and laser sintered on an EOS P100 Formiga system. Well-defined specimens having a simple rectangular shape were obtained, but through SEM micrographs of cross-sectional surfaces it was possible to notice that not all particles were fully melted.

Scaffolds having more complex shapes were realized for bone tissue engineering by Zhou *et al.*[118] using poly(L-lactide) and carbonated hydroxyapatite (CHAp) nanospheres within a poly(L-lactide) matrix. Also in this case, both neat polymer particles and nanocomposite microspheres were in-house synthesized. A Sinterstation 2000 SLS machine was modified in order to reduce the amount of powder required for each printing run. The tetragonal scaffold design consisted of a lower part which acted as a solid base (9 x 9 x 3 mm^3) to facilitate handling, and an upper macroporous part (8 x 8 x 16 mm^3) having a periodic architecture composed of orthogonal struts (Fig. 3.32a). Through laser sintering of layers 100 µm thick,

well-defined parts were obtained (Fig. 3.32d). However, the channels diameter was only about 600 μm instead of 800 μm owing to the penetration of the laser energy beyond the design scan area. The removal of excessive powder from the scaffolds was not problematic, the layers were generally well preserved and no powders were trapped in the channels (Fig. 3.32e).

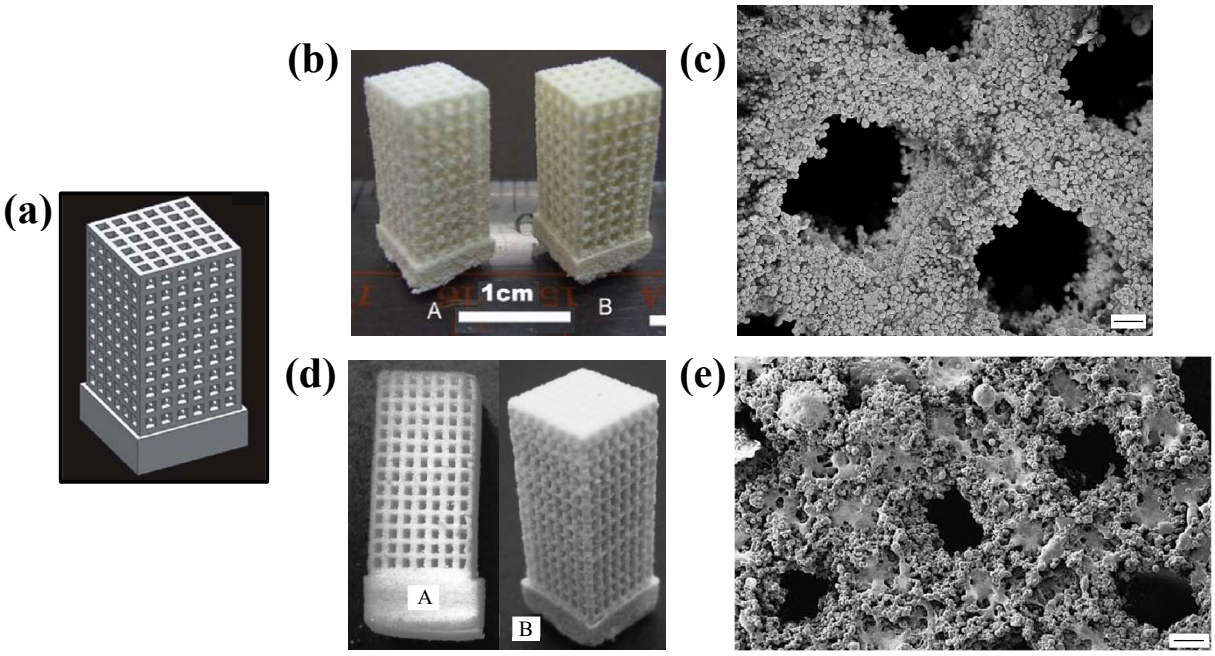

Figure 3.32 (a) Digital model of the tetragonal scaffold.[116] **(b)** Scaffolds printed from (A) PHBV and (B) Ca-P/PHBV. [115] **(c)** SEM image of PHBV scaffold.[115] **(d)** Scaffolds printed from (A) PLLA and (B) PLLA/CHAp. [118] **(e)** SEM image of PLLA scaffold.[118] (Scale bars: 200 μm)

During the laser sintering of a polymer, the exposure to high temperatures can have two negative consequences when dealing with objects for biomedical applications. First, the heat provided by the laser could degrade the polymer, leading to chemical and/or physical changes. Second, in tissue engineering applications, proteins are usually introduced to serve seeding molecules for tissue regeneration, thus proteins denaturation may occur due to high temperatures. To circumvent these issues, a modified laser sintering process was introduced.[119] This technology, namely surface-selective laser sintering, is based on a near-infrared (NIR) laser radiation which is not absorbed by the polymer. Distributing a small quantity of biocompatible carbon microparticles at the surface of the polymer particles, the NIR radiation is strongly absorbed by the carbon coating and only the surface of each particle reaches the molten state.[119]

A proof-of-concept of such approach was demonstrated by Antonov *et al.*[120] in the preparation of composite scaffolds. In the work, a small amount of furnace black carbon microparticles were homogeneously distributed across the surface of poly(D,L-lactic) acid particles. The printing process was performed using a custom system which consisted of a NIR laser and a precision moving platform. A two-layers scaffold and a fourteen-layers scaffold with dimensions of 5 x 5 x 5 mm^3 were built up through the deposition of layers 200 μm thick. SEM analysis demonstrated that PLA structures of high quality with a spatial resolution of 200 μm were obtained.

3.4.2. *Binder jetting*

3.4.2.1. Binder jetting generalities

In binder jetting, a liquid binding solution bonds powder particles within each layer as the result of adhesive forces. Thus, the printing setup comprises an inkjet printing head instead of the laser (Fig. 3.33). The liquid binder is deposited from the printhead through one of the dispensing mechanisms previously described in the section referred to DOD printing.[109] To improve mechanical properties, the green part is then post-processed by a high-temperature sintering treatment.

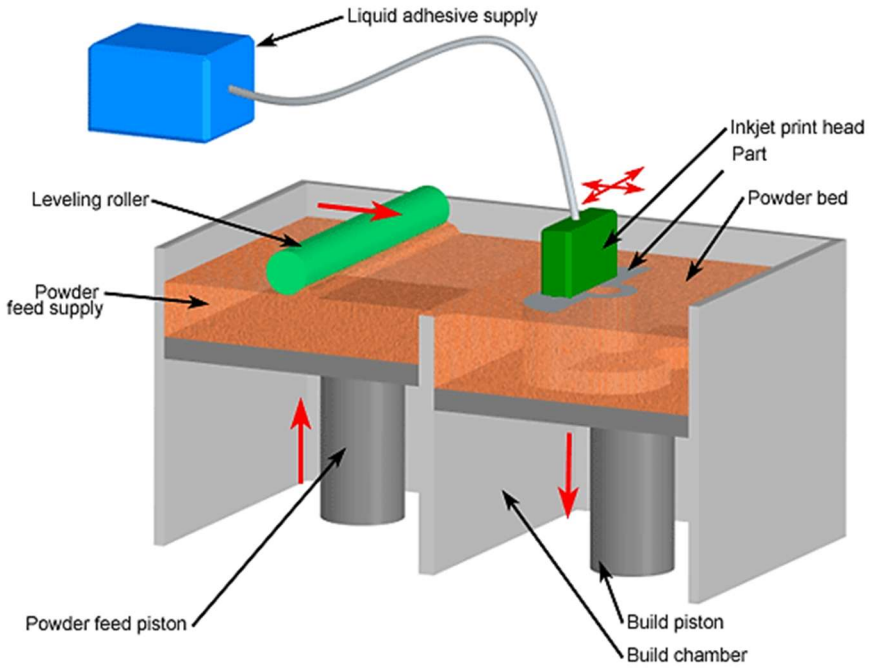

Figure 3.33 Schematic of binder jetting process. [121] (Copyright 2008 Custom Part Net).

Besides the characteristics of powder particles, the head nozzle diameter, the chemistry and reology of the binder, and chemical affinity between the powder and binder play an important role in the printing process. These parameters determine the initial size of the droplets, the velocity and path of the jetting heads, and the wettability of the powders.[80,109,110] Moreover, wettability affects the resolution: too low wetting of particles results in powder bed rearrangement that may have detrimental effects on the printing process, and too high wetting will reduce the smallest featue size.[109]

3.4.2.2. Biobased polymers for binder jetting and applications

Generally, the binder is embedded within the powder component and then activated by inkjet printing with an appropriate solvent. Inkjet printing of aqueous solvents is used if the powder is a hydrophilic polymer, such as starch, maltodextrin, and cellulose derivatives. While organic solvents like chloroform or other chlorinated solvents, are needed in case of hydrophobic polymers such as polylactid.[24]
The fabrication of drug implants and tablets is the main application of binder jetting technique when biobased polymers are employed. Such bulk structures have simple shapes in the millimeter scale and, since the main aim of research has been to study their drug release, little attention has been given given to the resolution assessment.

Implants for controlled delivery of antibiotics were manufactured by Huang *et al*.[122] using poly(L-lactic) acid as powder and a mixture of ethanol and acetone as binder solution. Using a machine designed and built by Fochif Mechatronics Technology Co. Ltd., three cylindrical implants (9 mm in diameter, 6 mm in height) with different drug gradients were printed. All the implants showed well-defined geometries and smooth surfaces (Fig. 3.34a).
Poly(L-lactide) implants with controlled drug release were also printed in another study.[123] The same binder solution and the same binder jetting machine of the previous work were used, while the implant designs were doughnut-shaped and multilayer doughnut-shaped with a central hole of 3 mm in diameter (Fig. 3.34b), in addition to the simpler columnar-shaped. The outer diameters were 9 mm and the heights were 5 mm and 7 mm for the multilayered one. The layer thickness was set to 200 µm and after printing, all implants were compact, in accordance with nominal dimensions, and no layers separation was observed.
Another material suitable for the fabrication of tablets via binder jetting is cellulose. Yu *et al*.[124] used powders based on ethylcellulose and hydroxypropyl methylcellulose, and a solution of ethylcellulose in ethanol as liquid binder, to print cylindrical tablets composed of three sections having different drug concentrations. The printing system was the same of the previous studies and the layer thickness was set to 200 µm as well. The tablet model had a diameter of 12 mm and the number of layers was 25 resulting in a overall height of 5 mm. After printig, the dimensions were measured with a caliper and the actual values were in accordance with the nominal ones.
Finally, an example of scaffolds printed from a blend is reported. Lam *et al*.[125] used a mixture of cornstarch, dextran, and gelatin as constituents of the powder and a water-based solution as binder. In this case, an available printer commercialized by Zcorp (Z402) was employed. A solid cylinder and four porous scaffolds having different designs were obtained (Fig. 3.34c). The overall dimensions were 12.5 mm in diameter and in height, while the pores size was 2.5 mm.

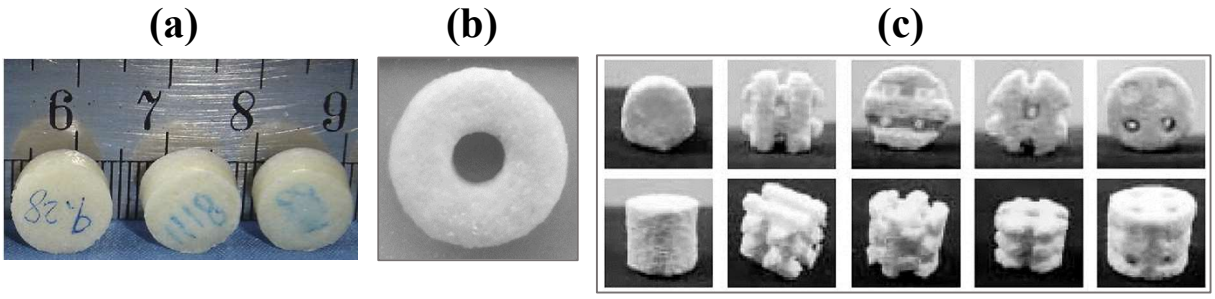

Figure 3.34 (a,b) Implants printed by binder jetting from poly(L-lactide).[122,123] **(c)** Scaffolds printed from the blend cornstarch-dextran-gelatin by binder jetting.[125]

4. Comparisons of the different techniques and conclusions

Four important additive manufacturing classes have been considered: technologies based on material extrusion, material jetting, vat photo-polymerization and powder bed printing. As far as the materials are concerned, literature data show that biobased polymers from all three groups, i.e. are natural polymers, synthetic polymers from biomass, and bacterial polymers, have been used in research works on 3D printing. Moreover, in order to tune the properties of the feedstock material or to enhance the mechanical performance of the final object, fully biobased blends have been formulated or reinforcing fillers, such as lignocellulosic fibers, have been added. In most cases, the printability of the raw material has been tested on commercial printers, sometimes with some modifications.

Generally, aesthetics and functionality of a printed component depend on the printing resolution and accuracy, which are affected by several factors. Firstly, the intrinsic characteristics of AM methodology rule the reproduction fidelity of the CAD virtual model. For instance, staircase effect and surface faceting are inherent features of layer by layer manufacturing and of surface discretization after conversion of the CAD model into the STL file, respectively. Secondly, both the specific AM technique and the processed material influence the quality of the final object. Considering these parameters, a comparison among the results reported in this thesis has been made in Table 4.1.

While the range of spatial resolutions of 3D printing from common petroleum-based polymers are widely reported in literature, less information regarding resolution of biobased polymers are available. Since few papers report the resolution in the XY plane while in most of them the height of the deposited layer is indicated, Table 4.1 gathers Z resolution. In comparing data, it is important to consider two aspects: first, the observations are referred to a restricted number of papers, therefore they can not have a general value; second, the setting of the layer thickness depends on the design of the object and its application, thus the indicated resolutions are not to be considered as the highest achievable.

Regarding FDM technique, almost all machines used in printing experiments are commercial printers. Objects with well-defined geometry and dimensions have been successfully obtained, it was possible to print quite complex constructs having overall dimensions from millimeters to centimeters and with layer thicknesses which vary in the range between 50 μm and 400 μm. The printability of natural polymers via LDM process has been evaluated mainly by printers available on the market, but also custom-made systems and adapted commercial printers have been employed. In some cases the modifications of commercial machines were necessary to have the proper temperature and consequently, ensure solidification of the extruded material. The major concern was to adjust the viscosity in order to allow the deposition of self-supporting structures. However, with the proper viscosity, self-standing structures having overall dimensions from millimeters to a few centimeters have been obtained and Z resolutions mainly in the range 200-750 μm could be achieved.

Less papers are available in literature regarding biobased-polymers printing by DOD. In the mentioned studies, custom-made printers and commercial machines with or without modifications have been employed.

Table 4.1 Additive manufacturing technologies and relative biobased feedstocks. The applications and dimensional features of printed objects, as well as the printing system, are reported.

AM approach	*AM technology*	*Biobased feedstock*	*Application*	*Features of printed objects*	*Printer*	*Reference*
Material extrusion	FDM	PLA	→ sacrificial mold for scaffold	Cylindrical scaffold (D = 5 mm, h=3mm) with a gradient distribution of pores (D≈250 µm) from the top to the bottom as the distance between pores increases from 240 to 560 µm	Solidoodle Workbench Apprentice 3D printer (D_{nozzle} = 0.250 mm, layer height = 0.3 mm)	[32]
			→ bone scaffold	"Square pore shaped" cylindrical scaffolds composed of stacked units with a 200 µm line distance (wall thickness ≈200 µm, pore size ≈200 µm, channel size ≈500 µm)	FDM printer (layer height = 0.250 mm)	[33]
			→ surgical instruments	Prototype replica of a common Army/Navy retractor (17 cm x 1.5 cm x 4 mm)	MakerBot Replicator 2 (layer height = 0.100 mm)	[34]
		bio-PC	→ daily life products	Test specimen (ASTM D638 type 1)	Custom-developed system (D_{nozzle} = 0.4 mm, layer height = 0.2 mm)	[35]
		PEF	→ prototypes with high chemical resistance	Cylinder (D = 7.8 mm) and other objects	Ultimaker^2 machine (minimum Dnozzle = 0.25 mm, minimum layer height = 0.05 mm)	[36]
		zein	→ pharmaceutical application	A "ring" geometry model (D = 1 cm, h = 2-3 layers)	ORD Bot-Hadron 3D printer (D_{nozzle} = 0.5 mm)	[37]

ethylcellulose	→ drug loaded implants	A hollow cylinder (D_{outer} = 5 mm, D_{inner} = 3 mm, h = 3 mm)	Multirap M420, Multec GmbH (D_{nozzle} = 0.5 mm, layer height = 0.1 mm)	[38]
hydroxypropyl cellulose	→ hollow capsule for drug release	Hollow structures to be assembled in capsulare devides (D≈7 mm, h≈13 mm, minimum thickness ≈ 300 ÷ 500 µm, maximum thickness ≈ 600 ÷800 µm)	MakerBot Replicator 2 (D_{nozzle} = 0.25 mm)	[39]
ethylcellulose, hydroxypropyl cellulose	→ capsule shells and coatings for immediate or modified release	A disk (D = 30 mm, h ≈ 600 mm)	MakerBot Replicator 2 (D_{nozzle} = 0.4 mm, layer height= 0.30 mm)	[40]
hydroxypropyl methylcellulose acetate succinate	→ delayed release tablets	Cylindrical printlet (D = 10 mm, h = 3.6 mm), discs (D = 23 mm, h = 1 mm)	MakerBot Replicator 2X (layer height = 0.10 mm)	[41]
ethylcellulose, hydroxypropyl cellulose, hydroxypropyl methylcellulose	→ controlled release tablets	Tablet (D = 10 mm, h = 4.5 mm)	Prusa i3 3D desktop printer (Dnozzle = 0.4 mm, layer height = 0.10 mm)	[42]
ethylcellulose + hydroxypropyl methylcellulose, ethylcellulose + alginate, ethylcellulose + xanthan gum	→ tablets	Tablet templates (D = 12.0 mm, h = 7.0 mm, shell thickness= 0.4 ÷ 1.2 mm)	Desktop FDM printer A3, JGAURORA (D_{nozzle} = 0.4 mm, layer height = 0.1 ÷ 0.3 mm)	[43]
starch + cellulose acetate	→ medical devices	Specimen (25 mm x 5 mm x 1.5 mm)	Ultimaker 2+ printer (D_{nozzle} = 0.6 mm, layer height = 0.15 mm)	[44]

	PLA + galactoglucomannan	→ tissue engineering and drug-eluting scaffolds	Scaffold (20 mm x 20 mm x 2 mm)	Me3D desktop printer (D_{nozzle} = 0.4 mm, layer height = 0.2 mm)	[45]
	PLA + microcrystalline cellulose	→ biomedical scaffold prototypes	Scaffold (D = 15 mm, h= 1 mm)	AutoMaker, Robox 3D printer	[46]
	PLA + spruce pulp fiber	→ antibacterial devices	3D model figures (D = 15 mm), dog bone specimens (80 mm x 3 mm x 3 mm)	Ultimaker Original 3D printer (D_{nozzle} = 0.4 mm)	[47]
	bio-PE functionalized with maleic anhydride + thermomechanical pulp fibers	→ prototyping	Squares (10 mm x 10 mm), model figure (D = 20 mm)	Ultimaker Original 3D printer (D_{nozzle} = 0.4 mm)	[48]
	PHA-g-MA + palm fiber	→ daily life products	Specimens	Flashforge, L2D Desktop Factory (layer height = 0.05 mm)	[49]
LDM	cellulose nanofibers	→ scaffold	Electrode scaffold with 6, 12, 15, 18, 21, 24 layers	Benchtop robot Fisnar F4200n (D_{nozzle} = 0.150 mm, layer height = 0.20 mm)	[57]
	carboxymethylated-periodate oxidized cellulose nanofibrils	→ wound dressing	Grid structure, cylindrical scaffold (D = 25 mm, h = 6 mm) with 9 layers each consisting of 12 × 12 tracks	Bioplotter EnvisionTEC GmbH	[58]

cellulose nanocrystals	→ textured cellular architectures	Structures with 1 to 8 layers each of which is composed of filamentary features (d = 410 µm) arrayed with a center-to-center spacing varying between 1.0 mm (grids) and 320 µm (blocks)	ABL 900010, Aerotech Inc. (D_{nozzle} = 0.200, 0.410 mm)	[59]
	→ scaffold	Simple 1 cm^3 cubic structure using nozzle tips of different sizes; octet cube, pyramid, hexagonally twisting vase, nose model, ear model, and honeycomb with a nozzle tip size of 500 µm (D_{pores} = 20 ÷ 800 µm); porous scaffold (filament width of 750 µm) with a nozzle tip size of 500 µm	DIW printer (D_{nozzle} = 0.200, 0.400, 0.500 mm)	[60]
cellulose acetate	→ pharmaceutical application	Cylindrical tablet (D = 12 mm, h = 5.85 mm) designed with internal separate compartments	RegenHU (D_{nozzle} = 0.500 mm)	[61]
	→ surgical instruments	Miniature eyeglass frames, a rose (≈ 1 cm^3), miniature forceps (length ≈ 3 cm) with custom circular grippers, dog bone specimens (57 x 4 x 0.65 mm^3)	Modified Printrbot Simple Metal with a Nordson HP7x mounted syringe (Dnozzle = 0.200 mm, nominal layer thickness = 0.180 mm)	[62]

		cellulose acetate, acetoxypropyl cellulose	→ textile surface tailoring and functionalizing	Test strips (10 x 40 mm^2, 10 x 10 mm^2) and 5 types of structures (refractive, thermoresponsive, rigid structuring, flexible structuring and smocking) printed on cellulosic fabrics	3Dn-300, nScrypt Inc. (D_{nozzle} = 0.84 mm) and an in-house built printer	[63]
		hemicellulose	→ biomedical application	Hollow cube (base 2 cm x 2 cm, heigh 1 cm), scaffold prototype (10.5 mm on the sides, 5.3 mm in height), flower-shaped model, three-layered grid structure	Custom-made 3D printer for high viscosity pastes (D_{nozzle} = 0.68 mm, layer heights ≈ 0.53, 0.68, 0.70, 0.74 mm)	[64]
		agar	→ tissue engineering	Cubic scaffold (edge length = 1 cm, strand diameter = 0.500 mm, gap between the strands in the layer = 0.500 mm)	3D plotter based on a CNC milling machine for 3D positioning of a dispenser; the milling head was replaced by a double jacket cartridge equipped with a standard Luer-Lock adaption for the dispensing nozzles (inner D_{nozzle} = 0.15 mm, layer height = 0.30 mm)	[65]
		alginate, alginate + methylcellulose	→ scaffolds	Pure alginate: exhibited poor applicability for the plotting of 3D scaffolds. Alg/MC: scaffolds with different edge lengths (6, 15, 20 mm), numbers of layers (4, 20, 28,	BioScaffolder 2.1, GeSiM (inner D_{nozzle} = 0.25 mm for alg/MC, inner D_{nozzle} = 0.20 mm for alginate)	[66]

				50) and strand distances (2.5, 2, 1.87, 1.5, 1, 0.75 mm); at a distance of 0.75 mm the scaffold resulted non-macroporous		
		methacrylated hyaluronic acid	→ scaffold for bone regeneration	Porous scaffolds (20 x 20 x 3 mm^3 with strand distances of 1 mm), non-porous lumbar scaffolds (20 x 25 x 1 mm^3 with strand distances of 0.2 mm)	Bioscaffolder dispensing system (SYS+ENG) (D_{nozzle} = 0.50 mm, strand thickness of 0.2 mm)	[67]
		chitosan	→ soft tissue regeneration	Scaffold (from 5 to 20 layers 47 mm × 47 mm) with a mesh structure having nominal opening of 0.40 mm	Modified (FDM) 3D printer (D_{nozzle} = 0.26 mm, $D_{filament}$ = 0.25 mm)	[68]
		collagen	→ cartilage tissue	Half-cylinders (D = 30 mm) with ≥90% geometric accuracy within 2 mm of targeted dimensions	Modified Fab@Home 3D printer (Seraph Robotics)	[69]
		gelatin methacrylamide	→ scaffold	Porous scaffold (1-3 mm thick constructs of 13 mm x 13 mm with strand spacing of 0.35 and 0.55 mm)	Bioplotter EnvisionTEC GmbH (internal D_{nozzle} = 0.15 - 0.20 mm, layer height = 0.15 – 0.20 mm)	[70]
		aneroin	→ scaffold, anatomical models	Rectangular parallelepiped lattices (20 x 5 x 0.5 mm^3) with strands of 400 µm, human ear model (35 x 50 x 18 mm^3), vascular graft, and nose model	Custom-made printing system (D_{nozzle} = 0.5, 0.41 mm, minimum strand width = 0.10-0.27 mm)	[71]
		silk fibroin	→ biophotonic implantable device	Straight and wavy optical waveguides (cross-section ≈ 5 µm x 5 µm)	ABL9000, Aerotech Inc. (D_{nozzle} = 0.005 mm)	[72]

		milk protein + whey protein	→ food products with customized designs	Chinese character (38 mm × 38 mm × 4.75 mm), cylinder (16 mm × 16 mm × 20 mm) and other objects	SHINNOVE-S2, SHIYIN Technologies Co. Ltd. (D_{nozzle} = 0.84 mm, layer height = 0.75 mm)	[73]
Material jetting	DOD	alginate	→ scaffold	Sheets, tubes (D ≈ 0.5 mm)	Custom-made printer with EPSON SEA-Jet™ inkjet nozzle head (Seiko Epson Corp.) (D_{bead} = 0.010-0.060 mm, positioning resolution = 0.0002 mm)	[76]
		collagen	→ biocompatible platform for immobilization of biological cells	Patterns: lines, rings (D = 2.55 mm), circles, dot arrays	Modified Canon Bubble Jet, BJC-2100 (D_{nozzle} = 0.020-0.030 mm, lateral resolution = 0.30-0.40 mm)	[77]
		silk fibroin	→ biocompatible platform for immobilization of biological cells	"Nest" shaped structures (D = 70-100 μm, several hundred nanometers in thickness)	JetLab II, MicroFab Technologies (D_{nozzle} = 0.050 mm)	[78]
Light-assisted printing	SLA	soybean oil epoxidized acrylate	→ scaffold	Scaffolds (minimum thickness ≤ 0.10 mm, minimum width = 0.25 mm)	Modified Solidoodle® 3D printer platform, with MarketTech laser (stepper motors with resolution of 0.10 mm in x, y, z-axis; spot size = 0.190 ± 0.050 mm)	[86]

resins formulated with different biobased acrylates (isobornyl acrylate, 1,10-decanediol diacrylate, pentaerythritol tetraacrylate, multifunctional acrylate oligomer)	→ complex shaped prototypes	Tensile bars (ISO 527-2-1BA), rook tower model (h = 24 mm)	Formlabs Form 2 (spot size = 0.14 mm, layer height = 0.050 mm)	[87]
methacrylated and acrylated epoxidized sucrose soyate	→ prototypes	Flexural rectangular samples (76.8 mm × 13 mm × 4 mm), tensile testing samples (ASTM D638 type IV), a ring with pinhole details	Peopoly Moai SLA printer, Firmware version 1.6 (layer height = 0.10 mm)	[88]
methacrylated vanillin	→ prototypes	1. A square part (50 mm x 50 mm) composed of 25 equal-area square tiles (25 layers, the first layer covering the area of 25 tiles, the second layer covering 24 tiles, and so on) 2. Tensile testing samples (ASTM D638 type IV), viscoelastic testing samples (35 × 12 × 2.5 mm^3 and 35 × 12 × 1.5 mm^3)	1. Peopoly Moai SLA printer (beam width = 0.07 mm) 2. Formlabs Form 2 (layer height = 0.10 mm)	[85]
methacrylated bovine serum albumin	→ medical devices	Cylindrical disks (D = 10 mm, h = 5 mm), resolution test structures (smallest fin printed = 0.243 mm, smallest square hole resolved = 0.700 mm, deviation from the CAD model = 0.0675 mm), lattice geometries (strands = 0.25 mm)	Formlabs Form 2 (resolution ≈ 0.2 mm, layer height = 0.05 mm)	[89]

	(SLA+FDM)	3,6-dioxa-1,8-octanedithiol eugenol acrylate + guaiacol methacrylate	→ mechanically robust objects	Logo “M” model (20.0 mm × 11.8 mm × 2.9 mm), standard dogbone specimen (31.8 mm × 4.8 mm × 1.6 mm)	Formlabs Form 1+ (spot size = 0.30 mm, Z resolution = 0.10 mm)	[90]
		methacrylated ethyl cellulose + 2-hydroxyethyl acrylate + rosin derived monomers	→ thermosets with shape memory and repairability; for flexible electronic and smart photoelectric materials	A chess piece and the missing part of a damaged chess piece	Creality LD 001 (layer height = 0.040 mm)	[91]
		gelatin methacrylate + PLA	→ complex bone scaffold	Cylindrical construct (D = 9 mm, h = 4 mm) composed of stacked units with a 0.20 mm line distance, 0.25 mm line width, and a 0.20 mm layer height, with 8 channels (D_{outer} = 0.5 mm) and a central channel (D_{outer} = 2 mm)	A dual 3D bioprinting platform comprised of a FDM 3D bioprinter and a SLA 3D bioprinter (spot size = 0.19 mm)	[92]
	DLP	acrylated waste cooking oil	→ commodities	A cm sized butterfly model with features down to ~100 micrometer resolution	Solus DLP (XY resolution = 0.0417 mm, layer height = 0.025 mm)	[96]
		acrylated epoxidized soy bean oil	→ rapid prototyping	Monolayer membranes on pillars (minimum thickness = 0.097 mm), cm sized chess-like models	Asiga Pico2 39 UV (XY resolution = 0.039 mm, spot size = 2 mm)	[97]
		methacrylated epoxidized soy bean oil	→ prototypes	Tensile bars (ISO 527-2-1 BA), test specimen (60 mm x 50 mm x 1 mm), rook tower prototype	Cubicon Lux Full HD (layer height = 0.10 mm)	[98]

methacrylated PDLLA oligomers	→ tissue engineering	Tensile test specimens (ISO 37-2), films (70 x 24 x 0.5 mm^3), scaffold with a gyroid architecture	EnvisionTec Perfactory Mini Multilens (XY resolution = 0.032 mm, layer height = 0.025 mm)	[99]
methacrylated carboxymethyl cellulose	→ tissue engineering and regenerative medicine	Cylinders, parallelepipeds, and more complex geometries with suspended structures or with thin walls having sub-millimetric details	Asiga UV-MAX DLP printer (XY resolution = 0.062 mm)	[100]
methacrylated silk fibroin	→ tissue engineering	Porous scaffolds (D_{pores} = 0.7, 1 mm), Eiffel Tower models (h = 50 mm), organ miniature models such as ear, brain, trachea (2 cm × 2.5 cm × 1 cm), heart, lung, and blood vessel network	Customized DLP printer with UV Digital Micro-mirror Device™ with a resolution of 0.030 mm (layer height = 0.050 mm; observable features were formed when nominal X and Z dimensions were at least 0.10 and 0.30 mm)	[101]
keratin	→ tissue engineering	Cylinders, cubes, and pyramids with dimensions of a few millimeters and features as small as 1 mm	EnvisionTec Perfactory 4	[102]

	DLW	acrylated epoxidized soybean oil	→ rapid prototyping, tissue engineering	Bi-layer scaffold (75 × 75 μm^2), 7 layers scaffold (1.065 mm x 1.065 mm with 25 µm wide logs), 2D grating (75 × 75 μm^2 with 0.8 µm wide and 2 µm high logs), chess-like bulky objects (“Tower”, “Marvin”,”Car”)	Custom setup (Pharos laser, Scanlab HurryScan II Galvano-scanners, Aerotech positioning system, Zeiss objectives)	[97]
		vanillin dimethacrylate, vanillin diacrylate	→ biomedical applications	Woodpile structures (two layers of 2D gratings, connected by vertical columns 0.020 mm high, the gratings comprised orthogonal sets of logs 0.015 mm wide and 0.075 mm long with a 0.015 mm gap between them)	Custom setup (Pharos laser, Aerotech positioning system, Zeiss and Nikon objectives)[51]	[107]
		mixture of acrylated epoxidized soybean oil / vanillin dimethacrylate	→ rapid prototyping, application in the fields of biomedicine, micro-optics and nanophotonics	A 3D model consisted of five rectangle-shaped columns which were 15 µm wide, 60 µm long and 15 µm high. Gaps between the columns varied from 5 µm to 20 µm every 5 µm. Five straight lines (< 2 µm thick) lie perpendicularly above the columns	Custom setup (Pharos laser, Aerotech positioning system, Zeiss and Nikon objectives)[51]	[108]
Powder bed-based printing	SLS	P3HB	→ tissue engineering	Porous cube (10.407 x 10.350 x 10.140 mm^3) with internal architecture composed of circular pins (minimum diameter = 1.641 mm)	Sinterstation 1 2000 SLS (3D Systems) (laser spot size = 0.450 mm, scan spacing = 0.15 mm, layer height = 0.18 mm)	[114]

	(SSLS)	P3HBV, P3HBV + calcium phosphate	→ tissue engineering	Tetragonal porous scaffolds (8 x 8 x 15.5 mm^3) composed of orthogonal struts 0.5 mm wide, intricate porous structures	Modified Sinterstation 2000 SLS (3D Systems) (spot size = 0.457 mm, scan spacing = 0.20 mm for PHBV and 0.10 mm for Ca-P/PBHV, layer thickness = 0.15 mm for PHBV and 0.10 mm for Ca-P/PHBV)	[115]
		P3HBV + calcium phosphate	→ tissue engineering	A cm sized human proximal femoral condyle model (strut size = 1 mm), two porous scaffolds in the shape of bars and rods, complex geometrical structures	Modified Sinterstation 2000 SLS (3D Systems) (scan spacing = 0.1 mm, layer thickness = 0.1 mm)	[116]
		PLA, PLA + nanoclay	→ medical applications	Flexural test specimens (ASTM D790)	EOS P100 Formiga system (laser scan = 0.25 mm)	[117]
		PLLA, PLLA + carbonated hydroxyapatite	→ tissue engineering	A tetragonal porous scaffold (8 x 8 x 16 mm^3) composed of orthogonal struts	Modified Sinterstation 2000 SLS (3D Systems) (spot size = 0.457 mm, scan spacing = 0.15 ÷ 0.21 mm, layer height = 0.10 mm)	[118]
		PDLLA	→ tissue engineering	Porous scaffold (5 mm x 5 mm x 5 mm) with an accuracy of 0.200 mm	Custom setup (laser spot = 0.200 mm, layer height = 0.200 mm)	[120]

	Binder Jetting	PLLA	→ drug implant	Three cylindrical implants: matrix structure, capsule structure, double-layer with a reservoir-like structure (D = 9 mm, h = 6 mm)	3DP machine was designed and built by Fochif Mechatronics Technique Co. Ltd	[122]
			→ tablets	Columnar-shaped tablet (D = 9 mm, h = 5 mm), doughnut-shaped tablet (D = 9 mm, h = 5 mm), multilayer doughnut-shaped tablet (D = 9 mm, h = 7 mm)	3DP machine was designed and built by Fochif Mechatronics Technique Co. Ltd (layer height = 0.200 mm)	[123]
		hydroxypropyl methylcellulose, ethylcellulose	→ tablets	Cylindrical multilayer tablet (D≈12 mm, h≈5 mm)	3DP machine assembled at Shanghai Folichif Co., Ltd (Dnozzles = 0.030 mm, layer height = 0.200 mm, spacing of droplets within the direction of raster motion = 0.040 mm, line-to-line spacing = 0.100 mm)	[124]
		cornstarch + dextran + gelatin	tissue engineering	A solid cylinder and 4 different porous cylindrical scaffolds (D = 12.5 mm, h = 12.5 mm)	Z402 3D printer, Zcorp	[125]

In all three cases, this technique has been used to create simple objects of micrometer size for cell culture experiments. Among these printing tests, the minimum value of lateral resolution, intended as the minimum diameter of the deposited drop, is between 10-60 μm, while the minimum layer thickness obtained is a hundred of nanometers.

Compared to the other AM technologies, vat photo-polymerization methods offer greater printing accuracy and reliability. The quality achieved by biobased resins were comparable to the printing performance of some of commercial resins.
Successful printing tests both via SLA and DLP have been performed using in almost all cases commercial printers. Both bulky and macroporous objects with complex shapes and high feature resolution have been realized. The overall dimensions ranged from millimeters to a few centimeters, and details with hundreds of micrometers size were well resolved. The most reported values of Z resolution are equal to or less than 100 μm.
As regards the DLW technology, three examples have been proposed. By means of custom printing systems, the fabrication of scaffolds and chess-like figures with dimensions from hundreds nanometers to millimeters was possible. In one case, some micrometric details have not been reproduced, while in the other two, the lateral resolution could reach 1 μm or even several hundreds nanometers.

For SLS process, commercial printers, sometimes modified to reduce the amount of raw powders, have been used to fabricate macroporous scaffolds in the centimeter scale. The critical issues which have been detected are the undesirable adhesion of loose particles, trapped powder in channels or macropores, unmelted particles and the penetration of the laser energy beyond the scan area. For these reasons, different results have been obtained resulting in medium to low printing resolutions.
A custom printing system and a commercial printer have been utilized in binder jetting manufacturing. Since this technique has been applied to the preparation of drug implants or tablets, constructs with mostly simple shapes, like cylinders, have been printed. The printed parts were in accordance with nominal dimensions and the model geometry.

Considering the resolution data reported in Table 3.1 and referring to oil-based polymers, in some cases the obtained resolutions are comparable to the typical resolution values achievable with the most common polymers. The cases referred to are FDM processing of PLA, PEF, cellulose derivatives, and PHA, all reported LDM studies, SLA processing of (meth)acrylates derived from soybean oil, vanillin, eugenol, guaiacol, cellulose derivative and rosin, DLP processing of (meth)acrylates derived from waste cooking oil, soybean oil, and poly(D,L-lactide), and DLW processing of acrylates from soybean oil and vanillin.
Certainly other efforts have to be done in order to expand the number of available polymers derived from renewable sources and to improve their printing resolution. Development of polymers that are environmentally sustainable and economically competitive is paramount for the success of additive manufacturing using biobased materials rather than those derived from petroleum.

References

[1] Piorkowska E. (2019). Overview of Biobased Polymers, in: "*Thermal Properties of Bio-Based Polymers, Advances in Polymer Science*", (Di Lorenzo M.L., Androsch R., Eds.) Springer International Publishing, Cham, pp. 1–35. [ISBN 978-3-030-39962-7]

[2] Gandini A., Naceur Belgacem M. (2012). The State of the Art of Polymers from Renewable Resource, in: "*Handbook of Biopolymers and Biodegradable Plastics: Properties, Processing and Applications*" (Ebnesajjad S.), Chap. 4. Elsevier Science & Technology Books, St. Louis, pp. 71-84. [ISBN 978-1-4557-3003-2]

[3] Wang, Z., Ganewatta, M.S., Tang, C. (2020). Sustainable polymers from biomass: Bridging chemistry with materials and processing. *Progress in Polymer Science* **101**, 101197. https://doi.org/10.1016/j.progpolymsci.2019.101197

[4] Yu, L., Dean, K., Li, L. (2006). Polymer blends and composites from renewable resources. *Progress in Polymer Science* **31**(6), 576–602. https://doi.org/10.1016/j.progpolymsci.2006.03.002

[5] Zong, A., Cao, H., Wang, F. (2012). Anticancer polysaccharides from natural resources: A review of recent research. *Carbohydrate Polymers* **90**(4), 1395–1410. https://doi.org/10.1016/j.carbpol.2012.07.026

[6] Taylor, W.R., May, A.C.W., Brown, N.P., Aszódi, A. (2001). Protein structure: geometry, topology and classification. *Rep. Prog. Phys*. **64**(4), 517–590. https://doi.org/10.1088/0034-4885/64/4/203

[7] Pollock, V. (2007). Proteins, in: "*The Comprehensive Pharmacology Reference"* (Enna, S.J., Bylund, D.B., Eds.), XPharm: Elsevier, New York, pp. 1–11. [ISBN 978-0-08-055232-3]

[8] Gupta, M.N. (2008). 2 - Purification of naturally occurring biomaterials, in: "*Natural-Based Polymers for Biomedical Applications*" (Reis, R.L., Neves, N.M., Mano, J.F., Gomes, M.E., Marques, A.P., Azevedo, H.S., Eds.), Woodhead Publishing Series in Biomaterials. Woodhead Publishing, pp. 54–84. [ISBN 978-1-84569-264-3]

[9] Thomas, A. (2000). Fats and Fatty Oils, in: *"Ullmann's Encyclopedia of Industrial Chemistry"* American Cancer Society. [ISBN 978-3-527-30673-2]

[10] Wolfmeier, U., Schmidt, H., Heinrichs, F.-L., Michalczyk, G., Payer, W., Dietsche, W., Boehlke, K., Hohner, G., Wildgruber, J. (2000). Waxes, in: "*Ullmann's Encyclopedia of Industrial Chemistry"* American Cancer Society. [ISBN 978-3-527-30673-2]

[11] Storz, H. (2014). Bio-based plastics: status, challenges and trends. *Landbauforschung Volkenrode* **63**, 321–332. https://doi.org/10.3220/LBF_2013_321-332

[12] Nakajima, H., Dijkstra, P., Loos, K. (2017). The Recent Developments in Biobased Polymers toward General and Engineering Applications: Polymers that are Upgraded from Biodegradable Polymers, Analogous to Petroleum-Derived Polymers, and Newly Developed. *Polymers* **9**(10), 523. https://doi.org/10.3390/polym9100523

[13] Wilbon, P.A., Chu, F., Tang, C. (2013). Progress in Renewable Polymers from Natural Terpenes, Terpenoids, and Rosin. *Macromolecular Rapid Communications* **34**(1), 8–37. https://doi.org/10.1002/marc.201200513

[14] Winnacker, M., Rieger, B. (2016). Biobased Polyamides: Recent Advances in Basic and Applied Research. *Macromolecular Rapid Communications* **37**(17), 1391–1413. https://doi.org/10.1002/marc.201600181

[15] Zacharopoulou, V., Lemonidou, A.A. (2018). Olefins from Biomass Intermediates: A Review. *Catalysts* **8**(1), 2. https://doi.org/10.3390/catal8010002

[16] Zhang, C., Garrison, T.F., Madbouly, S.A., Kessler, M.R. (2017). Recent advances in vegetable oil-based polymers and their composites. Progress in Polymer Science, Topical Volume on *Polymeric Biomaterials* **71**, 91–143. https://doi.org/10.1016/j.progpolymsci.2016.12.009

[17] Quirino, R.L., Monroe, K., Fleischer, C.H., Biswas, E., Kessler, M.R. (2020). Thermosetting polymers from renewable sources. *Polymer International,* 1-14. https://doi.org/10.1002/pi.6132

[18] Raquez, J.-M., Deléglise, M., Lacrampe, M.-F., Krawczak, P. (2010). Thermosetting (bio)materials derived from renewable resources: A critical review. Progress in Polymer Science, Topical Issue on *Biomaterials* **35**(4), 487–509. https://doi.org/10.1016/j.progpolymsci.2010.01.001

[19] Islam, M. R., Beg, M. D. H., & Jamari, S. S. (2014). Development of vegetable-oil-based polymers. *Journal of Applied Polymer Science*, **131**(18). https://doi.org/10.1002/app.40787

[20] Abraham, T. W., Höfer, R. (2012). Lipid-Based Polymer Building Blocks and Polymers, in: "*Polymer Science: A Comprehensive Reference"* (K. Matyjaszewski, M. Möller), Elsevier, pp 15–58. [ISBN 978-0-08-087862-1]

[21] Popa, E., Râpă, M., Popa, O. (2014). Biopolymers based on renewable resources - a review. *Scientific Bulletin. Series F. Biotechnologies* **18**, 188-195. [ISSN 2285-1364]

[22] Rajaguru, K., Karthikeyan, T., & Vijayan, V. (2020). Additive manufacturing – State of art. *Materials Today: Proceedings*, **21**, 628–633. https://doi.org/10.1016/j.matpr.2019.06.728

[23] Mohan, D., Teong, Z. K., Bakir, A. N., Sajab, M. S., & Kaco, H. (2020). Extending Cellulose-Based Polymers Application in Additive Manufacturing Technology: A Review of Recent Approaches. *Polymers*, **12**(9), 1876. https://doi.org/10.3390/polym12091876

[24] Han, T., Kundu, S., Nag, A., & Xu, Y. (2019). 3D Printed Sensors for Biomedical Applications: A Review. *Sensors*, **19**, 1706. https://doi.org/10.3390/s19071706

[25] Turner, B. N., Gold, S. A. (2015). A review of melt extrusion additive manufacturing processes: II. Materials, dimensional accuracy, and surface roughness. *Rapid Prototyping Journal*, **21**(3), 250–261. https://doi.org/10.1108/RPJ-02-2013-0017

[26] Vyavahare, S., Teraiya, S., Panghal, D., & Kumar, S. (2020). Fused deposition modelling: A review. *Rapid Prototyping Journal*, **26**(1), 176–201. https://doi.org/10.1108/RPJ-04-2019-0106

[27] Boschetto, A., Bottini, L. (2014). Accuracy prediction in fused deposition modeling. *The International Journal of Advanced Manufacturing Technology*, **73**(5), 913–928. https://doi.org/10.1007/s00170-014-5886-4

[28] Singh, R., Singh, S., Hashmi, M. S. J. (2016). Implant Materials and Their Processing Technologies, in: "*Reference Module in Materials Science and Materials Engineering*" Elsevier. [ISBN 978-0-12-803581-8]

[29] Harikrishnan, U., Soundarapandian, S. (2018). Fused Deposition Modelling based Printing of Full Complement Bearings. *Procedia Manufacturing*, ***26***, 818–825. https://doi.org/10.1016/j.promfg.2018.07.102

[30] Park, S. J., Lee, J. E., Lee, H. B., Park, J., Lee, N.-K., Son, Y., & Park, S.-H. (2020). 3D printing of bio-based polycarbonate and its potential applications in ecofriendly indoor manufacturing. *Additive Manufacturing*, **31**, 100974. https://doi.org/10.1016/j.addma.2019.100974

[31] https://www.sharebot.it/prodotti/

[32] Miao, S., Zhu, W., Castro, N. J., Leng, J., & Zhang, L. G. (2016). Four-Dimensional Printing Hierarchy Scaffolds with Highly Biocompatible Smart Polymers for Tissue Engineering Applications. *Tissue Engineering. Part C, Methods*, **22**(10), 952–963. https://doi.org/10.1089/ten.tec.2015.0542

[33] Cui, H., Zhu, W., Holmes, B., & Zhang, L. G. (2016). Biologically Inspired Smart Release System Based on 3D Bioprinted Perfused Scaffold for Vascularized Tissue Regeneration. *Advanced Science*, **3**(8), 1600058. https://doi.org/10.1002/advs.201600058

[34] Rankin, T. M., Giovinco, N. A., Cucher, D. J., Watts, G., Hurwitz, B., & Armstrong, D. G. (2014). Three-dimensional printing surgical instruments: Are we there yet? *Journal of Surgical Research*, **189**(2), 193–197. https://doi.org/10.1016/j.jss.2014.02.020

[35] Park, S. J., Lee, J. E., Lee, H. B., Park, J., Lee, N.-K., Son, Y., & Park, S.-H. (2020). 3D printing of bio-based polycarbonate and its potential applications in ecofriendly indoor manufacturing. *Additive Manufacturing*, **31**, 100974. https://doi.org/10.1016/j.addma.2019.100974

[36] Kucherov, F. A., Gordeev, E. G., Kashin, A. S., & Ananikov, V. P. (2017). Three-Dimensional Printing with Biomass-Derived PEF for Carbon-Neutral Manufacturing. *Angewandte Chemie International Edition*, **56**(50), 15931–15935. https://doi.org/10.1002/anie.201708528

[37] Chaunier, L., Leroy, E., Valle, G. D., Dalgalarrondo, M., Bakan, B., Marion, D., Madec, B., & Lourdin, D. (2017). 3D printing of maize protein by fused deposition modeling. *AIP Conference Proceedings*, **1914**(1), 190003. https://doi.org/10.1063/1.5016792

[38] Yang, J., An, X., Liu, L., Tang, S., Cao, H., Xu, Q., & Liu, H. (2020). Cellulose, hemicellulose, lignin, and their derivatives as multi-components of bio-based feedstocks for 3D printing. *Carbohydrate Polymers*, **250**, 116881. https://doi.org/10.1016/j.carbpol.2020.116881

[39] Kempin, W., Franz, C., Koster, L.-C., Schneider, F., Bogdahn, M., Weitschies, W., & Seidlitz, A. (2017). Assessment of different polymers and drug loads for fused deposition modeling of drug loaded implants. *European Journal of Pharmaceutics and Biopharmaceutics*, **115**, 84–93. https://doi.org/10.1016/j.ejpb.2017.02.014

[40] Melocchi, A., Parietti, F., Loreti, G., Maroni, A., Gazzaniga, A., & Zema, L. (2015). 3D printing by fused deposition modeling (FDM) of a swellable/erodible capsular device for oral pulsatile release of drugs. *Journal of Drug Delivery Science and Technology*, **30**, 360–367. https://doi.org/10.1016/j.jddst.2015.07.016

[41] Melocchi, A., Parietti, F., Maroni, A., Foppoli, A., Gazzaniga, A., & Zema, L. (2016). Hot-melt extruded filaments based on pharmaceutical grade polymers for 3D printing by fused deposition modeling. *International Journal of Pharmaceutics*, **509**(1), 255–263. https://doi.org/10.1016/j.ijpharm.2016.05.036

[42] Goyanes, A., Fina, F., Martorana, A., Sedough, D., Gaisford, S., & Basit, A. W. (2017). Development of modified release 3D printed tablets (printlets) with pharmaceutical excipients using additive manufacturing. *International Journal of Pharmaceutics*, **527**(1), 21–30. https://doi.org/10.1016/j.ijpharm.2017.05.021

[43] Zhang, J., Feng, X., Patil, H., Tiwari, R. V., & Repka, M. A. (2017). Coupling 3D printing with hot-melt extrusion to produce controlled-release tablets. *International Journal of Pharmaceutics*, **519**(1), 186–197. https://doi.org/10.1016/j.ijpharm.2016.12.049

[44] Yang, Y., Wang, H., Li, H., Ou, Z., & Yang, G. (2018). 3D printed tablets with internal scaffold structure using ethyl cellulose to achieve sustained ibuprofen release. *European Journal of Pharmaceutical Sciences*, **115**, 11–18. https://doi.org/10.1016/j.ejps.2018.01.005

[45] Paggi, R. A., Salmoria, G. V., Ghizoni, G. B., de Medeiros Back, H., & de Mello Gindri, I. (2019). Structure and mechanical properties of 3D-printed cellulose tablets by fused deposition modeling. *The International Journal of Advanced Manufacturing Technology*, **100**(9), 2767–2774. https://doi.org/10.1007/s00170-018-2830-z

[46] Xu, W., Pranovich, A., Uppstu, P., Wang, X., Kronlund, D., Hemming, J., Öblom, H., Moritz, N., Preis, M., Sandler, N., Willför, S., & Xu, C. (2018). Novel biorenewable

composite of wood polysaccharide and polylactic acid for three dimensional printing. *Carbohydrate Polymers*, **187**, 51–58. https://doi.org/10.1016/j.carbpol.2018.01.069

[47] Murphy, C. A., & Collins, M. N. (2018). Microcrystalline cellulose reinforced polylactic acid biocomposite filaments for 3D printing. *Polymer Composites*, **39**(4), 1311–1320. https://doi.org/10.1002/pc.24069

[48] Filgueira, D., Holmen, S., Melbø, J. K., Moldes, D., Echtermeyer, A. T., & Chinga-Carrasco, G. (2017). Enzymatic-Assisted Modification of Thermomechanical Pulp Fibers To Improve the Interfacial Adhesion with Poly(lactic acid) for 3D Printing. *ACS Sustainable Chemistry & Engineering*, **5**(10), 9338–9346. https://doi.org/10.1021/acssuschemeng.7b02351

[49] Filgueira, D., Holmen, S., Melbø, J. K., Moldes, D., Echtermeyer, A. T., & Chinga-Carrasco, G. (2018). 3D Printable Filaments Made of Biobased Polyethylene Biocomposites. *Polymers*, **10**(3), 314. https://doi.org/10.3390/polym10030314

[50] Wu, C.-S., Liao, H.-T., & Cai, Y.-X. (2017). Characterisation, biodegradability and application of palm fibre-reinforced polyhydroxyalkanoate composites. *Polymer Degradation and Stability*, **140**, 55–63. https://doi.org/10.1016/j.polymdegradstab.2017.04.016

[51] Xu, W., Wang, X., Sandler, N., Willför, S., & Xu, C. (2018). Three-Dimensional Printing of Wood-Derived Biopolymers: A Review Focused on Biomedical Applications. *ACS Sustainable Chemistry & Engineering*, **6**(5), 5663–5680. https://doi.org/10.1021/acssuschemeng.7b03924

[52] Murphy, S. V., Atala, A. (2014). 3D bioprinting of tissues and organs. *Nature Biotechnology*, **32**(8), 773–785. https://doi.org/10.1038/nbt.2958

[53] Guvendiren, M., Molde, J., Soares, R. M. D., & Kohn, J. (2016). Designing Biomaterials for 3D Printing. *ACS Biomaterials Science & Engineering*, **2**(10), 1679–1693. https://doi.org/10.1021/acsbiomaterials.6b00121

[54] Chia, H. N., & Wu, B. M. (2015). Recent advances in 3D printing of biomaterials. *Journal of Biological Engineering*, **9**(1), 4. https://doi.org/10.1186/s13036-015-0001-4

[55] Li, L., Lin, Q., Tang, M., Duncan, A. J. E., & Ke, C. (2019). Advanced Polymer Designs for Direct-Ink-Write 3D Printing. *Chemistry – A European Journal*, **25**(46), 10768–10781. https://doi.org/10.1002/chem.201900975

[56] Wang, Q., Sun, J., Yao, Q., Ji, C., Liu, J., & Zhu, Q. (2018). 3D printing with cellulose materials. *Cellulose*, **25**(8), 4275–4301. https://doi.org/10.1007/s10570-018-1888-y

[57] Cao, D., Xing, Y., Tantratian, K., Wang, X., Ma, Y., Mukhopadhyay, A., Cheng, Z., Zhang, Q., Jiao, Y., Chen, L., & Zhu, H. (2019). 3D Printed High-Performance Lithium Metal Microbatteries Enabled by Nanocellulose. *Advanced Materials*, **31**(14), 1807313. https://doi.org/10.1002/adma.201807313

[58] Rees, A., Powell, L. C., Chinga-Carrasco, G., Gethin, D. T., Syverud, K., Hill, K. E., & Thomas, D. W. (2015, maggio 19). 3D Bioprinting of Carboxymethylated-Periodate Oxidized Nanocellulose Constructs for Wound Dressing Applications. *BioMed Research International*, **2015**, 1-7. https://doi.org/10.1155/2015/925757

[59] Siqueira, G., Kokkinis, D., Libanori, R., Hausmann, M. K., Gladman, A. S., Neels, A., Tingaut, P., Zimmermann, T., Lewis, J. A., & Studart, A. R. (2017). Cellulose Nanocrystal Inks for 3D Printing of Textured Cellular Architectures. *Advanced Functional Materials*, **27**(12), 1604619. https://doi.org/10.1002/adfm.201604619

[60] Li, V. C.-F., Dunn, C. K., Zhang, Z., Deng, Y., & Qi, H. J. (2017). Direct Ink Write (DIW) 3D Printed Cellulose Nanocrystal Aerogel Structures. *Scientific Reports*, **7**(1), 8018. https://doi.org/10.1038/s41598-017-07771-y

[61] Khaled, S. A., Burley, J. C., Alexander, M. R., Yang, J., & Roberts, C. J. (2015). 3D printing of five-in-one dose combination polypill with defined immediate and sustained release

profiles. *Journal of Controlled Release*, **217**, 308–314. https://doi.org/10.1016/j.jconrel.2015.09.028

[62] Pattinson, S. W., & Hart, A. J. (2017). Additive Manufacturing of Cellulosic Materials with Robust Mechanics and Antimicrobial Functionality. *Advanced Materials Technologies*, **2**(4), 1600084. https://doi.org/10.1002/admt.201600084

[63] Tenhunen, T.-M., Moslemian, O., Kammiovirta, K., Harlin, A., Kääriäinen, P., Österberg, M., Tammelin, T., & Orelma, H. (2018). Surface tailoring and design-driven prototyping of fabrics with 3D-printing: An all-cellulose approach. *Materials & Design*, **140**, 409–419. https://doi.org/10.1016/j.matdes.2017.12.012

[64] Bahçegül, E. G., Bahçegül, E., & Özkan, N. (2020). 3D Printing of Hemicellulosic Biopolymers Extracted from Lignocellulosic Agricultural Wastes. *ACS Applied Polymer Materials*, **2**(7), 2622–2632. https://doi.org/10.1021/acsapm.0c00256

[65] Landers, R., Hübner, U., Schmelzeisen, R., & Mülhaupt, R. (2002). Rapid prototyping of scaffolds derived from thermoreversible hydrogels and tailored for applications in tissue engineering. *Biomaterials*, **23**(23), 4437–4447. https://doi.org/10.1016/S0142-9612(02)00139-4

[66] Schütz, K., Placht, A.-M., Paul, B., Brüggemeier, S., Gelinsky, M., & Lode, A. (2017). Three-dimensional plotting of a cell-laden alginate/methylcellulose blend: Towards biofabrication of tissue engineering constructs with clinically relevant dimensions. *Journal of Tissue Engineering and Regenerative Medicine*, **11**(5), 1574–1587. https://doi.org/10.1002/term.2058

[67] Poldervaart, M. T., Goversen, B., Ruijter, M. de, Abbadessa, A., Melchels, F. P. W., Öner, F. C., Dhert, W. J. A., Vermonden, T., & Alblas, J. (2017). 3D bioprinting of methacrylated hyaluronic acid (MeHA) hydrogel with intrinsic osteogenicity. *PLOS ONE*, **12**(6), e0177628. https://doi.org/10.1371/journal.pone.0177628

[68] Elviri, L., Foresti, R., Bergonzi, C., Zimetti, F., Marchi, C., Bianchera, A., Bernini, F., Silvestri, M., & Bettini, R. (2017). Highly defined 3D printed chitosan scaffolds featuring improved cell growth. *Biomedical Materials*, **12**(4), 045009. https://doi.org/10.1088/1748-605X/aa7692

[69] Rhee, S., Puetzer, J. L., Mason, B. N., Reinhart-King, C. A., & Bonassar, L. J. (2016). 3D Bioprinting of Spatially Heterogeneous Collagen Constructs for Cartilage Tissue Engineering. *ACS Biomaterials Science & Engineering*, **2**(10), 1800–1805. https://doi.org/10.1021/acsbiomaterials.6b00288

[70] Billiet, T., Gevaert, E., De Schryver, T., Cornelissen, M., & Dubruel, P. (2014). The 3D printing of gelatin methacrylamide cell-laden tissue-engineered constructs with high cell viability. *Biomaterials*, **35**(1), 49–62. https://doi.org/10.1016/j.biomaterials.2013.09.078

[71] Park, T. Y., Yang, Y. J., Ha, D.-H., Cho, D.-W., & Cha, H. J. (2019). Marine-derived natural polymer-based bioprinting ink for biocompatible, durable, and controllable 3D constructs. *Biofabrication*, **11**(3), 035001. https://doi.org/10.1088/1758-5090/ab0c6f

[72] Parker, S. T., Domachuk, P., Amsden, J., Bressner, J., Lewis, J. A., Kaplan, D. L., & Omenetto, F. G. (2009). Biocompatible Silk Printed Optical Waveguides. *Advanced Materials*, **21**(23), 2411–2415. https://doi.org/10.1002/adma.200801580

[73] Liu, Y., Liu, D., Wei, G., Ma, Y., Bhandari, B., & Zhou, P. (2018). 3D printed milk protein food simulant: Improving the printing performance of milk protein concentration by incorporating whey protein isolate. *Innovative Food Science & Emerging Technologies*, *49*, 116–126. https://doi.org/10.1016/j.ifset.2018.07.018

[74] Gudapati, H., Dey, M., & Ozbolat, I. (2016). A comprehensive review on droplet-based bioprinting: Past, present and future. *Biomaterials*, **102**, 20–42. https://doi.org/10.1016/j.biomaterials.2016.06.012

[75] Aguilar-de-Leyva, Á., Linares, V., Casas, M., & Caraballo, I. (2020). 3D Printed Drug Delivery Systems Based on Natural Products. *Pharmaceutics*, **12**(7), 620. https://doi.org/10.3390/pharmaceutics12070620

[76] Nishiyama, Y., Nakamura, M., Henmi, C., Yamaguchi, K., Mochizuki, S., Nakagawa, H., & Takiura, K. (2009). Development of a Three-Dimensional Bioprinter: Construction of Cell Supporting Structures Using Hydrogel and State-Of-The-Art Inkjet Technology. *Journal of Biomechanical Engineering*, **131**(3). https://doi.org/10.1115/1.3002759

[77] Roth, E. A., Xu, T., Das, M., Gregory, C., Hickman, J. J., & Boland, T. (2004). Inkjet printing for high-throughput cell patterning. *Biomaterials*, **25**(17), 3707–3715. https://doi.org/10.1016/j.biomaterials.2003.10.052

[78] Suntivich, R., Drachuk, I., Calabrese, R., Kaplan, D. L., & Tsukruk, V. V. (2014). Inkjet Printing of Silk Nest Arrays for Cell Hosting. *Biomacromolecules*, **15**(4), 1428–1435. https://doi.org/10.1021/bm500027c

[79] Bose, S., Ke, D., Sahasrabudhe, H., & Bandyopadhyay, A. (2018). Additive manufacturing of biomaterials. *Progress in Materials Science*, **93**, 45–111. https://doi.org/10.1016/j.pmatsci.2017.08.003

[80] Ngo, T. D., Kashani, A., Imbalzano, G., Nguyen, K. T. Q., & Hui, D. (2018). Additive manufacturing (3D printing): A review of materials, methods, applications and challenges. *Composites Part B: Engineering*, **143**, 172–196. https://doi.org/10.1016/j.compositesb.2018.02.012

[81] Semba, J. A., Mieloch, A. A., & Rybka, J. D. (2020). Introduction to the state-of-the-art 3D bioprinting methods, design, and applications in orthopedics. *Bioprinting*, **18**, e00070. https://doi.org/10.1016/j.bprint.2019.e00070

[82] Melchels, F. P. W., Feijen, J., & Grijpma, D. W. (2010). A review on stereolithography and its applications in biomedical engineering. *Biomaterials*, **31**(24), 6121–6130. https://doi.org/10.1016/j.biomaterials.2010.04.050

[83] Sutton, J. T., Rajan, K., Harper, D. P., & Chmely, S. C. (2018). Lignin-Containing Photoactive Resins for 3D Printing by Stereolithography. *ACS Applied Materials & Interfaces*, **10**(42), 36456–36463. https://doi.org/10.1021/acsami.8b13031

[84] Skliutas, E., Kašėtaitė, S., Grigalevičiūtė, G., Jonušauskas, L., Rekštytė, S., Ostrauskaitė, J., & Malinauskas, M. (2017). Bioresists from renewable resources as sustainable photoresins for 3D laser microlithography: Material synthesis, cross-linking rate and characterization of the structures. *Advanced Fabrication Technologies for Micro/Nano Optics and Photonics X*, **10115**, 1011514. https://doi.org/10.1117/12.2249600

[85] Bassett, A. W., Honnig, A. E., Breyta, C. M., Dunn, I. C., La Scala, J. J., & Stanzione, J. F. (2020). Vanillin-Based Resin for Additive Manufacturing. *ACS Sustainable Chemistry & Engineering*, **8**(14), 5626–5635. https://doi.org/10.1021/acssuschemeng.0c00159

[86] Miao, S., Zhu, W., Castro, N. J., Nowicki, M., Zhou, X., Cui, H., Fisher, J. P., & Zhang, L. G. (2016). 4D printing smart biomedical scaffolds with novel soybean oil epoxidized acrylate. *Scientific Reports*, **6**(1), 27226. https://doi.org/10.1038/srep27226

[87] Voet, V. S. D., Strating, T., Schnelting, G. H. M., Dijkstra, P., Tietema, M., Xu, J., Woortman, A. J. J., Loos, K., Jager, J., & Folkersma, R. (2018). Biobased Acrylate Photocurable Resin Formulation for Stereolithography 3D Printing. *ACS Omega*, **3**(2), 1403–1408. https://doi.org/10.1021/acsomega.7b01648

[88] Silbert, S. D., Simpson, P., Setien, R., Holthaus, M., La Scala, J., Ulven, C. A., & Webster, D. C. (2020). Exploration of Bio-Based Functionalized Sucrose Ester Resins for Additive Manufacturing via Stereolithography. *ACS Applied Polymer Materials*, **2**(7), 2910–2918. https://doi.org/10.1021/acsapm.0c00417

[89] Patrick T. Smith, benjaporn narupai, Jonathan H. Tsui, S. Cem Millik, Ryan T. shafranek, Deok-Ho Kim, Alshakim Nelson (2019). Additive Manufacturing of Bovine Serum Albumin-Based Hydrogels and Bioplastics. *ChemRxiv*.

[90] Ding, R., Du, Y., Goncalves, R. B., Francis, L. F., & Reineke, T. M. (2019). Sustainable near UV-curable acrylates based on natural phenolics for stereolithography 3D printing. *Polymer Chemistry*, **10**(9), 1067–1077. https://doi.org/10.1039/C8PY01652F

[91] Lu, C., Wang, C., Yu, J., Wang, J., & Chu, F. (2020). Two-Step 3 D-Printing Approach toward Sustainable, Repairable, Fluorescent Shape-Memory Thermosets Derived from Cellulose and Rosin. *ChemSusChem*, **13**(5), 893–902. https://doi.org/10.1002/cssc.201902191

[92] Cui, H., Zhu, W., Nowicki, M., Zhou, X., Khademhosseini, A., & Zhang, L. G. (2016). Hierarchical Fabrication of Engineered Vascularized Bone Biphasic Constructs via Dual 3D Bioprinting: Integrating Regional Bioactive Factors into Architectural Design. *Advanced Healthcare Materials*, **5**(17), 2174–2181. https://doi.org/10.1002/adhm.201600505

[93] Berry, D. B., Yu, C., & Chen, S. (2020). Biofabricated three-dimensional tissue models, in: "*Principles of Tissue Engineering (Fifth Edition)"* (R. Lanza, R. Langer, J. P. Vacanti, & A. Atala), Chap. 75, Academic Press, pagg. 1417–1441. [ISBN 978-0-12-818422-6]

[94] Huh, J. T., Yoo, J. J., Atala, A., & Lee, S. J. (2020). Three-dimensional bioprinting for tissue engineering, , in: "*Principles of Tissue Engineering (Fifth Edition)"* (R. Lanza, R. Langer, J. P. Vacanti, & A. Atala), Chap. 74, Academic Press, pagg. 1391–1415. [ISBN 978-0-12-818422-6]

[95] Ko, D. H., Gyak, K. W., & Kim, D. (2017). Emerging Microreaction Systems Based on 3D Printing Techniques and Separation Technologies. *Journal of Flow Chemistry*, **7**, 1–10. https://doi.org/10.1556/1846.2017.00013

[96] Wu, B., Sufi, A., Ghosh Biswas, R., Hisatsune, A., Moxley-Paquette, V., Ning, P., Soong, R., Dicks, A. P., & Simpson, A. J. (2020). Direct Conversion of McDonald's Waste Cooking Oil into a Biodegradable High-Resolution 3D-Printing Resin. *ACS Sustainable Chemistry & Engineering*, **8**(2), 1171–1177. https://doi.org/10.1021/acssuschemeng.9b06281

[97] Skliutas, E., Lebedevaite, M., Kasetaite, S., Rekštytė, S., Lileikis, S., Ostrauskaite, J., & Malinauskas, M. (2020). A Bio-Based Resin for a Multi-Scale Optical 3D Printing. *Scientific Reports*, **10**(1), 9758. https://doi.org/10.1038/s41598-020-66618-1

[98] Guit, J., Tavares, M. B. L., Hul, J., Ye, C., Loos, K., Jager, J., Folkersma, R., & Voet, V. S. D. (2020). Photopolymer Resins with Biobased Methacrylates Based on Soybean Oil for Stereolithography. *ACS Applied Polymer Materials*, **2**(2), 949–957. https://doi.org/10.1021/acsapm.9b01143

[99] Melchels, F. P. W., Feijen, J., & Grijpma, D. W. (2009). A poly(d,l-lactide) resin for the preparation of tissue engineering scaffolds by stereolithography. *Biomaterials*, **30**(23), 3801–3809. https://doi.org/10.1016/j.biomaterials.2009.03.055

[100] Melilli, G., Carmagnola, I., Tonda-Turo, C., Pirri, F., Ciardelli, G., Sangermano, M., Hakkarainen, M., & Chiappone, A. (2020). DLP 3D Printing Meets Lignocellulosic Biopolymers: Carboxymethyl Cellulose Inks for 3D Biocompatible Hydrogels. *Polymers*, **12**(8), 1655. https://doi.org/10.3390/polym12081655

[101] Kim, S. H., Yeon, Y. K., Lee, J. M., Chao, J. R., Lee, Y. J., Seo, Y. B., Sultan, M. T., Lee, O. J., Lee, J. S., Yoon, S., Hong, I.-S., Khang, G., Lee, S. J., Yoo, J. J., & Park, C. H. (2018). Precisely printable and biocompatible silk fibroin bioink for digital light processing 3D printing. *Nature Communications*, **9**(1), 1620. https://doi.org/10.1038/s41467-018-03759-y

[102] Placone, J. K., Navarro, J., Laslo, G. W., Lerman, M. J., Gabard, A. R., Herendeen, G. J., Falco, E. E., Tomblyn, S., Burnett, L., & Fisher, J. P. (2017). Development and Characterization of a 3D Printed, Keratin-Based Hydrogel. *Annals of Biomedical Engineering*, **45**(1), 237–248. https://doi.org/10.1007/s10439-016-1621-7

[103] Geng, Q., Wang, D., Chen, P., & Chen, S.-C. (2019). Ultrafast multi-focus 3-D nano-fabrication based on two-photon polymerization. *Nature Communications*, **10**(1), 2179. https://doi.org/10.1038/s41467-019-10249-2

[104] Xing, J.-F., Zheng, M.-L., & Duan, X.-M. (2015). Two-photon polymerization microfabrication of hydrogels: An advanced 3D printing technology for tissue engineering and drug delivery. *Chem. Soc. Rev.*, **44**. https://doi.org/10.1039/C5CS00278H

[105] Nguyen, A. K., & Narayan, R. J. (2017). Two-photon polymerization for biological applications. *Materials Today*, **20**(6), 314–322. https://doi.org/10.1016/j.mattod.2017.06.004

[106] Wu, S., Serbin, J., & Gu, M. (2006). Two-photon polymerisation for three-dimensional micro-fabrication. *Journal of Photochemistry and Photobiology A: Chemistry*, **181**(1), 1–11. https://doi.org/10.1016/j.jphotochem.2006.03.004

[107] Navaruckiene, A., Skliutas, E., Kasetaite, S., Rekštytė, S., Raudoniene, V., Bridziuviene, D., Malinauskas, M., & Ostrauskaite, J. (2020). Vanillin Acrylate-Based Resins for Optical 3D Printing. *Polymers*, **12**(2), 397. https://doi.org/10.3390/polym12020397

[108] Lebedevaite, M., Ostrauskaite, J., Skliutas, E., & Malinauskas, M. (2019). Photoinitiator Free Resins Composed of Plant-Derived Monomers for the Optical μ-3D Printing of Thermosets. *Polymers*, **11**(1), 116. https://doi.org/10.3390/polym11010116

[109] Shirazi, S. F. S., Gharehkhani, S., Mehrali, M., Yarmand, H., Metselaar, H. S. C., Kadri, N. A., & Osman, N. A. A. (2015). A review on powder-based additive manufacturing for tissue engineering: Selective laser sintering and inkjet 3D printing. *Science and Technology of Advanced Materials*, **16**(3), 033502. https://doi.org/10.1088/1468-6996/16/3/033502

[110] Yuan, S., Shen, F., Chua, C. K., & Zhou, K. (2019). Polymeric composites for powder-based additive manufacturing: Materials and applications. *Progress in Polymer Science*, **91**, 141–168. https://doi.org/10.1016/j.progpolymsci.2018.11.001

[111] Leong, K.-F., Liu, D., Chua, C.-K. (2014). Tissue Engineering Applications of Additive Manufacturing, in: "*Comprehensive Materials Processing"* (S. Hashmi, G. F. Batalha, C. J. Van Tyne, & B. Yilbas), Chap. 10.09, Elsevier, pag. 251–264. [ISBN 978-0-08-096533-8]

[112] Chiulan (Negru), I., Frone, A., Brandabur, C., & Panaitescu, D. (2017). Recent Advances in 3D Printing of Aliphatic Polyesters. *Bioengineering*, **5**, 2. https://doi.org/10.3390/bioengineering5010002

[113] Oliveira, M. F., Maia, I. A., Noritomi, P. Y., Nargi, G. C., Silva, J. V. L., Ferreira, B. M. P., & Duek, E. A. R. (2007). Construção de Scaffolds para engenharia tecidual utilizando prototipagem rápida. *Matéria (Rio de Janeiro)*, **12**(2), 373–382. https://doi.org/10.1590/S1517-70762007000200016

[114] Pereira, T. F., Oliveira, M. F., Maia, I. A., Silva, J. V. L., Costa, M. F., & Thiré, R. M. S. M. (2012). 3D Printing of Poly(3-hydroxybutyrate) Porous Structures Using Selective Laser Sintering. *Macromolecular Symposia*, **319**(1), 64–73. https://doi.org/10.1002/masy.201100237

[115] Duan, B., Cheung, W. L., & Wang, M. (2011). Optimized fabrication of Ca–P/PHBV nanocomposite scaffolds via selective laser sintering for bone tissue engineering. *Biofabrication*, **3**(1), 015001. https://doi.org/10.1088/1758-5082/3/1/015001

[116] Duan, B., & Wang, M. (2010). Customized Ca–P/PHBV nanocomposite scaffolds for bone tissue engineering: Design, fabrication, surface modification and sustained release of

growth factor. *Journal of the Royal Society Interface*, **7**(Suppl 5), S615–S629. https://doi.org/10.1098/rsif.2010.0127.focus

[117] Bai, J., Goodridge, R. D., Hague, R. J. M., & Okamoto, M. (2017). Processing and characterization of a polylactic acid/nanoclay composite for laser sintering. *Polymer Composites*, **38**(11), 2570–2576. https://doi.org/10.1002/pc.23848

[118] Zhou, W. Y., Lee, S. H., Wang, M., Cheung, W. L., & Ip, W. Y. (2008). Selective laser sintering of porous tissue engineering scaffolds from poly(l-lactide)/carbonated hydroxyapatite nanocomposite microspheres. *Journal of Materials Science: Materials in Medicine*, **19**(7), 2535–2540. https://doi.org/10.1007/s10856-007-3089-3

[119] Van den Eynde, M., & Van Puyvelde, P. (2018). 3D Printing of Poly(lactic acid), in: "*Industrial Applications of Poly(lactic acid)",* (M. L. Di Lorenzo & R. Androsch), Springer International Publishing, pag. 139–158. [ISBN 978-3-319-75459-8]

[120] Antonov, E. N., Bagratashvili, V. N., Whitaker, M. J., Barry, J. J. A., Shakesheff, K. M., Konovalov, A. N., Popov, V. K., & Howdle, S. M. (2005). Three-Dimensional Bioactive and Biodegradable Scaffolds Fabricated by Surface-Selective Laser Sintering. *Advanced Materials*, **17**(3), 327–330. https://doi.org/10.1002/adma.200400838

[121] http://www.custompartnet.com/wu/3d-printing

[122] Huang, W., Zheng, Q., Sun, W., Xu, H., & Yang, X. (2007). Levofloxacin implants with predefined microstructure fabricated by three-dimensional printing technique. *International Journal of Pharmaceutics*, **339**(1), 33–38. https://doi.org/10.1016/j.ijpharm.2007.02.021

[123] Wu, G., Wu, W., Zheng, Q., Li, J., Zhou, J., & Hu, Z. (2014). Experimental study of PLLA/INH slow release implant fabricated by three dimensional printing technique and drug release characteristics in vitro. *BioMedical Engineering OnLine*, **13**(1), 97. https://doi.org/10.1186/1475-925X-13-97

[124] Yu, D. G., Yang, X. L., Huang, W. D., Liu, J., Wang, Y. G., & Xu, H. (2007). Tablets With Material Gradients Fabricated by Three-Dimensional Printing. *Journal of Pharmaceutical Sciences*, **96**(9), 2446–2456. https://doi.org/10.1002/jps.20864

[125] Lam, C. X. F., Mo, X. M., Teoh, S. H., & Hutmacher, D. W. (2002). Scaffold development using 3D printing with a starch-based polymer. *Materials Science and Engineering: C*, **20**(1), 49–56. https://doi.org/10.1016/S0928-4931(02)00012-7

Appendix A

Categories of Additive Manufacturing according to ASTM [23]:

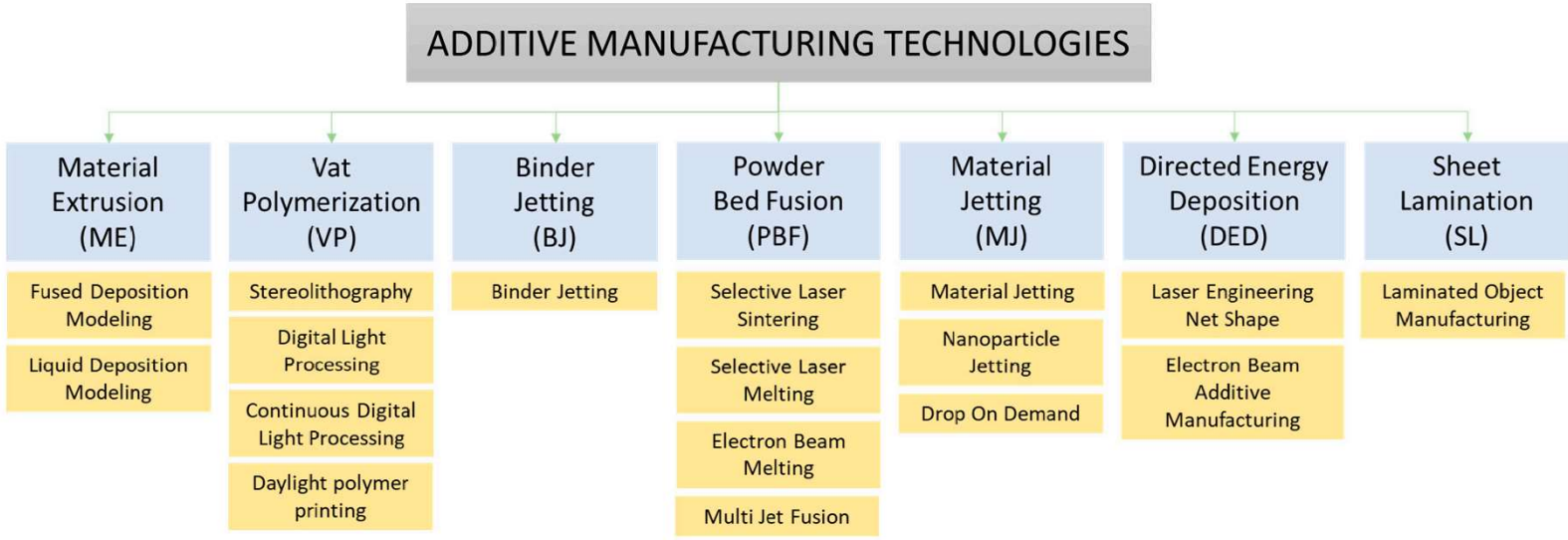

Appendix B

Chemical structures of mentioned biobased polymers/monomers:

Fused Deposition Modeling

- Polylactic acid (PLA)

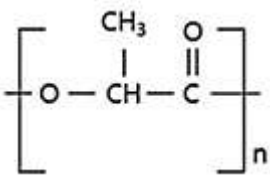

- Bio-polycarbonate (bio-PC)

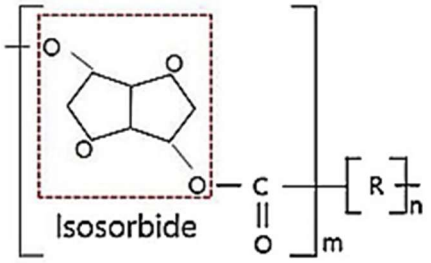

- Polyethylene-2,5-furandicarboxylate (PEF)

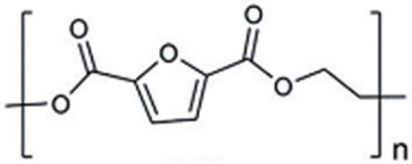

- Cellulose

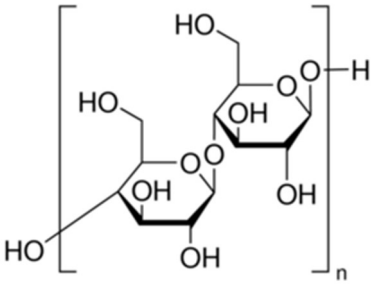

- Ethylcellulose

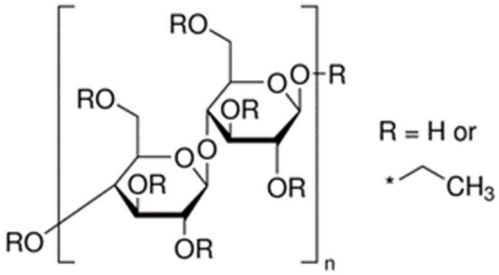

- Hydroxypropyl cellulose

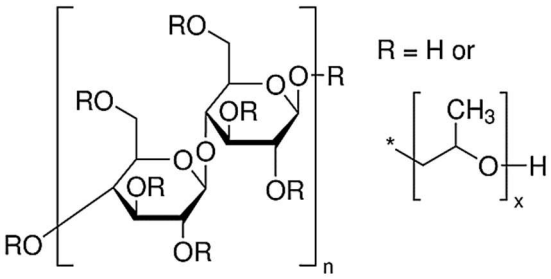

- Hydroxypropyl methyl cellulose

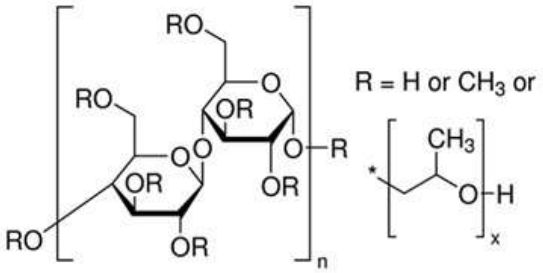

- Cellulose acetate

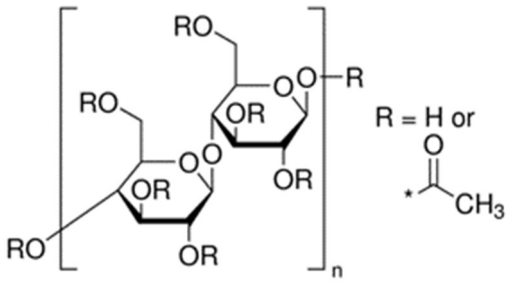

- Galactoglucomannan

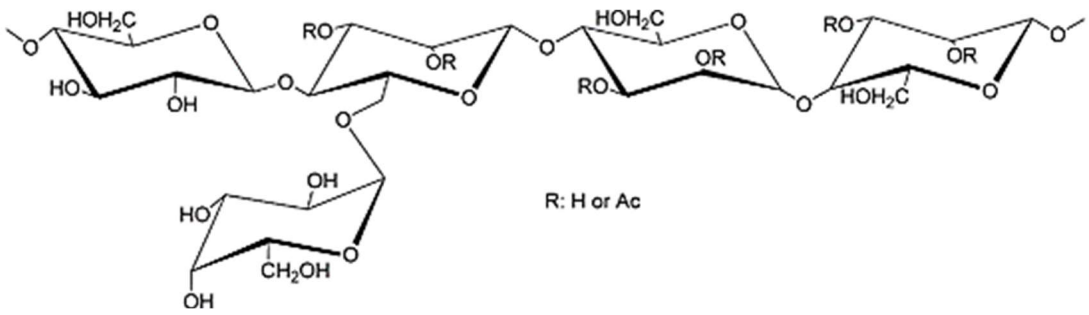

- Polyhydroxyalkanoates

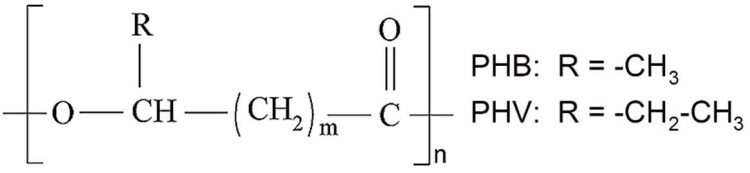

Liquid Deposition Modeling

- Agar

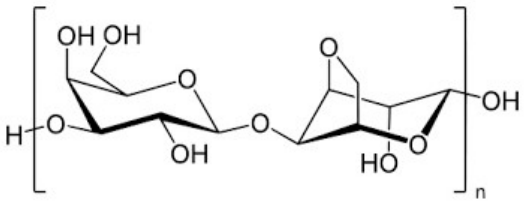

- Sodium alginate

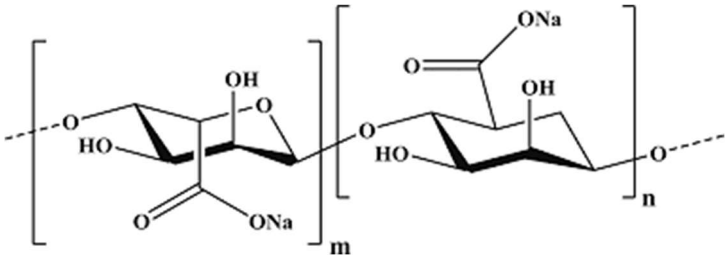

- Hyaluronic acid

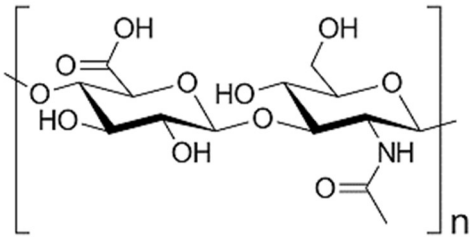

- Methacrylated hyaluronic acid

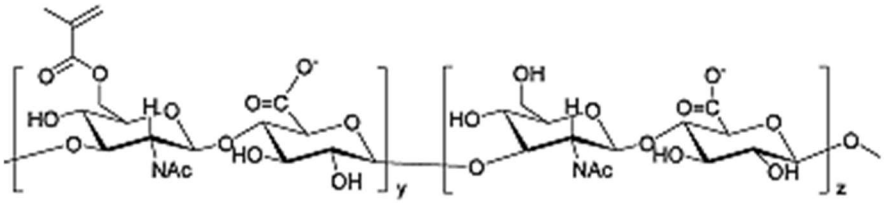

- Chitosan

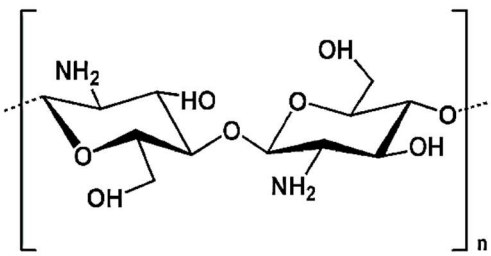

Stereolithography

- Epoxidized linseed oil

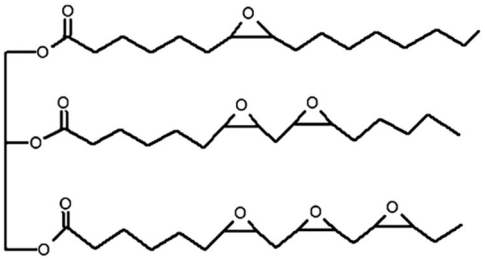

- Soybean oil epoxidized acrylate

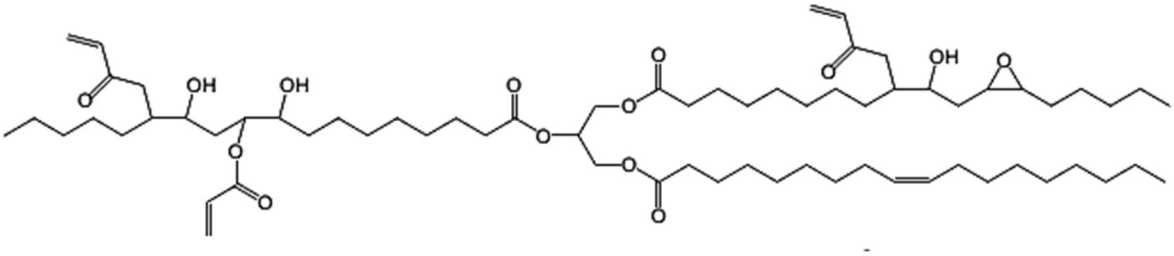

- Isobornyl acrylate

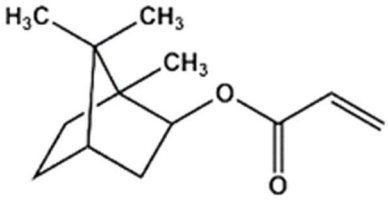

- 1,10-decanediol diacrylate

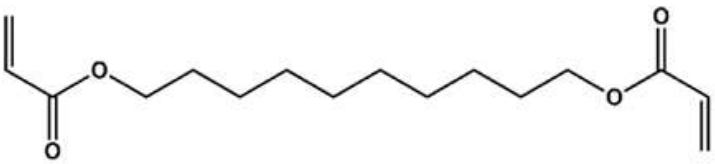

- Pentaerythritol tetraacrylate

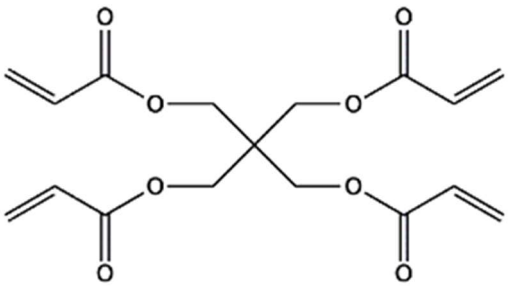

- Epoxidized sucrose soyate

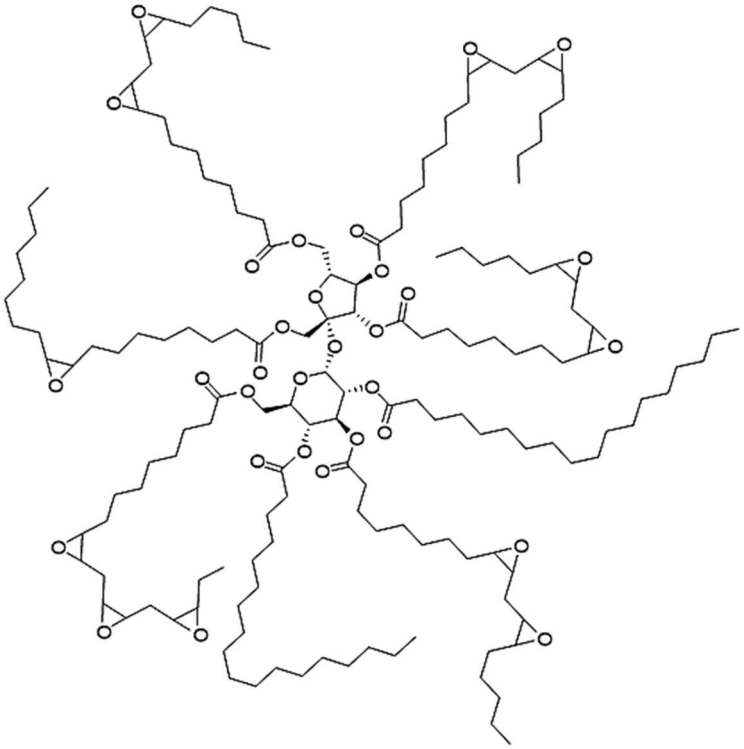

- Methacrylated vanillin

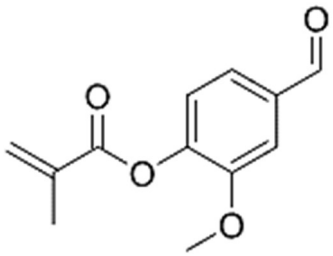

- 3,6-dioxa-1,8-octanedithiol eugenol acrylate

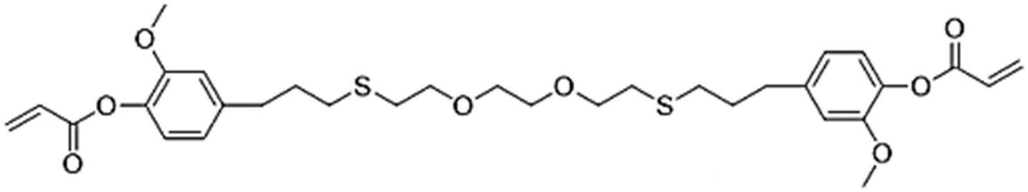

- Guaiacol methacrylate

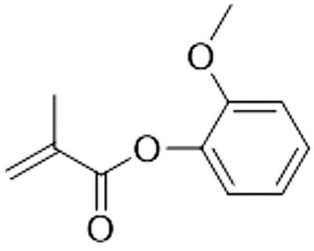

- 2-hydroxyethyl acrylate

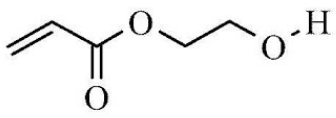

- Rosin derived monomer (DAGMA)

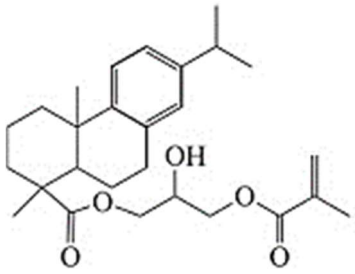

Direct Light Projection

- Methacrylated epoxidized soybean oil

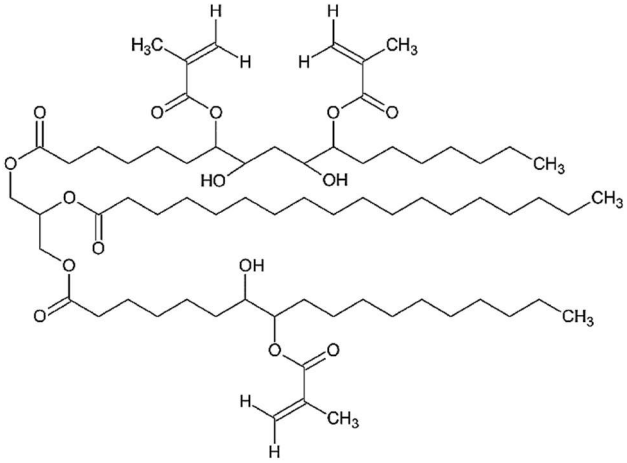

- Methacrylated carboxymethyl cellulose

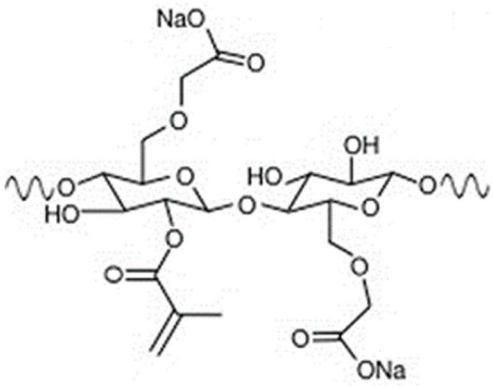

Direct Laser Writing

- Vanillin diacrylate

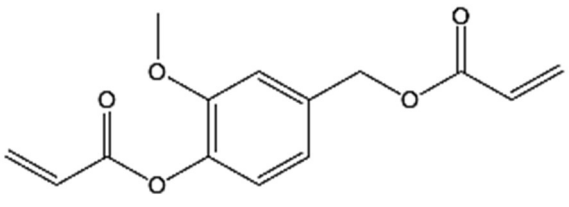

- Vanillin dimethacrylate